NTNU

Department of Structural Engineering
Faculty of Engineering Science and Technology

Floating Wind Turbines at Medium Water Depths

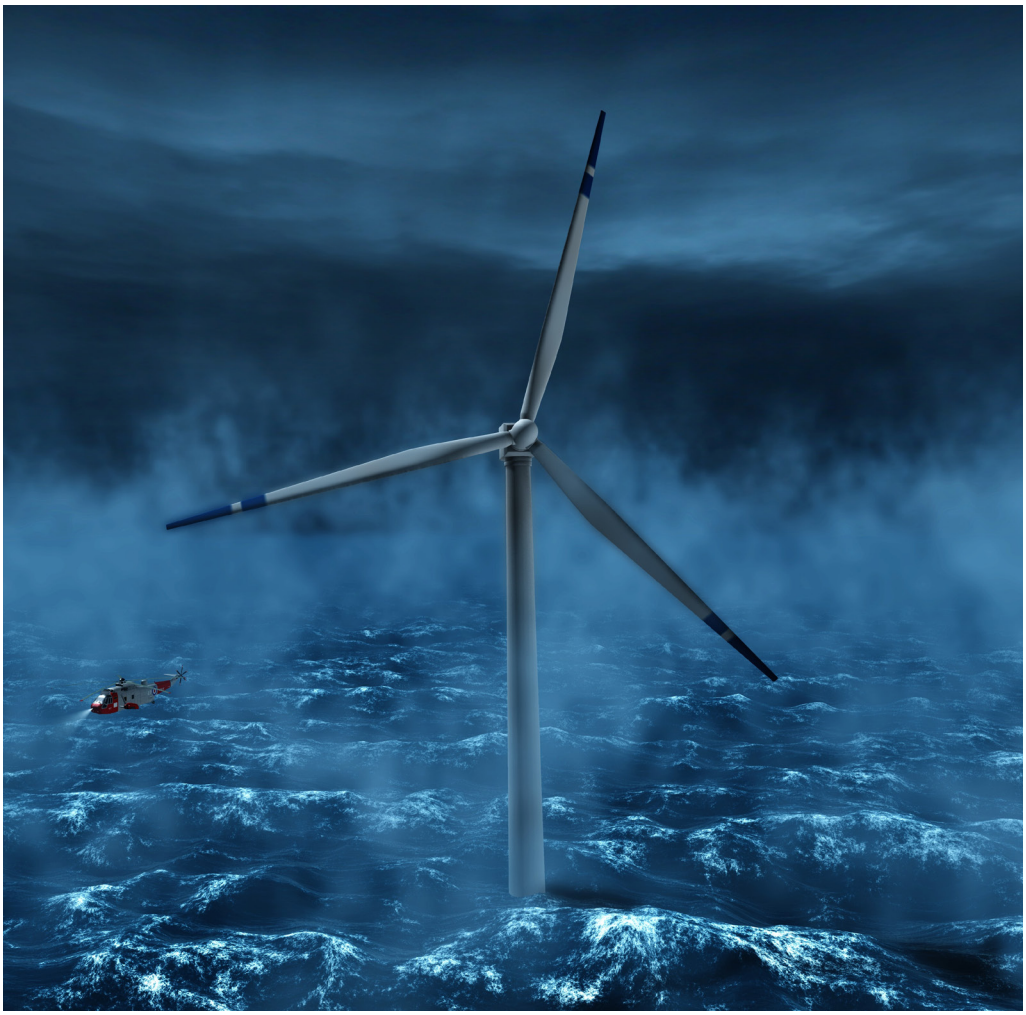

TKT4900 - Structural Engineering, Master Thesis

by

Eirik Wie Furunes

Spring 2010
Norwegian University of Science and Technology

Department of Structural Engineering
Faculty of Engineering Science and Technology
NTNU - Norwegian University of Science and Technology

ACCESSIBILITY

RESTRICTED

MASTER THESIS 2010

SUBJECT AREA:	DATE:	NO. OF PAGES:
Dynamic analyses, Floating offshore wind turbines	14th of June, 2010	135

TITLE:

Floating wind turbines at medium water depths
Flytende offshore vindmøller på moderate vanndyp

BY:

Eirik Wie Furunes

SUMMARY:
Offshore wind turbines have an enormous potential in terms of larger average wind speeds and low surface roughness compared to their onshore counterpart. Shallow water fixed wind turbines are ranked as a mature technology but are also limited by the price tag of creating and installing fixed installations for increasing depths. Hywind, which is a floating wind turbine concept developed by Statoil with focus on larger depths but may prove beneficial for shallower depths and fill the present void between floating and fixed wind turbines.

Hywind is limited for shallower waters by among others its large draft and the thesis focus is on a reduction of the draft with the inclusion of a heave plate for possible increased performance. The performance in ultimate limit state (ULS) and fatigue limit state (FLS) are utilized as a base for comparisons between different draft configurations.

Non-linear time domain analyses are carried out in FLS and ULS by the coupled computer codes SIMO/RIFLEX including wind, wave and current loads. In the non-linear analyses performed the hydrodynamic loads are calculated at the actual displaced position of the structure and instability effects as the Mathieu instability are accounted for, and also investigated in combination with a second order heave force contribution.

The analysis procedures and theory for floating offshore wind turbines are investigated and analysis parameters are defined in terms of ULS and FLS load cases, natural frequencies, a simplified wind turbine control system, damping estimates and heave plate properties.

In FLS the draft length has proven as an integral parameter and reduction in lifetime is shown for reduced draft configurations. The inclusion of a heave plate is shown to give an increase in lifetime, although minimal. In ULS peak values are increased for the reduced draft configurations and inclusion of the heave plate has shown to reduce dynamic heave motion but increase dynamic pitch motion.

RESPONSIBLE TEACHER: Professor Arild Holm Clausen, NTNU.

SUPERVISOR(S): Principal researchers Tor David Hanson and Rune Yttervik, Statoil.

CARRIED OUT AT: Statoil Research Center Bergen.

NORGES TEKNISK-NATURVITENSKAPELIGE UNIVERSITET
INSTITUTT FOR KONSTRUKSJONSTEKNIKK

MASTEROPPGAVE 2010

Eirik Wie Furunes

Floating wind turbines at medium water depths

(Flytende offshore vindmøller på moderate vanndyp)

As non-renewable energy resources at some point will be nearly depleted and global warming is increasing, the world is looking to extend the renewable energy resources' potential. The renewable energy is generated from natural resources such as sunlight, wind, waterfalls, tides and geothermal heat. Wind power, which can be used to run wind turbines, is growing at the rate of 30 percent annually and is widely used in the European countries. While wind turbines on land and fixed in shallow waters are ranked as a mature technology and commercialized, floating wind turbines are ranked as a new technology and still require extensive studies and testing.

Statoil has developed and installed a floating wind turbine prototype (Hywind) for deeper waters (120 m – 700 m). But there is also a desire to study floating wind turbines in waters more shallow than 120 m, which in turn might be a more attractive concept than fixed offshore wind turbines at these water depths. This calls for an investigation of the dynamic behaviour of floating wind turbines in waters more shallow than the Hywind prototype.

The candidate is supposed to cover these issues in the thesis work:

- Explore the literature on modeling and analysis of floating wind turbines
- Assess the dynamic response of floating wind turbines by performing parameter studies
- Compare the numerical predictions with results from more simple design models

The candidate can agree with the supervisors to exclude one or more of these issues, or include other topics in the investigation.

The thesis has to be written as a research report, and it should be organised in accordance with the guidelines provided by Department of Structural Engineering, NTNU.

Supervisors: Tor David Hanson and Rune Yttervik, Statoil

The thesis is to be handed in at Department of Structural Engineering not later than 14 June 2010.

NTNU, 15 January 2010

Arild H. Clausen
Professor

Preface

The written work herein constitutes the final work with my Master's degree within the program of study Engineering Science and ICT (Ingeniørvitenskap og IKT), at the Norwegian University of Science and Technology (NTNU). The work has been carried out in the spring of 2010 in cooperation with the Statoil research center in Bergen, where I have spent most of the time during the semester.

The thesis investigate properties related to a new and emerging field of offshore structures, namely offshore floating wind turbines. The offshore floating wind turbines is still defined as a young technology, and much research needs to be devoted to the understanding and analyses of among others the complex loading situations in terms of wind and wave loads.

As the author's background is within structural engineering, it has been both challenging and rewarding to extend the knowledge within structural dynamics to the broad field of marine dynamics as well as wind dynamics. With the authors background, time has been devoted to get the proper knowledge within especially marine dynamics and the reader should be aware of that. Although the thesis' focus is on a reduction of the draft, time has also been devoted to explain dynamic challenges related to the Hywind concept as the understanding of theoretical foundations and physical nature of what is analysed is deemed integral by the author to obtain reliability and confidence with the results.

Many people have contributed to the work herein and firstly I would like to thank my main supervisor during the semester, Tor David Hanson. He has during the whole semester followed my work and given competent advice whenever needed. I would like to thank my co-supervisor Rune Yttervik, which has given me much feedback in regards to the analysis tools as well as discussions during the semester. Sincere gratitude is given to Finn Gunnar Nielsen for his guidance in the physical behavior of the Hywind concept and Bernt Karsten Lyngvær for his guidance in the analysis program WAMIT. Everyone at the department in Bergen have shown a positive attitude towards my work and have made the months in Bergen memorable. Sincere gratitude is also given to my Professor Arild Holm Clausen in Trondheim for invaluable feedback on the written work.

Eirik Wie Furunes

Bergen, 14th of June 2010

Abstract

Offshore wind turbines have an enormous potential in terms of larger average wind speeds and low surface roughness compared to their onshore counterpart. Shallow water fixed wind turbines are ranked as a mature technology but are also limited by the price tag of creating and installing fixed installations for increasing depths. Hywind, which is a floating wind turbine concept developed by Statoil with focus on larger depths but may prove beneficial for shallower depths and fill the present void between floating and fixed wind turbines.

Hywind is limited for shallower waters by among others its large draft and the thesis focus is on a reduction of the draft with the inclusion of a heave plate for possible increased performance. The performance in ultimate limit state (ULS) and fatigue limit state (FLS) are utilized as a base for comparisons between different draft configurations.

Non-linear time domain analyses are carried out in FLS and ULS by the coupled computer codes SIMO/RIFLEX including wind, wave and current loads. In the non-linear analyses performed the hydrodynamic loads are calculated at the actual displaced position of the structure and instability effects as the Mathieu instability are accounted for, and also investigated in combination with a second order heave force contribution.

The analysis procedures and theory for floating offshore wind turbines are investigated and analysis parameters are defined in terms of ULS and FLS load cases, natural frequencies, a simplified wind turbine control system, damping estimates and heave plate properties.

In FLS the draft length has proven as an integral parameter and reduction in lifetime is shown for reduced draft configurations. The inclusion of a heave plate is shown to give an increase in lifetime, although minimal. In ULS peak values are increased for the reduced draft configurations and inclusion of the heave plate has shown to reduce dynamic heave motion but increase dynamic pitch motion.

Contents

List of Figures

List of Tables

1 Introduction

1.1 Motivation

When looking at the energy consumption of the world today and its energy dependence, it is quite clear that non-renewable energy resources as it is today, is not the solution of the future. As these energy resources are shrinking and global warming is increasing, research is devoted to expand the potential of renewable energy in many different forms.

One of the renewable energy resources that have been utilized in many decades is wind power. Wind turbines, which utilize wind power, are increasing in numbers, efficiency and where they are placed. Onshore wind turbines is a proven technology that has been utilized for quite some time, but raising wind turbines onshore has met a lot of public resistance in terms of their aesthetics and intervention with the nature.

Turning to offshore wind turbines, which are out of sight of the public, there is an enormous potential in terms of larger average wind speeds and low surface roughness which leads to less turbulence. Even though there are a lot of benefits with offshore locations, the potential of rough seas combined with wind is a challenge for the designers. Fixed offshore wind turbines are increasing in numbers but are also limited by the price tag of creating and installing fixed installations for increasing depths. New and exciting offshore floating wind turbine concepts are emerging as a consequence of the limitations of the fixed offshore wind turbines.

1.2 Thesis focus

Hywind, which is a floating wind turbine concept developed by Statoil, utilizing their vast experience with offshore conditions and structures, is developed with focus on larger depths but may prove beneficial for shallower depths in the range 70 m - 100 m and fill the present void between floating and fixed wind turbines.

As Hywind is limited for shallower waters by among others its large draft, modifications to reduce the draft may prove beneficial for taking the concept to shallower depths. The long draft provides for beneficial hydrodynamic properties, and the thesis investigates the possibility to compensate in loss of draft by a heave plate, which properties are thoroughly investigated within the thesis. Mooring line properties are also important factors for taking the concept to shallower waters, but are in general not investigated to limit the scope of the thesis. An important factor, which has not been found in previous literature and investigated in the thesis, is possible positive effects of the heave plate in terms of the ultimate and fatigue limit state for the floating wind turbine.

As a base for comparisons coupled wind and wave analyses are carried out. The states investigated are 50-year ultimate limit state analyses with comparisons of motions and structural forces, as well as fatigue limit state analyses where lifetime assessments are done at the mean water line with environmental data based on 50-year scatter tables.

1.3 Thesis outline

A large focus within the thesis work has been to gain the proper theoretical knowledge to be able to carry out analyses and understand the physical behavior of what is observed. The majority of the theoretical background material is presented in Chapter 3, 4 and 5, but also smaller sections with theoretical explanations related to material in other chapters are included.

Chapter 2 presents important properties with the Hywind concept, the configuration used as a base case for the analyses in the thesis and some introductory details with the heave plate.

Chapter 3 and 4 presents a brief overview of the theoretical foundation for numerical wave and wind calculation, respectively. These are theoretical chapters and deemed by the author as integral for the understanding of the underlying processes in the analysis programs.

Chapter 5 deals with more specialized theory in regards to the floating support structure. Properties such as added mass, damping estimation, excitation forces as well as key parameter extraction for the support structure are discussed from a theoretical point of view.

Chapter 6 presents the analysis programs, important properties with them and their coupling. Analysis model properties as well as fatigue calculation procedures are also presented.

Chapter 7 deals with added mass calculations by the panel program WAMIT. Analytical expressions are verified and frequency dependencies investigated.

Chapter 8 deals with the extraction of environmental conditions applied in the ultimate and fatigue limit state analyses.

Chapter 9 deals with a thorough investigation of the base case configuration. This chapter lays the foundation for the analyses done on all configurations and investigates possible resonance issues as well as the theoretical foundations for what is observed.

Chapter 10 presents reduced draft configurations and compare performance in the ultimate and fatigue limit state.

The appendix mainly contains Matlab scripts developed during the thesis work. The appendix also includes a batch script for running coupled analyses in parallel and sequentially, analysis models and tables with dynamic response characteristics.

2 The Hywind Concept

The concept developed by Statoil is a wind turbine mounted on to a spar buoy and moored with three mooring lines. The concept is currently being tested in full scale outside Karmøy north of Stavanger, Norway. The test program started in September 2009 and will run for about two years to collect data from the many sensors mounted on board as well as experience challenges and potential improvements with the concept.

The Hywind concept is ballast stabilized which means that the center of gravity is located below the center of buoyancy and gives excellent stability conditions. There is also other floating wind turbine concepts which utilizes other stability conditions, i.e. mooring line stabilized and buoyancy stabilized, but these concepts are not investigated nor further explained in the thesis.

2.1 Definition of motions

The author believes it is proper to give a clear definition of what is meant by the different motions used throughout the thesis. The rigid-body translatory motions are referred to as surge, sway and heave which depending on if the coordinate system follows the body can be referred to local x-, y- and z-coordinates respectively. The angular motions are referred to as roll, pitch and yaw. The numbering of the motions are from 1-6 and the motions with corresponding numbering are exemplified in Figure 2.1 for a circular cylinder. What also should be observed is that the circular cylinder in the figure as well as the Hywind concept have symmetrical properties, thus surge and sway as well as roll and pitch are the same.

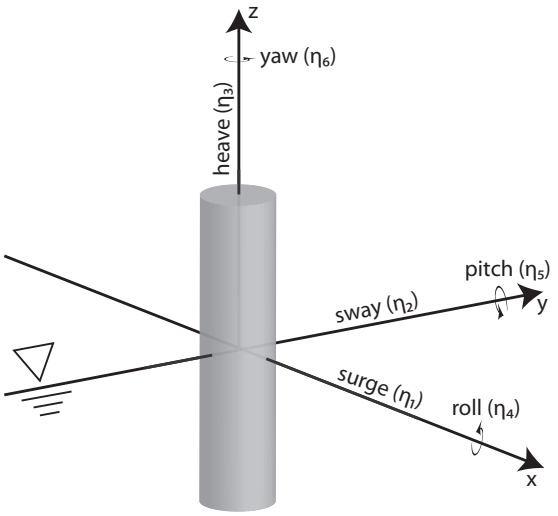

Figure 2.1: Definitions of motions, exemplified by a circular cylinder.

2.2 Base case

The structure being tested outside Karmøy is built with a steel draft, but the original concept was with a concrete draft and that is also what is used as a base case for the thesis. Table 2.1 summarizes some key dimensions of the concrete draft structure used as a base case for the investigations in the thesis.

Turbine size	2.3 MW
Turbine weight	136 tons
Turbine height	64 m
Rotor diameter	82.4 m
Draft hull	110 m
Displacement	6274 tons
Diameter at waterline	6 m
Diam. submerged body	8.6 m

Table 2.1: Dimensions for Base case

2.3 Mooring system

Hywind is moored with three mooring lines distributed evenly around the hull with a 120° spacing, made of steel and chain. To increase the line tension clump weights are attached to each mooring line. A bridle (delta line) is used in the connection between the mooring line and Hywind to increase the restoring in yaw. The reader may confer to the illustration in Figure 2.2 for a better understanding of the mooring line arrangement. It should be noted that the length of the mooring lines in Figure 2.2 are much shorter than the actual mooring lines and only two of the three mooring lines are shown.

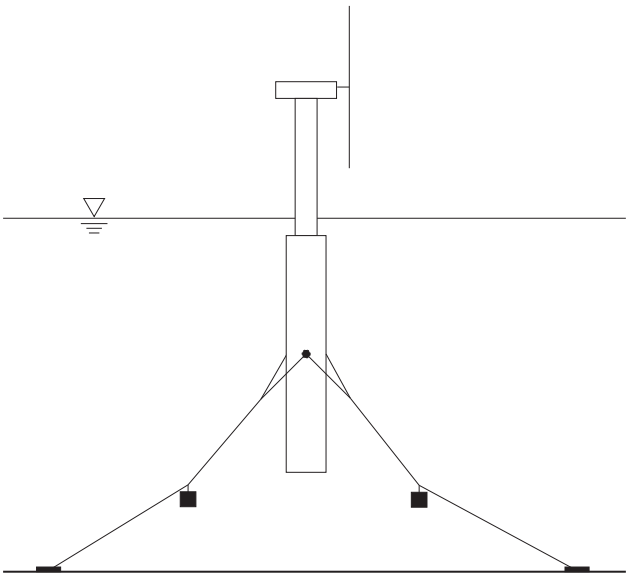

Figure 2.2: Hywind concept, mooring line arrangement. Not in scale.

Different water depths will require different mooring systems where mooring line length, clump weight and attachment point are just a few of the parameters that must be considered. To reduce the complexity of the thesis and to keep a focus on the support structure, the mooring system will be kept constant, and as a consequence the water depth will be

kept constant for all analyses. It should also be mentioned that with different configurations of the support structure, the attachment point can be kept at a constant water level or kept constant in regards to the draft hull. The latter is utilized in the thesis.

The strategy for the mooring line attachment point is based on argumentations in a memo on the Hywind concept by F. G. Nielsen [1]. Attaching the mooring lines near the mean water line, which is beneficial for the structure in terms of its rotation, may induce extreme loading in the mooring lines. Attaching the mooring lines at the bottom of the draft, which is beneficial for the loading of the mooring lines, may increase the rotation of the structure to an unbeneficial magnitude. The mooring line system dimensions utilized in the thesis is summarized in Table 2.2.

Mooring line segment	Length [m]	Diameter [mm]	Weight in water [kg/m]
Upper steel wire	180	90	35.48
Clump weight	1	-	50×10^3
Lower steel wire	420	90	35.48

Table 2.2: Dimensions for mooring system

The upper steel wire contains the bridle, which is 50 m. The vertical and horizontal projection for the base case is 174 m and 558 m, respectively. This will be different for other cases with lower draft because of the change in attachment point.

2.4 Turbine control system

The turbine of 2.3 MW which is utilized in the thesis requires some extra attention. Wind turbines do in general have control systems to ensure the most beneficial power production and the turbine considered has a cut-in wind speed at 3-5 $\mathrm{m\,s^{-1}}$, which is the required wind speed before the turbine starts to produce electricity. There is also a cut-out wind speed at 25 $\mathrm{m\,s^{-1}}$ where the blades are pitched so they experience the least lift possible and are thus in an idling mode to reduce structural loads at extreme wind velocities.

The thrust force on the structure is at its maximum approximately at a wind velocity of 12 $\mathrm{m\,s^{-1}}$, this can be seen from Figure 2.3a where the thrust force versus the wind velocity is plotted. A brief overview of the theory behind the simplified thrust force can be reviewed in Section 4.3. After the wind thrust has reached its maximum, the thrust force will reduce on the structure and the turbine is at its rated power production, this can be seen from Figure 2.3b where the power production versus the wind velocity is plotted. The simplified estimate for power production is based on the same theoretical assumptions as the thrust force.

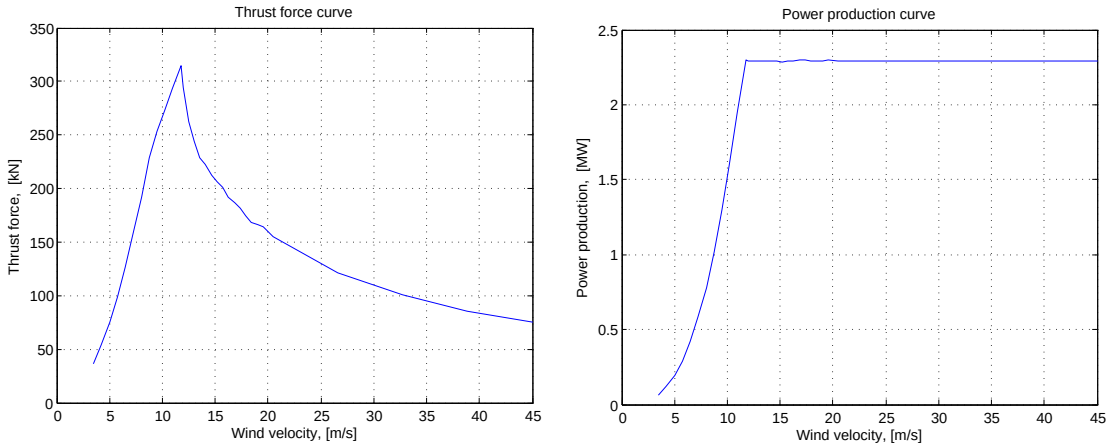

(a) Thrust force curve

(b) Power production curve

Figure 2.3: Simplified models for thrust force and power production

In terms of turbine control strategies, below rated wind speed the control system needs to ensure maximum possible power production by varying rotor speed and keeping a constant blade pitch angle.

Above rated wind speed, what is named conventional control should not be used for floating wind turbines, the conventional control strategies is to control for constant power production by keeping a constant rotor speed and vary the blade-pitch angle, which is excellent for fixed wind turbines, but in terms of floating wind turbines the control system must also strive for active damping of the structures pitch motions when varying the blade-pitch angle. The relevance of the active damping is further described and analysed in Section 9.6.

2.5 Modification to the Hywind concept

The thought is, to reduce the draft and investigate the possibility to compensate in loss of hydrodynamic stability by a circular concrete mass plate at the bottom. The mass plate which goes under different names in the literature, i.e. mass plate, heave plate or damping plate, is reported with important beneficial factors within heave motion, heave damping and the heave natural period [2, 3, 4]. It is referred to as a heave plate in the thesis.

The increase of mass at the bottom of the structure may prove beneficial for the dynamic pitch performance, which is a driving factor for structural forces, in terms of a lower center of gravity compared to a reduction without the heave plate. All of the mentioned factors will be further discussed in the thesis and are mentioned here as a brief introduction to the possible beneficial factors for the Hywind concept. The modification of the Hywind concept with a heave plate is illustrated in Figure 2.4.

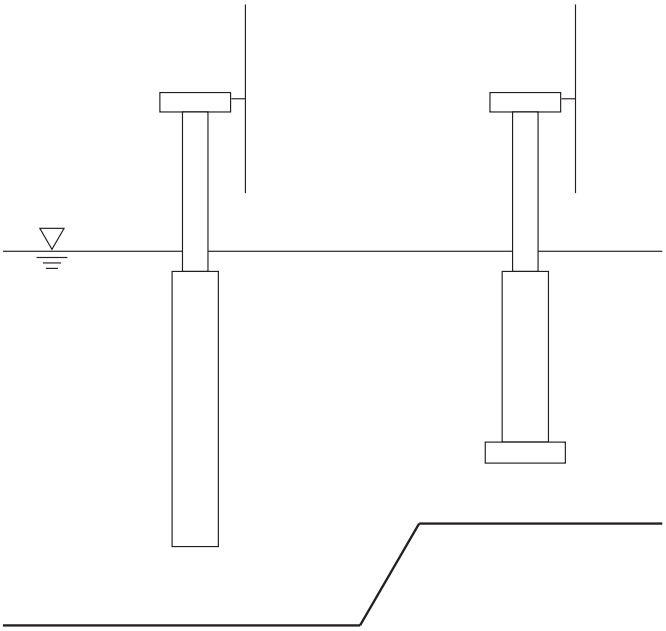

Figure 2.4: Hywind modification, illustration.

3 Wave Theory

The theory in this chapter is mainly based on the book "Sea loads on ships and offshore structures" by O. M. Faltinsen [5].

3.1 Linear wave theory

This section identifies some of the main assumptions in the development of linear wave theory, which is by the author seemed as integral for the understanding of numerical wave calculations, the reader may refer to [6] for a more thorough discussion of the subject.

3.1.1 Laplace's equation

The usual starting point for linear wave theory, also called Airy[1] wave theory, is Laplace's equation:

$$\nabla^2\phi = \frac{\partial^2\phi}{\partial x^2} + \frac{\partial^2\phi}{\partial z^2} = 0 \tag{3.1}$$

Presented here in two dimensions in the x-y plane, where ϕ represents the potential function.

The potential function is introduced because it is convenient in the mathematical analysis of irrotational fluid motion. The equation is valid for fluid assumed incompressible and inviscid. Also, the fluid motion is assumed irrotational. Equation (3.1) expresses fluid motion with the mentioned assumptions. The relation between the potential function and the velocity of fluid particles can be written as:

$$\frac{\partial\phi}{\partial x} = u \tag{3.2a}$$

$$\frac{\partial\phi}{\partial z} = w \tag{3.2b}$$

Where u is velocity in x-direction and w is velocity in z-direction.

3.1.2 Boundary conditions - finite water depth

By assuming a horizontal sea bottom and a free-surface of infinite horizontal extent, the boundary conditions for the x-direction do not have to be explicitly stated. In what follows the boundary conditions in z-direction is considered.

For a finite water depth, the following boundary condition can be stated for the sea bottom:

$$w = (\frac{\partial\phi}{\partial z})|_{z=-h} = 0 \tag{3.3}$$

[1] Sir George Biddell Airy (1801 - 1892)

Where z = 0 at mean water level and h is the vertical distance to the sea bottom. The boundary condition can easily be interpreted as it says that no flow will go through the sea bottom.

A boundary condition for the sea surface is more tedious to develop and only the paramount requirements are stated here. The derivation of the surface condition is based on a kinematic boundary condition and a dynamic boundary condition. The kinematic boundary condition states that a fluid particle will follow the free surface $\zeta(x,t)$ at all times. The dynamic boundary condition states that the pressure at the surface must be equal to the atmospheric pressure, which is assumed constant.

With these boundary conditions a solution to Laplace's equation is very difficult to obtain, thus an assumption that the waves are very small i.e. $\zeta(x,t)$ is very small compared to the variations in the x-direction. Thus the relevant boundary conditions are linearized and the boundary condition for the free surface can be obtained as:

$$(\frac{\partial^2\phi}{\partial t^2} + g\frac{\partial\phi}{\partial z})|_{z=0} = 0 \tag{3.4}$$

3.2 Regular wave theory

By using the sea bottom condition (3.3) and the free surface condition (3.4), the velocity potential for finite water depth can be written as:

$$\phi = \frac{g\zeta_a}{\omega}\frac{cosh(k(z+h))}{cosh(kh)}cos(\omega t - kx) \tag{3.5}$$

The development of boundary conditions for infinite water depth is similar and can be obtained by assuming no fluid disturbance when z $\rightarrow -\infty$. The velocity potential for infinite water depth can be written as:

$$\phi = \frac{g\zeta_a}{\omega}e^{kz}cos(\omega t - kx) \tag{3.6}$$

Where, for both equations:

- g: acceleration of gravity
- ζ_a: wave amplitude
- d: water depth
- ω: angular frequency ($\omega = \frac{2\pi}{T}$, where T is the wave period)
- k: wave number (k = $\frac{2\pi}{\lambda}$, where λ is the wave length)

From the velocity potential given by (3.5) and (3.6) particle velocities can be found from the expressions in (3.2), and accelerations can be found by differentiating the particle velocities. Wave properties are also shown in Figure 3.1.

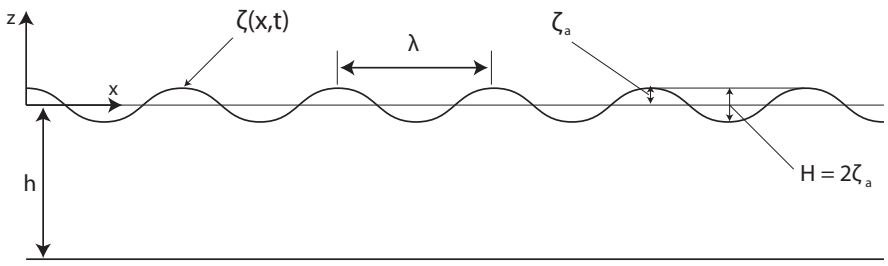

Figure 3.1: Wave properties.

An important result from the derivation of linear wave theory is the dispersion relation:

$$\frac{\omega^2}{g} = k\ tanh(kh) \tag{3.7}$$

The dispersion relation gives the relationship between the wave number k and the angular frequency ω, or in other words; the wave length and the wave period.

The expression is the same for both finite and infinite water depth, but for small values of kh which represents shallow waters $tanh(kh) \rightarrow kh$. For large values of kh which represents deep waters $tanh(kh) \rightarrow 1$. A Matlab script used to solve the dispersion relation for slender body evaluation can be seen in Appendix A.1.

3.3 Irregular wave theory

The only waves in the ocean which may resemble the regular waves described in the previous section is swell, i.e. waves generated by a distant storm. So to obtain a more useful usage of regular wave theory one must look at the simplification that made it possible, linearity.

Being linear one can superimpose regular waves of different amplitudes, angular frequency and wave number to obtain an irregular sea state. The one-dimensional wave elevation can be written as:

$$\zeta = \sum_{j=1}^{N} A_j sin(\omega_j t - k_j x + \epsilon_j) \tag{3.8}$$

Where A_j is the wave amplitude, k_j and ω_j are related by the dispersion relation and ϵ_j is a random phase angle. The random phase angles are uniformly distributed between 0 and 2π and constant with time.

Since the wave phases are considered as random variables, they represent the randomness in the simulation of irregular waves and the wave surface becomes a random surface. The wave amplitude A_j can be expressed by a wave spectrum by the following relation:

$$\frac{1}{2}A_j^2 = S(\omega_j)\Delta\omega \tag{3.9}$$

Where $\Delta\omega$ represents the frequency discretization interval of the wave spectrum.

The sea state, which is the condition of the ocean surface, is considered as a stochastic field and can be represented by the wave spectrum. The wave spectrum which is the frequency domain representation of the waves can be estimated from wave measurements, and a commonly used wave spectrum is the Joint North Sea Wave Project (JONSWAP) type spectrum, the reader may also refer to [5] for more information.

The JONSWAP spectrum can be written as:

$$S(\omega) = 155\frac{H_{1/3}^2}{T_1^4\omega^5}\exp\left(\frac{-944}{T_1^4\omega^4}\right)(3.3)^Y \tag{3.10}$$

Where

$$Y = \exp\left(-\left(\frac{0.191\omega T_1 - 1}{2^{\frac{1}{2}}\sigma}\right)^2\right) \tag{3.11}$$

and

$$\sigma = \begin{cases} 0.07 & \text{if } \omega \leq 5.24/T_1, \\ 0.09 & \text{if } \omega > 5.24/T_1. \end{cases} \tag{3.12}$$

Where $H_{1/3}$ is the significant wave height defined as the mean of the one third highest waves, it is often redefined as $H_{1/3} = 4\sqrt{m_0}$ where m_0 is the variance of the surface elevation. The latter is a simplification, but for a narrow-banded Gaussian sea elevation process, the two definitions will converge. T_1 is a mean wave period, it has a relation with the peak period of the spectrum as $T_p = 1.199T_1$ which is most commonly used. The JONSWAP spectrum is used in the analysis part of the thesis.

4 Wind Theory

The theory described here is relevant for the understanding of wind as well as generation of thrust forces through a numerical model of thrust from a wind turbine onto the nacelle. Most of the theory presented can be regarded as a theoretical basis for the numerical thrust force model TDHMILL utilized in the analyses, TDHMILL is further described in Section 6.1.1.

4.1 Wind field

The theoretical background in the following is based on the book "Theory of Bridge Aerodynamics" by E. Strømmen [7].

A wind field is a complex process that is randomly distributed in time and space, being randomly distributed it can be seen as a stochastic process described mathematical by different stochastic variables as expectation value and variance.

A structure under the influence of wind will experience static forces as well as dynamic forces. The wind velocity causing this can be divided into a static velocity, i.e. a time independent, and a time dependent fluctuating velocity. For a slender structure as a wind turbine, i.e. the velocity is regarded as constant with regards to the thickness of the structure, the total velocity in terms of height and time can be written as:

$$U(z,t) = V(z) + u(z,t) \tag{4.1}$$

The turbulent component $u(z,t)$ is selected so that it has an expectation value equal to zero and will fluctuate around the mean velocity $V(z)$, see Figure 4.1. Because of friction the wind velocity will decrease nearing mean water level, but the friction will be less over water than over land.

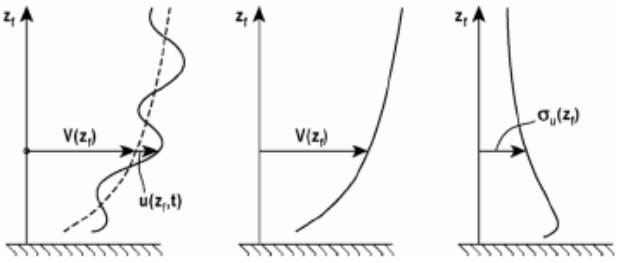

Figure 4.1: Wind field variation with height $z_f = z$ [7]

Theoretical the mean wind velocity can be written as a logarithmic function of the height:

$$\frac{V_{10}(z)}{V_{10}(10)} = \begin{cases} k_t ln(\frac{z}{z_0}) & \text{when } z > z_{min} \\ k_t ln(\frac{z_{min}}{z_0}) & \text{when } z \leq z_{min} \end{cases} \tag{4.2}$$

Where $V_{10}(10)$ is the wind velocity at reference height 10m, the subscript 10 means that the wind measurements used to determine the terrain specific parameters k_t, z_{min} and z_0 had a period of 10 minutes. Measurements are often done over several years. The turbulence intensity factor of the fluctuating part u(z) is defined as:

$$I_u(z) = \frac{\sigma_u(z)}{V(z)} \tag{4.3}$$

Where $\sigma_u(z)$ is the standard deviation of the fluctuating velocity component u(z).

4.2 IEC 61400-1 Standard

In the IEC 61400-1 standard [8] for wind turbines two turbulence models are given for design load calculations, the Mann and the Kaimal model. The latter is included in TDHMILL for generation of wind time series. The IEC standard states the Kaimal spectrum for the fluctuating part u on the following form:

$$\frac{fS_u(f)}{\sigma_u^2} = \frac{4fL_u/V_{hub}}{(1+6fL_U/Vhub)^{5/3}} \tag{4.4}$$

Where L_u is the velocity component integral scale parameter and V_{hub} is the wind speed at hub height. The normal turbulence model standard deviation and the velocity integral scale parameter in the Kaimal spectrum, as defined in the IEC standard, can be written as:

$$\sigma_u = I_{ref}(0.75V_{hub} + 5.6) \tag{4.5}$$

and

$$L_u = 8.1\Lambda_1, \text{ where } \Lambda_1 = \begin{cases} 0.7z_{hub} & \text{when } z_{hub} \leq 60m \\ 42m & \text{when } z_{hub} \geq 60m \end{cases} \tag{4.6}$$

Where I_{ref} is given for different turbulence characteristics in the IEC standard.

The spectrum in equation (4.4) as stated in the IEC standard is not a function of the height variable, which is a simplification with regards to the theory considered earlier.

The IEC standard also recommends a simpler mean wind velocity model than the one in equation (4.2), which is also suitable for the mean wind velocity over water where terrain specific parameters are of less concern. The model recommended is given as a power law:

$$V(z) = V_{hub}(\frac{z}{z_{hub}})^{\alpha} \tag{4.7}$$

Where α is the wind shear exponent and is usually set to 0.2 over land [8], over water the surface roughness is less and a typical value for α over water is 0.14 [9]. The effect of different wind shear exponent can be seen in Figure 4.2.

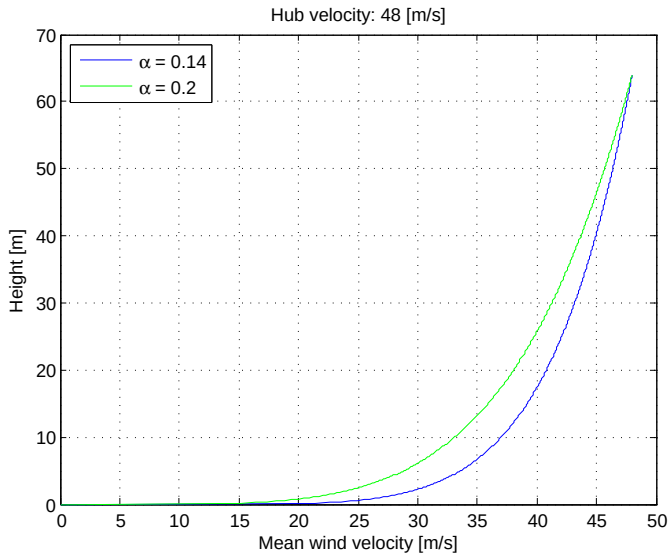

Figure 4.2: Mean wind velocity model, effect of wind shear exponent.

4.3 One-Dimensional Momentum Theory

The following is based on the book "Wind energy explained" by J. Wiley [10] and the theory is in general attributed to Albert Betz (1885 - 1968). Assumptions for the following derivation are:

- Homogenous, incompressible and steady state fluid flow.
- No frictional drag.
- An infinite number of blades.
- Uniform thrust over the disk or rotor area.
- A nonrotating wake.
- The static pressure far upstream and far downstream of the rotor is equal to the undisturbed ambient static pressure.

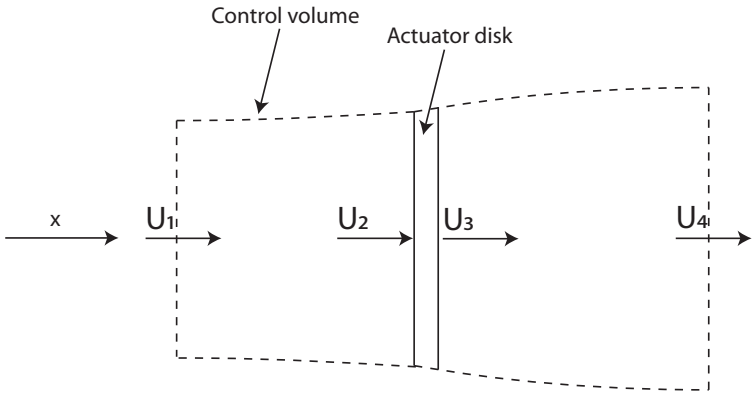

Figure 4.3: Control volume with flow over actuator disk, U_i is velocity for location 1, 2, 3 and 4.

Referring to Figure 4.3 and applying the one-dimensional conservation of linear momentum to the control volume one can find the net force acting on the control volume:

$$\sum F_x = \dot{m}_4 U_4 - \dot{m}_1 U_1 = (\rho_a A_4 U_4) U_4 - (\rho_a A_1 U_1) U_1 \tag{4.8}$$

Where $\dot{m}$ is mass flow rate, ρ_a is the density of air, U is velocity in x-direction, A_i is the cross sectional area and subscripts are locations as stated in Figure 4.3. Thus, the thrust force T on the disk may be written as:

$$T = -\sum F_x = (\rho_a A_1 U_1) U_1 - (\rho_a A_4 U_4) U_4 = \dot{m}(U_1 - U_4) \tag{4.9}$$

The last transition is from the assumption of steady state flow, i.e. $(\rho_a A_4 U_4) = (\rho_a A_4 U_4) = \dot{m}$. Using Bernoulli's equation from 1 to 2 and from 3 to 4 it can be shown that the thrust force can be written as:

$$T = \frac{1}{2} \rho_a A_2 (U_1^2 - U_4^2) \tag{4.10}$$

By defining the fractional decrease in wind velocity between the the velocities at 1 and 2, one obtains what is called the axial induction factor:

$$a = \frac{U_1 - U_2}{U_1} \tag{4.11}$$

Rearranging equation (4.11) for U_2 and U_4 as well as introducing them in equation (4.10) the thrust force can be written as:

$$T = \frac{1}{2} \rho_a A_2 U_1^2 (4a(1-a)) = \frac{1}{2} \rho_a \pi R^2 U_1^2 C_T \tag{4.12}$$

Where R is the radius of the actuator disk. In the last transition C_T is introduced for $(4a(1-a))$, C_T is a non-dimensional thrust coefficient which is further explained in Section 6.1.1.

5 Floating Support Structure

Described here is theory important for validation and understanding of properties related to the structure as well as the analysis model. Yaw motion is not considered as it is mostly related to the mooring line stiffness.

5.1 The equation of motion

The equation of motion for a multiple degree of freedom (MDOF) system can be written as:

$$[M]\{\ddot{\eta}\} + \{F_D(\dot{\eta})\} + \{F_C(\eta)\} = \{F(t,\eta)\} \tag{5.1}$$

Where [M] is the mass matrix, $\{F_D(\dot{\eta})\}$ is the non-linear damping force vector, $\{F_C(\eta)\}$ is the non-linear restoring force vector, $\{F(t,\eta)\}$ is the non-linear external force vector and $\{\eta\}$ is the motion vector containing the translatory and rotational degrees of freedom.

By linearization of equation (5.1), "the hydrodynamic problem" can be divided into two sub-problems and added together:

- "The diffraction problem": The forces and moments on the body when the body is restrained from oscillating and there are incoming waves. The hydrodynamic forces are composed of *Froude-Kriloff*[1] and *diffraction* forces and moments. Which are pressure forces and moments due to the undisturbed fluid flow and due to the changes in the pressure field by the body's presence in the water, respectively.
- "The radiation problem": The forces and moment on the body when the body is forced to oscillate with the wave excitation frequency and there are no incident waves. The hydrodynamic loads are identified as added mass, damping and restoring terms.

The main focus of this chapter is on the hydrodynamic effects, but in e.g. the external force matrix there is also a thrust force from the wind and the theory behind the thrust force can be seen in Section 4.3.

5.2 Added mass

Remembering the symmetry shown in Figure 2.1, the mass matrix in equation (5.1) for a three degree of freedom system (surge, heave and pitch) referred to the waterline can be written as:

$$[M] = \begin{bmatrix} M + A_{11} & 0 & Mz_g + A_{15} \\ 0 & M + A_{33} & 0 \\ Mz_g + A_{51} & 0 & I_{55} + Mz_g^2 + A_{55} \end{bmatrix} \tag{5.2}$$

Where M is the total dry mass, A_{ij} are the added mass, I_{55} is the moment of inertia referred to the center of gravity and z_g is the vertical position of the center of gravity. The subscripts 1, 3 and 5 refer to surge, heave and pitch, respectively.

[1] Named after William Froude (1810 - 1879) and Alexei Krylov (1863 - 1945)

Added mass or virtual mass depending on which literature one is exploring, comes from the fact that a body accelerating in a fluid medium with a certain density must move some of the surrounding fluid. For simplicity this is in many cases modeled as a finite volume of fluid being accelerated, though in reality all of the surrounding fluid will be accelerated to a certain degree. The added mass is usually expressed as a dimensionless added mass coefficient, i.e. the added mass divided by the displaced fluid mass.

The added mass of the system, which in many cases can be quite difficult to determine because of its frequency dependency, can be estimated with sufficient accuracy for many bodies. Especially a vertical cylinder where the diameter is small compared to the wavelength [11].

5.2.1 Strip theory

A strip theory approach is often used to determine coefficients involved in equation (5.2). The method is based on summing the added masses of individual two-dimensional strips. The following definitions are taken from the book "Mechanics of wave forces on offshore structures" by Sarpkaya and Isaacson [11] and the two-dimensional strip of a cylinder can be written as:

$$A_{11}^{2D} = \rho_w \frac{\pi D^2}{4} \tag{5.3}$$

Where D is the diameter of the cylinder. Thus by a strip theory approach A_{11}, $A_{15} = A_{51}$ and A_{55} can be written as:

$$A_{11}^{2D} = \int_{-L}^{0} A_{11}^{2D}\, dz \tag{5.4}$$

$$A_{15} = A_{51} = -\int_{-L}^{0} A_{11}^{2D} z\, dz \tag{5.5}$$

$$A_{55} = -\int_{-L}^{0} A_{11}^{2D} z^2\, dz \tag{5.6}$$

Where the integration is carried out from the bottom of the cylinder (z = -L) to the mean water line (z = 0). By this approach end effects near the water line and the bottom of the cylinder are assumed small.

For the heave added mass A_{33}, numerical studies have shown that the heave added mass for a semi-infinite cylinder can be approximated as $0.258\rho_w D^3$ [12], which is quite close to the mass of a half sphere of water. Thus, the added mass in heave for a cylinder is approximated as:

$$A_{33} = \rho_w \frac{\pi}{12} D^3 \tag{5.7}$$

This is also the expression which is used in the analysis basis for the Hywind concept [13]. As will be shown in Chapter 7 by a WAMIT analysis, this is in good correspondence with a finite-cylinder as well.

5.2.2 Heave plate - Adaption of theory

If one extend the logic for the added mass of a cylinder, one could assume that the added mass of a cylinder with a heave plate would be the mass of a sphere of water, and reduce for the volume occupied by the cylinder, see Figure 5.1.

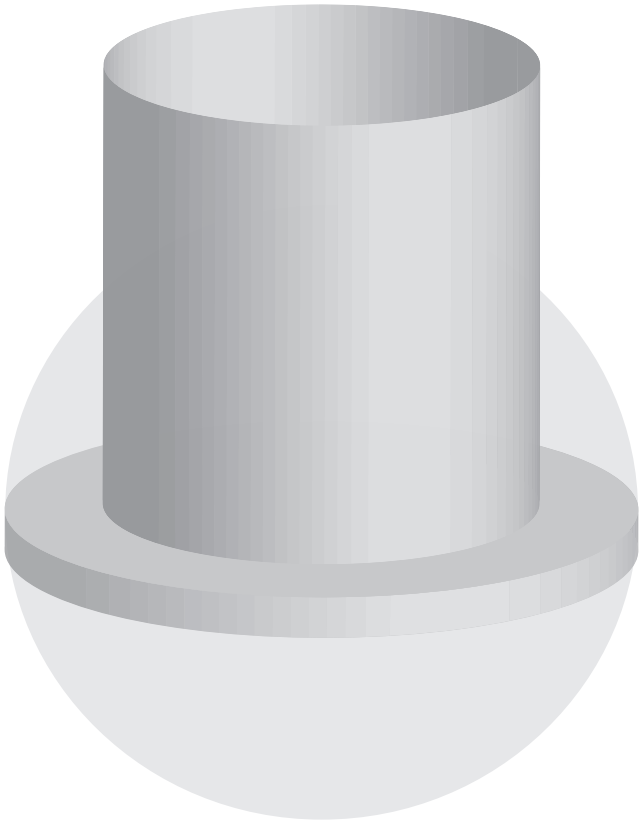

Figure 5.1: Added mass of a cylinder with a heave plate

The height of the intersection between the sphere and the cylinder can be written using Pythagoras theorem as:

$$H = \frac{1}{2}\sqrt{D_d^2 - D_c^2} \tag{5.8}$$

Where D_d and D_c is the diameter of the heave plate and cylinder, respectively.

By using a mathematical handbook [14] the expression for the segment of the sphere, with two parallel planes, which intersects the plate and the intersection between the sphere and the cylinder can be written as:

$$V_{seg} = \frac{\pi H}{6}(3(\frac{D_d}{2})^2 + 3(\frac{D_c}{2})^2 + H^2) \tag{5.9}$$

Reducing for the volume of the cylinder within the segment, the final expression for the added mass for a cylinder and heave plate can be written as:

$$A_{33}^{pl} = A_{33} + \rho_w \pi H[\frac{1}{6}(\frac{3}{4}D_d^2 + \frac{3}{4}D_c^2 + H^2) - \frac{1}{4}\pi D_c^2 H] \tag{5.10}$$

Where A_{33} is from equation (5.7). What will be shown in Chapter 7 by the panel program WAMIT is that this approach overestimates the added mass in heave.

An article by Longbin et al. [2] investigates an analytical expression for the added mass in heave for a cylinder with a heave plate. They use an expression presented by Sarpkaya

et al. [11] for only a plate and reduce for the volume of a cylinder over the intersection with the sphere as well as an reduction for the cap of the sphere. The expression is written as:

$$A_{33}^{pl} = \frac{1}{3}\rho_w D_d^3 - [\frac{\pi\rho_w}{8}D_c^2(D_d - \sqrt{D_d^2 - D_c^2}) + \frac{\pi\rho_w}{24}(D_d - \sqrt{D_d^2 - D_c^2})^2(2D_d + \sqrt{D_d^2 - D_c^2})] \tag{5.11}$$

The first term is the added mass of a thin plate, the second term is the mass of a cylinder with height $(D_d - H)$ and the last term is the mass of a spherical cap.

The reason for mentioning this expression is that it is in good agreement with WAMIT analyses in Chapter 7.

5.3 Wave excitation forces

Here the excitation force in the horizontal direction is considered. Excitation forces for circular cylinders are much discussed in many textbooks and the reader may refer to [5] for a more through discussion.

5.3.1 Inertia loads

For a two dimensional fixed cylinder, in infinite fluid, the horizontal excitation force on a two-dimensional strip, based on potential theory, can be written as:

$$f_I^{2D} = (A_{11}^{2D} + \rho_w \pi D_c^2)a_1 \tag{5.12}$$

Where a_1 is the x-component of the undisturbed water particle acceleration. The first term is the diffraction force based on a long wavelength assumption and the second term is the Froude-Kriloff force.

This expression corresponds to the inertia term in Morison's equation with an inertia coefficient $C_M = 2$.

5.3.2 Drag loads

The drag loads for a fixed cylinder can be expressed by a Morison type drag formulation as:

$$f_D^{2D} = \frac{\rho_w}{2}C_D D|u|u \tag{5.13}$$

Where C_D is the drag coefficient and u is the x-component of the undisturbed water particle velocity.

The drag coefficient, C_D, is among others influenced by the *Reynolds number* and the roughness and form of the body. Thus, finding the "correct" coefficient to use is a bit unpractical. For a circular cylinder in the horizontal direction a coefficient $C_D = 1$ is most commonly used [15].

5.3.3 Morison's equation

Seeing that the floating structure is not fixed, the total expression for Morison's equation can be expressed based on equations (5.12) and (5.13) in terms of relative velocity as:

$$f_M^{2D} = \frac{1}{2}\rho_w C_D D(u - \dot{\eta_1})|u - \dot{\eta_1}| + \rho_w C_M \frac{\pi D^2}{4}a_1 - \rho_w(C_M - 1)\frac{\pi D^2}{4}\ddot{\eta_1} \tag{5.14}$$

Since the body is moving, u and a_1 are position dependent. The | bracket represents absolute value. By integrating over the cylinder height, as for the added mass in Section 5.2, the total excitation force can be found.

The relative velocity term in equation (5.14) is of interest as it is also a source of damping. By assuming $u > \dot{\eta_1}$ the relative velocity term can be written as:

$$(u - \dot{\eta_1})^2 = u^2 - 2u\dot{\eta_1} + \dot{\eta_1}^2 \tag{5.15}$$

In equation (5.15) it can be seen that a negative excitation term corresponding to a damping term is found. By assuming $u < \dot{\eta_1}$ the relative velocity term can then be written as:

$$(u - \dot{\eta_1})(-u + \dot{\eta_1}) = 2u\dot{\eta_1} - (u^2 + \dot{\eta_1}^2) \tag{5.16}$$

Here, a negative excitation term, which corresponds to a damping term, is also observed.

With a current present the undisturbed water particle velocity (u) can become large and give beneficial damping effects so that it may be conservative to not include current, and is an important factor to remember by this simple approach.

5.4 Damping and motion decay

Assuming quadratic damping, the damping force for a one degree of freedom (1DOF) system can be written as:

$$F_D(\dot{x}) = B_1\dot{x} + B_2|\dot{x}|\dot{x} \tag{5.17}$$

Where B_1 is the linear damping, B_2 is the quadratic damping and x is a motion either translatory or angular.

The term quadratic damping is not widely used in classic dynamics, whereas the linear damping force is of large importance with low velocities the quadratic damping force is of more significance for higher velocities where the second term in equation (5.17) may become large. The quadratic damping is of importance for considerations in regards to the analysis model done later in the thesis.

To have some physical meaning to the words linear and quadratic damping one can review "the hydrodynamic problem" as defined in Section 5.1. The radiation damping, i.e. the body's ability to generate waves, can be related to the linear damping. The quadratic damping is related to the drag coefficient in Morison's equation. If one were to linearize the equation of motion one could say that the linear damping contained the drag damping as well as the radiation damping.

In reality damping may not follow this kind of expressions with good approximation. One could of course also talk about damping following polynomials of n-degrees, where n being an unknown number larger than two, or any other mathematical function for that matter. The fact being, is that one approximate physical quantities with mathematical expressions to be able to analyse problems before actually realizing it.

5.4.1 Motion decay

By using equation (5.17) for $F_D(\dot{x})$ in equation (5.1) and dividing by the mass M, the freely floating 1DOF equation of motion can be written as:

$$\ddot{x} + p_1\dot{x} + p_2|\dot{x}|\dot{x} + p_3x = 0 \tag{5.18}$$

Where p_1, p_2 and p_3 are linear damping, quadratic damping and system stiffness divided by M, respectively.

In a decay simulation the analysis of equation (5.18) can be done by the solution of a linear oscillating system and a technique named total equivalent linear damping. For each cycle of oscillation the terms in equation (5.17) is replaced by an equivalent total linear damping requiring that the energy contained in each expression is equal to the other. For more details on the procedure the reader may refer to [16]. The linearized equation of motion can then be written as:

$$\ddot{x} + p\dot{x} + p_3 x = 0 \tag{5.19}$$

Where

$$p = p_1 + \frac{16}{3}\frac{X_i}{T_i}p_2 \tag{5.20}$$

X_i is the amplitude of oscillation and T_D is the freely damped oscillation period.

For measuring damping, the logarithmic decrement is commonly used in the analysis process. The logarithmic decrement can for two successive amplitudes at a time interval T_d be written as:

$$\delta = ln(\frac{X_i}{X_{i+1}}) \tag{5.21}$$

A more common damping measurement is the relative damping which can be expressed in terms of the logarithmic decrement as:

$$\zeta = \frac{\delta}{\sqrt{4\pi^2 + \delta^2}} \tag{5.22}$$

The denominator in equation (5.22) can be approximated as 2π as the decrement is usually small compared to 2π, but that is not done in the following. The relative damping can also be expressed as:

$$\zeta = \frac{p}{p_{cr}} = p\frac{T_e}{4\pi} \tag{5.23}$$

Where T_e is the undamped natural period. Using equation (5.23) and (5.22) the linearized damping can be expressed in terms of the logarithmic decrement as:

$$p = \frac{4\pi}{T_e}\frac{\delta}{\sqrt{4\pi^2 + \delta^2}} \tag{5.24}$$

By fitting equation (5.20) to the measurements in equation (5.24) the linear and quadratic damping coefficients can be estimated. A Matlab script decay.m is written to perform this, and is used for evaluating damping related to the analysis model. The Matlab script can be seen in Appendix A.2.

5.5 Rigid body motions - Key parameters

Presented here is simplified theory important for understanding the rigid body motions of the floating support structure and identifying the key parameters controlling it. The focus is on the support structure and the mooring lines' contribution is in most cases neglected.

5.5.1 Static pitch angle

The static pitch is dominated by the wind thrust on the rotor. The static pitch should be less than a specific value and the following simplified analysis will show how to obtain a relation between the thrust force and hydrostatic forces. Main assumptions for the derivation are:

- Pitch restoring from mooring lines not considered.
- Small rotations, i.e. $sin(\eta_{5s}) \approx \eta_{5s}$ where η_{5s} is the static pitch angle
- z = 0 at the mean water line and z is positive upwards.

As described in Section 4.3 the wind thrust on the rotor can be expressed according to equation (4.12). Assuming the wind thrust constant and taking moment about the mooring line attachment point, the overturning moment due to wind thrust on the support structure can be written as:

$$M_w = T(z_a - z_m) \tag{5.25}$$

Where z_a is the distance between the water line and the center of the rotor and z_m is the distance to the mooring line attachment point. By giving the structure an imaginary pitch rotation the hydrostatic moment counteracting this can be written as:

$$M_h = (\rho_w g I_{wline} + \rho_w g V z_B - m g z_G)\eta_{5s} \tag{5.26}$$

Where ρ_w is the density of water, V is the displaced volume of the structure, m is the mass of the system including mass contribution from the mooring lines and I_{wline} is the second moment of inertia of the water plane. z_B and z_G is the vertical distance of center of buoyancy and center of gravity, respectively.

Equating equations (5.25) and (5.26), neglecting I_{wline} as it has a small contribution with a low water line radius and neglecting the vertical component of the mooring lines, i.e. $\rho_w V = mg$, the static pitch angle can be approximated as:

$$\eta_{5s} \approx \frac{T(z_a - z_m)}{\rho_w g V (z_B - z_G)} \tag{5.27}$$

To keep a low static pitch it is observed that $(z_a - z_m)$, which is the distance between the rotor and the mooring line attachment point, should be as low as possible, while reducing the draft the mooring line attachment point will be moved in a relative position with regards to the base case, thus it is dependent on the draft reduction. The distance $(z_B - z_G)$ which is the distance between the center of buoyancy and center of gravity as well as the buoyancy is also identified as important parameters to keep the static pitch low.

5.5.2 Natural periods

To avoid excessive motions the natural periods should be kept away from most wave periods occurring in the open sea. The most common wave periods in the open seas, i.e. the range of significant wave energy, is between 4 s - 20 s [5]. For practical considerations the natural periods in surge, heave and pitch should be kept over 20 s. When neglecting damping the general expression for eigen period in degree of freedom i is:

$$T_i = 2\pi \sqrt{\frac{M_{ii}}{C_{Hii} + C_{Mii}}} \tag{5.28}$$

For the translatory periods M_{ii} is mass including the body's mass and the added mass. For the angular oscillatory periods, M_{ii} is the moment of inertia of the body's mass and added mass. C_{Hii} is the hydrostatic stiffness and C_{Mii} is the mooring stiffness. Following this reasoning and choosing a vertical center of reference close to the center of gravity, where the motions in surge and pitch are almost uncoupled, the natural periods of the rigid body motions can be derived.

In surge the only stiffness contribution is from the mooring lines, and realizing that from a strip theory approach the added mass can be approximated as $\rho_w V$, the natural period in surge can be written as:

$$T_1 = 2\pi\sqrt{\frac{\rho_w V + A_{11}}{C_{M11}}} \approx 2\pi\sqrt{\frac{2\rho_w V}{C_{M11}}} \tag{5.29}$$

The surge natural period is typically in the matter of minutes and is seen to be controlled by the displaced volume and mooring line stiffness.

Considering the natural period in heave, the added mass in heave can be approximated as a half sphere and higher for the support structure with a heave plate. The restoring stiffness from the mooring lines in heave is of little significance, thus the natural period in heave can be written as:

$$T_3 = 2\pi\sqrt{\frac{\rho_w V + A_{33}}{C_{H33} + C_{M33}}} \approx 2\pi\sqrt{\frac{\rho_w V + A_{33}}{\rho_w g \pi R_{wline}^2}} \tag{5.30}$$

Where R_{wline} is the radius at the water line, and the water line stiffness (C_{H33}) can easily be understood by giving a freely floating body a heave motion and the change in buoyancy will force the body back to equilibrium. The heave natural period provides key parameters, if the volume of the structure decreases, the heave natural period can be increased by reducing the water plane radius and increasing the added mass in heave by the heave plate. The waterline radius is also observed as a key parameter controlling the hydrostatic stiffness in heave.

In pitch one must remember that it is an oscillatory period and that M_{55} will be the moment of inertia contribution referred to the center of gravity, the stiffness will be the same as for the static pitch angle in Section 5.5.1, and the natural period in pitch can be written as:

$$T_5 = 2\pi\sqrt{\frac{I_{55} + A_{55}}{C_{H55} + C_{M55}}} \approx 2\pi\sqrt{\frac{I_{55} + A_{55}}{\rho_w g V (z_B - z_G)}} \tag{5.31}$$

Where I_{55} is the dry mass moment of inertia. Here a conflicting key parameter is observed, by lowering the hydrostatic stiffness, thus increasing the natural period in pitch, the static pitch is increased. Considering the mass moment of inertia the tower is not to be changed, this means dimensions for the heave plate will be key parameters to keep the pitch natural period larger than the wave periods.

5.5.3 Mathieu instability - coupled heave/pitch

A coupling between heave and pitch may cause an instability effect, which does not explicitly provide any new key parameters, but is important for the closeness of the natural periods in heave and pitch. This instability effect is much discussed in the literature, and the reader may refer to e.g. [3] for a more thorough discussion. Here, only main results are stated.

Mooring line stiffness, wave excitation, surge coupling and damping effects are disregarded. The Mathieu equation on general form can be written as [3]:

$$\ddot{\eta_5} + \bar{\omega}^2(1 - \varepsilon cos(\omega_3 t))\eta_5 = 0 \tag{5.32}$$

Where physically ε represents the change in pitch restoring stiffness ($\Delta C_{55}/C_{55}$) which is influenced by the heave motion. $\bar{\omega}$ represents the relative frequency of this change in stiffness (ω_5/ω_3).

For certain values of the pairs $(\varepsilon, \bar{\omega})$, equation (5.32) has unstable solutions and can be represented in a stability diagram, see Figure 5.2.

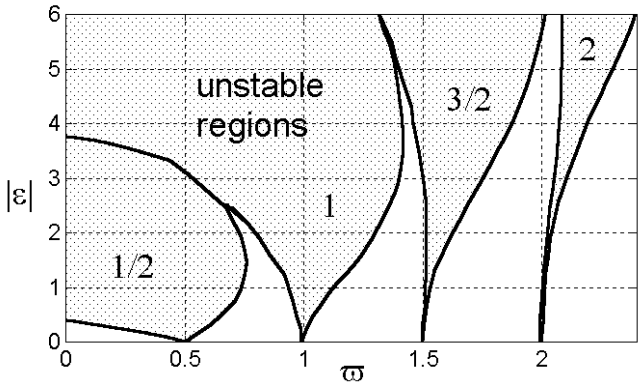

Figure 5.2: Mathieu instability diagram [3].

It is seen from Figure 5.2 that there exist instabilities even where $\varepsilon \to 0$. Considering the lowest angular frequency ($\bar{\omega} = 0.5$) in the diagram where $\varepsilon = 0$. In an instability context this corresponds to heave motion with a period half the natural period in pitch which can happen in two cases:

- The natural period in heave is half the natural period in pitch.
- There is considerable wave energy half the natural period in pitch.

For the Hywind system the latter of these two is likely to occur and is further studied in Section 9.3. Considering the second instability region $\bar{\omega} = 1$, which represents a natural period in heave equal to the natural period in pitch, an important factor when changing parameters is to keep the two natural periods apart to avoid this instability.

Inclusion of damping, excitation, mooring stiffness and coupling between pitch and surge will change the curves separating the different unstable regions in Figure 5.2, but unstable solutions still occur for periods close to the critical periods [3].

5.5.4 Summary key parameters

The key parameters extracted from the previous reasoning and influence on some of the properties discussed can be summarized as follows:

- **Diameter at waterline**: Natural period in heave, pitch restoring stiffness(C_{55}).
- **Diameter submerged body**: Displacement (Volume), pitch restoring stiffness(C_{55}).
- **Diameter heave plate**: Keep a low center of gravity, natural period in heave(A_{33}).
- **Thickness heave plate**: Keep a low center of gravity.
- **Draft hull**: Shallower water depths, displacement, pitch restoring moment(C_{55}).

Also, with reference to Section 5.5.3, the natural period in pitch and heave should be kept apart.

6 Method - Analysis Techniques and Modeling

Described here are the computer codes used for the analyses, modeling properties and fatigue calculation basis. To be able to include wind loads in ULS and FLS time domain analyses two programs are coupled together, the coupling is also described in the following.

6.1 SIMO/TDHMILL

Simulation of Marine Operations (SIMO) is a program developed by MARINTEK, it is a time domain simulation program for multi body systems. SIMO models all structures as rigid bodies with a given number of degrees of freedom, thus only rigid body movement is obtained. This makes it unsuitable for evaluating internal structural forces, but it has a valuable feature that can be used to include force generation from an external source through dynamic link libraries (DLL). This is utilized to generate coupled wind loads and is explained in the following.

6.1.1 TDHMILL

TDHMILL[1] is a simplified computer tool that generates thrust from a wind turbine rotor onto the nacelle. It is actualized through a DLL and communicates with SIMO. The numerical model of the thrust is based on one-dimensional momentum theory (see Section 4.3), and utilize coefficients for thrust tabulated as a function of relative velocity between the rotor and the wind. Wind time series are generated internally in TDHMILL and as mentioned in Section 4.2 the Kaimal spectrum is used.

The thrust force as defined in the user manual [17] is a slight rewrite of the thrust force found in Section 4.3 by introducing the relative velocity (U_{rel}) between the wind and the rotor hub and is written as:

$$T(t) = KC_T(U_{rel})U_{rel}(t)^2 \tag{6.1}$$

Where the thrust constant K is defined as:

$$K = \frac{1}{2}\rho_a \pi R^2 \tag{6.2}$$

R is the rotor radius and C_T is a thrust coefficient tabulated as a function of U_{rel}, the tabulated values are supplied in the input files from Statoil. The thrust coefficient is dependent on rotor blade pitch angle and tip-speed ratio and the values are usually found from simulations [15].

Translational and angular velocity of the SIMO body at a time step is computed by SIMO before the thrust force to be used for advancing to the next time step is computed

[1]The newest version which is utilized in the thesis is named THDMILL3D, but it is referred to as TDHMILL in the thesis.

[17], this information is used to compute the relative velocity based on transforming the velocities between the TDHMILL local coordinate system and the global SIMO coordinate system.

When the rotor is running with a constant angular speed, gyro moments will be induced in the hub if the orientation of the rotor plane is altered when the floating structure moves, further details are for the interested reader explained in the user manual [17].

An important factor with TDHMILL is that it includes a notch filter to filter out pitch velocity at a given frequency band. The purpose of the notch filter is to simulate a rotor blade-pitch control system which strive for active damping in pitch motion, the importance of this is further discussed in Section 9.6. The filtered pitch velocity is calculated in the time domain at each time step and it is important to notice that it is the pitch motion that is filtered, thus the wind velocity may include resonant frequencies in the relative velocity (U_{rel}).

The notch filter is determined by three parameters, which is the wanted frequency (pitch natural frequency) and two parameters that determines steepness and broadness (ζ_N,ζ_D). In Figure 6.1 a plot of the notch filter with different ζ_N and ζ_D factors are given. To avoid filtering out wind induced pitch motions at other frequencies than the pitch natural frequency the two parameters $\zeta_N = 0.001$ and $\zeta_D = 0.2$ are utilized which gives a satisfying frequency band. The significance of the parameter broadness and steepness is also investigated in Section 9.6.3.

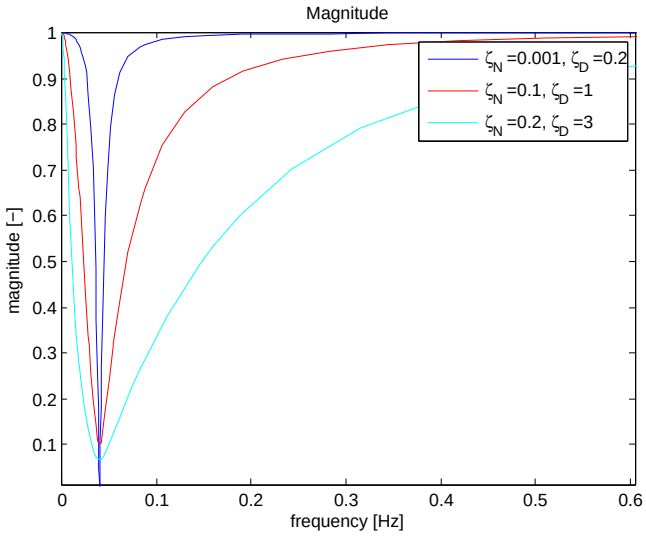

Figure 6.1: Notch filter parameters [18]

6.2 RIFLEX

Flexible Riser System Analysis Program (RIFLEX) is a *finite element method* (FEM) program for static and dynamic analysis of slender marine structures, and computes the structural response as global deformations and stress resultants.

In the non-linear analyses performed the hydrodynamic loads are calculated at the actual displaced position of the structure and *true Newton-Raphson* equilibrium iterations are carried out at each time step. All geometry is modeled in RIFLEX and further explained in the following

6.2.1 RIFLEX Analysis model

The analysis model of the floating wind turbine and mooring system is modeled using three dimensional elements. The floating structure is modeled with beam elements described in a *co-rotated ghost* formulation. The mooring system is modeled with bar elements described in a *total Lagrangian* formulation. This is combined with linearized *Green strain*, thus infinitesimal strains are assumed. The reader may refer to the RIFLEX theory manual [19] for more details.

The masses of the rotor and blades are not explicitly modeled but lumped as masses to the tower top. The ballast is added as distributed mass to the lower concrete section of the structure, and distributed according to estimated height of the ballast. A plot of the base case analysis model represented by its element nodes can be seen in Figure 6.2.

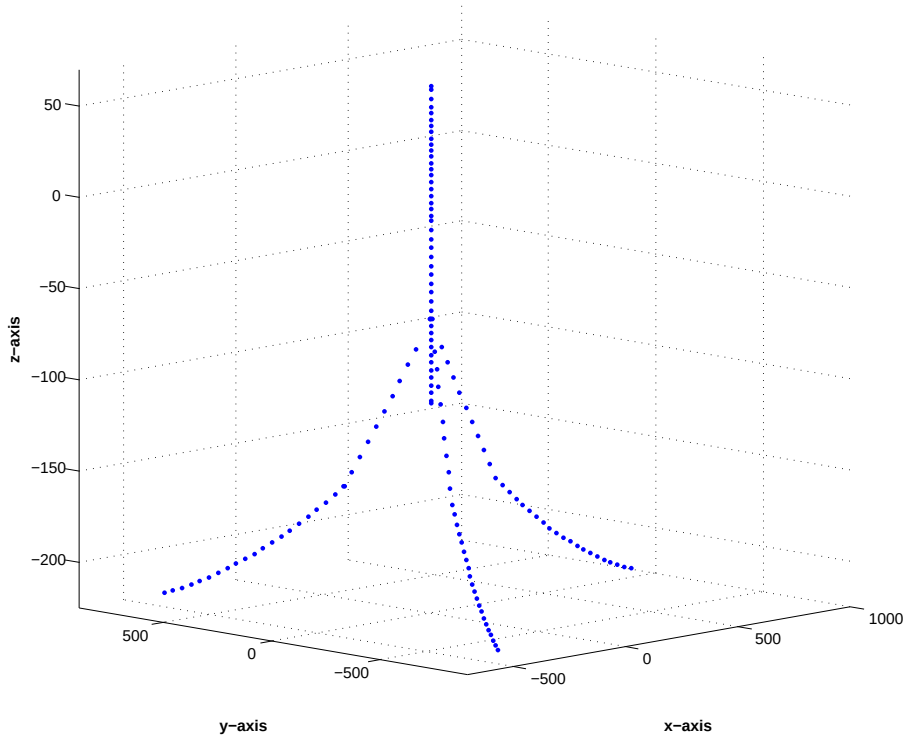

Figure 6.2: Base case analysis model, plot of element nodes.

An important factor to mention is that due to a difficulty of acquiring equilibrium in the static analysis, which is performed prior to the dynamic analysis, the node at the bottom of the structure is fixed throughout the static analysis in a position of estimated equilibrium position, and released at the first time step in the dynamic analysis. The difference in estimated equilibrium and actual equilibrium is small, and due to linearized damping the transient response is quickly damped out. The reader may refer to Section 9.2 for further clarifications.

6.3 SIMO/RIFLEX coupling

The coupling between the two analysis programs SIMO and RIFLEX, provides the environmental conditions (current, wave and wind thrust) represented by SIMO and the FEM modeling represented by RIFLEX. The coupling is run by a series of command prompts for the two different analysis programs in the following order:

RIFLEX inpmod → SIMO stamod → RIFLEX stamod → SIMO dynmod → RIFLEX dynmod.

For more information on the different modules the reader may refer to the analysis program's respective user manuals [20, 21].

Running these modules can be done by e.g. command prompts and manually setting values such as seed numbers for generation of waves. For the analyst's convenience, both programs come with the possibility to generate macro files for these internal settings in the programs.

In the work with the thesis the author has created a batch script to run the different modules in the coupling, as well as checking for possible unsuccessful completions of the RIFLEX modules. The batch script can be seen in Appendix B. The developed batch script also makes it easier to run more analyses sequentially or in parallel, and the script has proven as an invaluable tool during the thesis work.

6.4 Excel sheets for establishment of structural properties

Excel sheets developed at Statoil for the Hywind concept were acquired, these excel sheets contains structural geometry and mass properties for both the wind turbine structure and mooring lines. They also contain design rules developed for floating wind turbines, in terms of certain geometry properties with the tower and transition pieces. An important design rule that will be enforced due to the change in parameters in this thesis, is the amount of ballast needed for the mean water line to be at the expected position.

The waterline diameter, which is a key parameters found in Section 5.5, can not be changed when changing the parameters of the support structure. The reason for this is a design rule for the tower, where the waterline diameter controls the diameter of the waterline part of the tower, increasing the waterline diameter will give an overall increase in tower diameter and thus redesign the tower.

To establish the structural geometry and properties in RIFLEX a Matlab script developed by Tor David Hanson was acquired, it utilizes the information in the excel sheets to write RIFLEX model files. As the new concept (heave plate) studied deviate somewhat from the original Hywind concept, better estimates for added mass are acquired in Chapter 7 and the new analysis models are made to reflect this.

6.5 Fatigue calculations

For structures under cycling loading fatigue may be an important factor to account for in the analysis and design process. For onshore wind turbines fatigue calculations are of outmost importance and wind turbines are often called the "perfect fatigue machines".

For the Hywind concept, which has cyclic loading in terms of wind and waves, fatigue calculations have been an integral part of the design process. Therefore in terms of structural stresses, focus is devoted to fatigue calculations based on the bending moment at the mean waterline. As mentioned earlier the waterline diameter is not changed, thus the effect of changes to the structure in terms of fatigue is best "measured" at the mean waterline.

The fatigue lifetime estimates are based on "DNV Recommended Practice: Fatigue Design of Offshore Steel Structures" [22] with a stress-cycle (S-N) curve for steel structures in seawater with cathodic protection. The structure has welded connection corresponding to the detail category D [15], to utilize a higher category, which gives longer fatigue life, more thorough inspections and detail work must be done to the welds. Another approach that can increase which S-N curve one can use is testing of the concept, and the Hywind

test program outside Karmøy may produce data that gives the analyst evidence to use higher S-N curves. The S-N curve is given in the DNV Recommended Practice as:

$$log(N) = log(\bar{a}) - mlog(\Delta\sigma) \tag{6.3}$$

Where log is the base-10 logarithm, N is the predicted number of cycles to failure for stress range $\Delta\sigma$, m is the negative inverse slope of the S-N curve and $log(\bar{a})$ is the intercept of the log N-axis by the S-N curve.

This is combined with the assumption of a linear cumulative damage (*Palmgren-Miner rule*), where the damage for one analysis can be calculated as:

$$D = \sum_{i=1}^{k} \frac{n_i}{N_i} \tag{6.4}$$

Where n_i is number of stress cycles in stress block i and N_i is the number of cycles to failure at a constant stress range $\Delta\sigma_i$ from equation (6.3).

To find the long term fatigue life, each damage from analyses with different environmental conditions is multiplied with its relative probability of occurrence, and a lifetime estimate based on 50-year scatter tables is established by the sum of these. The reader may refer to Section 8.1 for the environmental conditions and their relative probability.

To find stress ranges the author utilizes *rainflow counting* which is a common cycle counting method for irregular loading. The WAFO-Toolbox [23] for Matlab has a built in rainflow cycle counting algorithm which is used in combination with a developed Matlab script. The developed Matlab script can be reviewed in Appendix A.3.

The interested reader may refer to the "ASTM Standard Practices for Cycle Counting in Fatigue Analysis" [24] for examples on the rainflow counting algorithm and other cycle counting algorithms.

6.6 WAMIT

WAMIT is a state of the art wave interaction analysis program. It is based on the linear and second-order potential theory for analyzing of floating or submerged bodies in the presence of ocean waves. By linearized potential theory it is meant that the free-surface condition is linearized, see equation (3.4).

This program is used for an evaluation of the change in added mass for changes to the analysis model compared to the strip theory approach used in RIFLEX. The panel method is used to solve for the velocity potential and fluid pressure on the submerged surfaces of the bodies. Solutions are carried out for the radiation problem, i.e. the added mass, pressure and fluid velocity is induced by forced motions of the body. These solutions are then used in WAMIT to obtain the added mass relevant for the evaluation carried out in Chapter 7.

Analysis files used to evaluate Hywind were obtained, the geometry was changed to reflect the studies carried out on added mass.

7 WAMIT Analyses - Added Mass

To verify and study the added mass, analyses are carried out in the panel program WAMIT and compared with the strip theory approach used in RIFLEX.

7.1 WAMIT Configurations

Three different cylinder configurations are presented here, their dimensions can be seen in Table 7.1. The W1 configuration is a cylinder without the heave plate.

Dimensions	W1	W2	W3
Cylinder draft [m]	80	80	80
Cylinder diam. (D_c) [m]	9.5	9.5	9.5
Plate thickness [m]	3	3	3
Plate diam. (D_d) [m]	9.5	14.0	18.5
Volume [m^3]	5659	5908	6254

Table 7.1: Dimensions for WAMIT configurations, plate diameter is varied.

Since the configurations have symmetrical properties only one quarter is modeled, see Figure 7.1, this also means that $A_{11} = A_{22}$, $A_{15} = A_{51} = -A_{24} = -A_{42}$ and $A_{55} = A_{44}$. That the symmetrical properties are present in the WAMIT results are confirmed, and results are presented only for one of each identical value. The results presented in the following are for frequency $f = 0.05\,\text{Hz}$, and yaw added mass A_{66} is for all analyses approximately zero as one would expect.

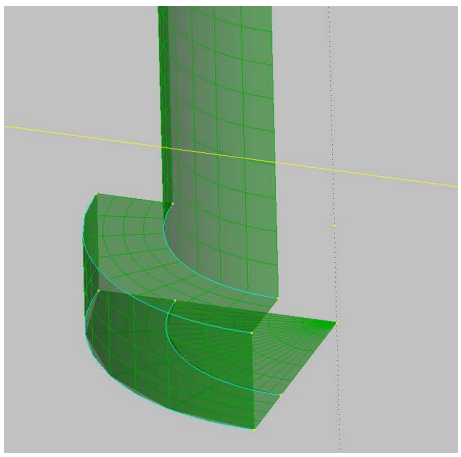

Figure 7.1: WAMIT analysis model, plate configuration.

7.2 W1: Circular cylinder

The W1 analysis is run on a circular cylinder which has less end effects, i.e. three-dimensional effects are smaller at the bottom. The results can be seen in Table 7.2.

Added mass	WAMIT (W)	Strip theory (S)	Difference W-S
A_{11} [kg]	5.63×10^{06}	5.80×10^{06}	2.9 %
A_{15} [kg m]	-2.18×10^{08}	-2.32×10^{08}	6.6 %
A_{33} [kg]	2.26×10^{05}	2.29×10^{05}	1.6 %
A_{55} [kg m^2]	1.11×10^{10}	1.24×10^{10}	11.4 %

Table 7.2: WAMIT analysis, configuration W1.

What can be seen from Table 7.2 is that strip theory gives acceptable results for the added mass. The difference is in the edge and free surface effect that is not accounted for when calculating the added mass by the two-dimensional strips. The edge effect can be accounted for by applying a reduction factor for segments near edges, i.e. equation (5.3) can be written as:

$$A_{11}^{2D} = \alpha \rho_w \frac{\pi D^2}{4} \tag{7.1}$$

Where α is a factor less than one. This will be studied further with the other configurations which has larger end effects.

7.3 W2: Heave plate

The W2 analysis has a heave plate with a diameter 1.47 times larger than the bare cylinder. The results can be seen in Table 7.3.

Added mass	WAMIT (W)	Strip theory (S)	Difference W-S	Difference W1-W*
A_{11} [kg]	5.76×10^{06}	6.06×10^{06}	5.1 %	2 %
A_{15} [kg m]	-2.28×10^{08}	-2.52×10^{08}	10.6 %	5 %
A_{33} [kg]	7.72×10^{05}	7.32×10^{05}	-5.2 %	242 %
A_{55} [kg m^2]	1.19×10^{10}	1.40×10^{10}	17.1 %	7 %

Table 7.3: WAMIT analysis, configuration W2. *Difference in WAMIT result in configurations W1 and W2

The heave added mass in Table 7.3 is calculated by equation (5.11), which is the expression obtained from the article on heave suppression by Longbin et al. [2], it is observed that it gives a reasonable estimate for the heave added mass. If one were to use equation (5.10), which is the intersection of the sphere with the cylinder, to calculate the added mass in heave a value of 1.03×10^{06} kg is obtained, which is 33 % larger than obtained in WAMIT and overestimates the heave added mass significantly.

The other estimates in added mass obtained by strip theory is also increasing in difference with larger end effects. By applying a factor $\alpha = 0.4$ for the 3 m long plate segment the differences are reduced which is shown in Table 7.4. It should also be noted that the free surface effect also contributes to the difference in added mass, but that is not accounted for in the reduction here.

Added mass	WAMIT (W)	Strip theory (S)	Difference W-S
A_{11} [kg]	5.76×10^{06}	5.77×10^{06}	0.1 %
A_{15} [kg m]	-2.28×10^{08}	-2.30×10^{08}	0.8 %
A_{55} [kg m^2]	1.19×10^{10}	1.22×10^{10}	2.4 %

Table 7.4: WAMIT analysis, configuration W2. $\alpha = 0.4$

7.4 W3: Heave plate

The W3 analysis has a heave plate with a diameter 1.95 times larger than the bare cylinder. The results can be seen in Table 7.5.

Added mass	WAMIT (W)	Strip theory (S)	Difference W-S	Difference W1-W*
A_{11} [kg]	5.86×10^{06}	6.41×10^{06}	9.3 %	4 %
A_{15} [kg m]	-2.36×10^{08}	-2.80×10^{08}	18.5 %	9 %
A_{33} [kg]	2.03×10^{06}	2.02×10^{06}	-0.28 %	799 %
A_{55} [kg m^2]	1.26×10^{10}	1.61×10^{10}	27.8 %	14 %

Table 7.5: WAMIT analysis, configuration W3. *Difference in WAMIT result in configurations W1 and W3

The heave added mass estimate is also in Table 7.5 calculated with the expression by Longbin et al. [2], and is by these few analyses in good agreement with the WAMIT analyses. Using equation (5.10) to calculate the heave added mass gives a value 37% larger than the WAMIT result.

It should also be observed that the added mass in heave is significantly larger from the bare cylinder configuration, which can be used to increase the natural period in heave, see equation (5.30) for the natural period in heave.

The other estimates in added mass can be reduced to the same difference as for the previous configuration by applying a factor $\alpha = 0.35$, this also shows that for larger D_d/L ratios, where L is the plate segment length, three-dimensional effects are larger and without a reduction the added mass may be largely overestimated. This is also in agreement with experiments conducted on cylinders with different diameter to length ratios, where results from experiments can be found in e.g. [11].

7.5 Summary and frequency dependence of surge added mass

The added mass that was presented in the preceding was for low frequencies which means higher periods, and by the dispersion relation (see equation (3.7)) longer wavelengths.

All WAMIT analyses were run over a broad specter of wave frequencies, and in the range of significant wave energy ($f = 0.05\,\text{Hz}$ to $f = 0.2\,\text{Hz}$) the maximum difference in added mass for all configurations between the two frequencies is 5 %. The maximum difference is found for the added mass in surge/sway. This confirms the low frequency dependence of the added mass for slender circular bodies also with the plate configuration. It should also be noted that the heave added mass has a difference of maximum 0.5 % for the two frequencies and for all configurations, which insinuate it is only an end effect and not influenced by the free surface condition (which is the reason for the frequency dependence).

To see more of the influence of the frequency dependence of added mass, the surge normalized added mass, i.e. the added mass divided by the structure's displaced mass,

for all configurations is plotted for frequencies $f = 0.025\,\text{Hz}$ to $f = 0.33\,\text{Hz}$, see Figure 7.2. To clarify any possible confusions, these are the WAMIT results for added mass as the strip theory estimates are not a function of frequency.

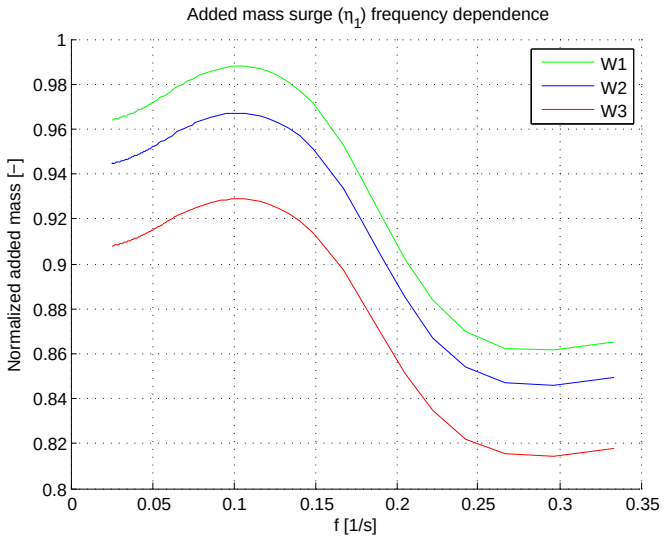

Figure 7.2: Normalized added mass in surge for all configurations.

The surge normalized added mass is on average reduced when introducing the heave plate, this is also clear from Figure 7.2. The frequency dependence has a similar trend for all configurations, and a negligible difference is seen when introducing the heave plate. The frequency dependence can also be related to the general "limit" which is usually set on the slender body approximation, see Figure 7.3. The slender body "limit" is usually for a circular cylinder set to $\lambda/D_c > 5$ where λ is the wave length.

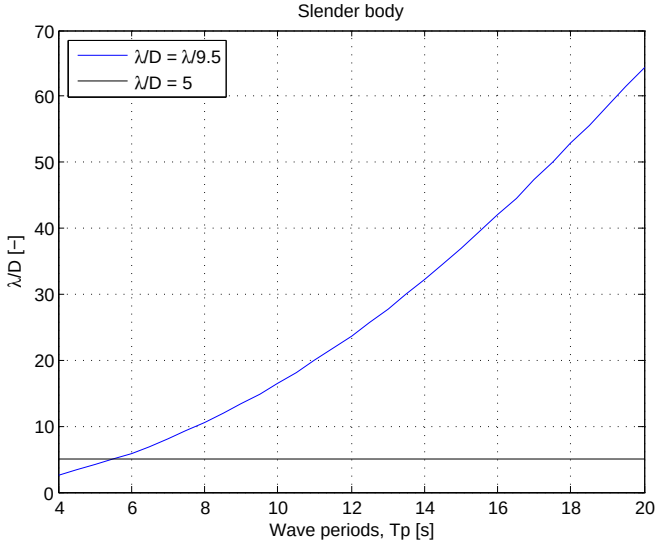

Figure 7.3: Slender body approximation, diameter 9.5 m

What can be concluded from the the investigations carried out in this chapter is that the heave added mass can be estimated from equation (5.11) which is the expression by Longbin et al. [2]. Using equation (5.10), which is the intersection of the sphere with the

cylinder, for estimation of the heave added mass largely overestimates it and is therefore deemed as inappropriate to use.

The heave plate introduces a reduction in surge added mass by strip theory for the segment containing the heave plate, which based on these studies is set to $\alpha = 0.7$ for further analyses in RIFLEX. The reason for not using a lower alpha value is that the bare cylinder configuration in RIFLEX utilizes no reduction for end effects, and thus a large reduction in added mass at the end for the heave plate configuration will make the analysis model design different. The reduction $\alpha = 0.7$ also gives the heave plate configurations the same difference between WAMIT results and strip theory as for the bare cylinder configuration (not shown). Frequency dependence is also seen as insignificant at the low frequencies where the largest wave energy resides.

8 Environmental Conditions

The environmental conditions presented in this chapter are based on the Hywind meteorological and oceanographic (metocean) design basis [25]. The metocean data presented is site specific for the Hywind location about 10 km outside Karmøy where the water depth is approximately 220 m. Different water depths have different locations, and will require further investigations into the site specific metocean data.

For shallower waters the driving factor in terms of environmental loads may not be the wave induced loads but the wind induced loads. Since the author does not have other site specific data for shallower waters, and also to have a better correspondence between the concepts, the environmental loads for all cases are based on the Hywind metocean data.

The I_{ref} mentioned in Section 4.2 is set to 0.12, which represents the category for lower turbulence characteristic [8]. Due to the low surface roughness of the sea one can expect that offshore locations have less turbulence than onshore locations and it is deemed reasonable to use the lowest reference value. In the following all wind velocities are given at hub height if nothing else is mentioned.

What also should be mentioned is that for a certain environmental state, different seed numbers (the randomness in the simulation) should be used for the wind and waves to check for realization dependence. This is not done in the thesis to limit the amount of analyses run.

8.1 Fatigue limit state

For an offshore floating wind turbine where the loading is periodic in terms of both wind and waves, the governing design criteria has been towards fatigue life. Therefore a larger number of environmental cases are made for the fatigue limit state (FLS). Current is for the fatigue limit state not included because of limited current data, as well as possible beneficial damping effects in surge and pitch motion, due to the relative velocity quadratic drag terms, see Section 5.3.3.

The environmental cases, hereby referred to as load cases, are based on simulated scatter tables for waves and wind, which represent long term statistics over a period of 50 years. The simulated scatter tables are from the Hywind metocean data. Scatter tables gives a sample distribution, which can be thought of as observations per parameter over longer time. There are two separate scatter tables, one for significant wave height (H_s) and spectral peak period (T_p), and one for significant wave height (H_s) and mean wind speed at hub height (U_{mean}). The two scatter tables are joined through the significant wave height, which means that the mean wind speed is assumed uncorrelated with the spectral peak period. Thus the load cases are based on significant wave height.

If one first consider the scatter table for H_s and T_p, the significant wave height in the scatter table has a spacing of size one (0-1, 1-2, etc.). For each H_s the upper limit in the spacing is used, which also makes the load cases conservative. For any H_s there is a number of possible T_p, each with different probability. To limit the number of load cases T_p is weighted for each H_s.

The weighting method can be written as:

$$T_p = \frac{\sum n_i T_i}{\sum n_i} \tag{8.1}$$

Where n_i is the number of samples for each spectral peak period T_i in the scatter table.

The weighting method can be thought of as finding the most probable spectral peak period for each significant wave height. The same strategy is utilized for the mean wind speed scatter table. The driving factor for the rigid body movements as well as the structural stresses is assumed as H_s, thus the probability for each load case is based on the probability for H_s occurring within the 50 years the scatter table covers. It should also be noted that there is little or no samples for $T_p > 20\,\text{s}$, which gives more validity of using the weighting method in terms of excitation periods near the natural periods of the rigid body movements.

The discretization in the mean wind scatter table is different, where a spacing of 0.5 m is utilized for H_s starting at 0.25 m. Thus to find U_{mean} for each H_s the closest values are linearly interpolated to the given H_s. The load cases are limited with a maximum H_s of 10 m, the reason for this is that the mean wind samples are somewhat scattered after a H_s of 10 m, which implies a lower statistical trend. There is also a low number of samples, especially for the mean wind scatter table after a H_s of 10 m, this implies that the probability for occurrence is low, but it does not say that the probability is zero which is an important fact to remember, their influence is however neglected for the load cases calculated. The sample distribution can be seen in Figure 8.1.

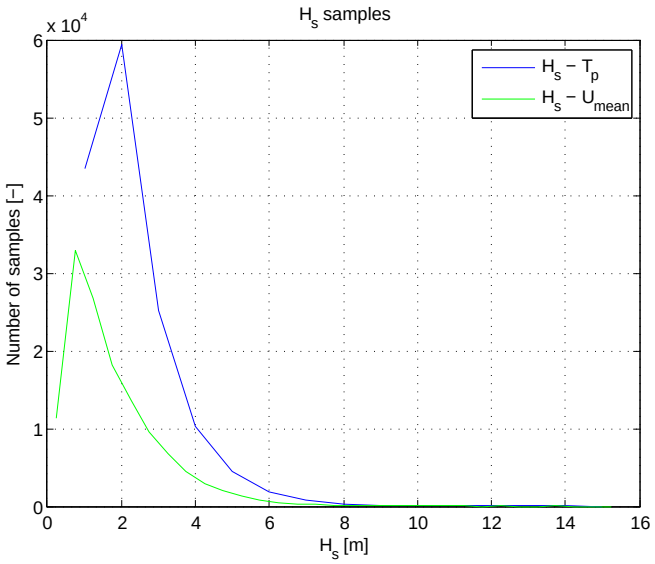

Figure 8.1: H_s samples for T_p and U_{mean}, both weighted.

Based on the procedure described in the preceding, the FLS load cases can be presented based on the significant wave height H_s, the weighted spectral peak period T_p as defined in equation (8.1), the mean wind velocity U_{mean} which is based on the same procedure as the spectral peak period, and the probability of H_s occurring which is based on the wave scatter table. The load cases are presented in Table 8.1.

Load case	H_s [m]	T_p [s]	U_{mean} [m/s]	P(H_s)
FLS1	1	7.8	6.7	0.2978
FLS2	2	8.8	10.7	0.4062
FLS3	3	9.6	14.0	0.1730
FLS4	4	10.3	17.3	0.0709
FLS5	5	11.0	19.6	0.0310
FLS6	6	11.6	22.0	0.0129
FLS7	7	12.2	23.9	0.0052
FLS8	8	12.8	25.7	0.0020
FLS9	9	13.4	28.1	0.0008
FLS10	10	14.0	28.6	0.0004

Table 8.1: Load cases, fatigue limit state.

8.2 Ultimate limit state

The ultimate limit state (ULS) is carried out to check maximum structural stresses in the wind turbine as well as compare rigid body movements in an extreme sea state. The ULS cases are based on a combination of 50-year conditions for waves and wind, as well as a 10-year condition for current. In terms of annual probability of exceedance, which is defined as [25]:

$$q = 1 - e^{(-\frac{T}{R})} \tag{8.2}$$

Where T = 1 year and R is the R-year condition. It can be seen that q is approximately 0.1 and 0.02 for 10-year and 50-year conditions, respectively.

8.2.1 ULS Load cases

The 50-year condition for the waves is based on probability contour lines of H_s and T_p, see Figure 8.2. The contour lines are are defined as lines with constant probability density [25].

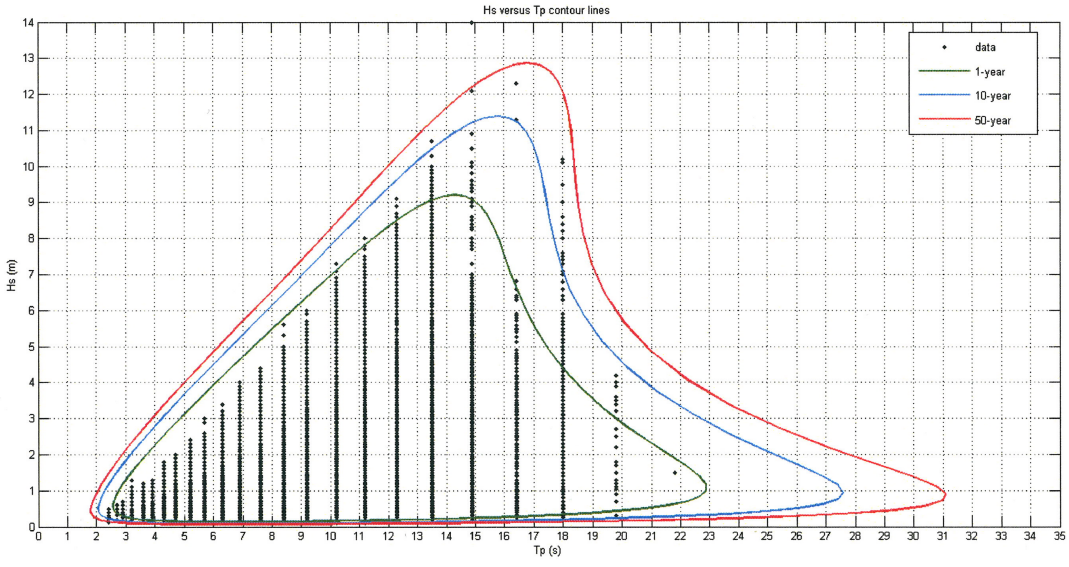

Figure 8.2: Probability contour lines of H_s - T_p [25].

What can be seen from Figure 8.2 is that the contour lines show a protruding behavior for the higher periods, periods which as will be shown in the analyses chapters are within the natural periods of the rigid body movements. As there are no actual data within these periods, and the significant wave height is low in this area, the wave load cases are based on the highest significant wave height within the 50-year contour line. See Table 8.2, where also the mean wind velocity based on the metocean data is presented.

Load case	H_s [m]	T_p [s]	U_{mean} [m/s]
ULS1	12.5	16	48
ULS2	12.8	16.5	48
ULS3	13	17	48
ULS4	12.5	17.5	48

Table 8.2: Load cases, ultimate limit state. See Table 8.3 for current

The 10-year current combined with all ULS cases in Table 8.2, is obtained in the Hywind metocean data report by assuming a current profile similar to the current profile at the Troll Field, where data from measurements are available. The current velocity with depth can be seen in Table 8.3

Depth [m]	Current velocity [m/s]
3	1.59
25	1.14
50	1.06
100	0.72
100	0.68

Table 8.3: Current velocity with depth. Combined with each load case in Table 8.2

8.2.2 Wind load in ULS condition

The wind load induced in the ULS condition requires some more attention. When the wind turbine is experiencing environmental conditions at this magnitude the turbine will be shut down [15], thus the wind induced load on the tower will be the significant part of the wind induced load. To be able to include this by the tools that are at hand, i.e. THDMILL which simulates the wind load as a point load, some simplifications have to be made.

The tower has a varying diameter from 6 m at the mean water lever to 2.4 m at the tower top and the tower height, when excluding the turbine is, 62 m. See Figure C.1 in the appendix for more information on the dimensions. By using the data from the analysis model an average diameter is found as $D_{avg} = 4\,\text{m}$. The specific constants and expressions in the following reasoning are obtained from the book "Fluid mechanics" by F. M. White [26] and Reynolds number can for this specific circular cylinder be written as:

$$Re = \frac{D_{avg}U_{mean}}{\nu} = \frac{4m \times 48m/s}{1.33 \times 10^{-5}m^2/s} = 1.44 \times 10^7 \tag{8.3}$$

Where U_{mean} is the mean wind velocity from the ULS cases and ν is the kinematic viscosity for air at a temperature of 0 °C. By using a graph for smooth circular cylinders [26] a drag coefficient $C_D = 0.7$ is found from the specific Reynolds number. The definition of a drag force can be written as:

$$F_D = \frac{1}{2}C_D\rho_a U^2 A \tag{8.4}$$

Where ρ_a is the density of air, A is here the frontal area of the circular cylinder.

By setting equation (8.4) equal to the thrust force derived earlier in equation (4.12), an expression for what is here named an equivalent radius can be derived:

$$R_{eqv} = \sqrt{\frac{C_D A}{C_T \pi}} = \sqrt{\frac{0.7 \times (62m \times 4m)}{1 \times \pi}} = 7.43m \tag{8.5}$$

Where the thrust coefficient C_T is set to 1, as it is user defined in TDHMILL.

There is one more question that needs to be answered before one has the information needed for this simplified approach, i.e. the action point of the point load. There is mainly two things influencing this, the fact that the tower varies in diameter with height and that the mean wind velocity varies with height, see Figure 4.2 for the mean wind velocity.

Since this is already a simplified approach, and the previous mentioned factors will make most parameters height dependent (drag, diameter and wind velocity), the wind velocity and diameter is assumed constant over height, and the loading is as a consequence constant over height. Thus, the resultant force is set to a convenient height at 32 m which is half of the tower height.

8.3 Simulation time

For onshore wind turbines it is ordinary to perform several 10 minute time-domain simulations to obtain statistical reliability in the estimates of characteristic loads.

For offshore structures the duration of the sea states governs the simulation length, the duration of the sea states considered in this chapter are 3 hours and to obtain reliable results in a statistical point of view, i.e. one want the number of samples to be large so characteristic response is more certain, the simulation length for all cases are 3 hours. This also means that the wind and current is assumed to be stationary within the 3 hours, which is considered acceptable as it will be conservative keeping them at their upper limits while the waves generate more statistical data.

For all analyses, if nothing else is mentioned, 400 s in the beginning of each time series are removed for transient effects.

8.4 Unidirectional loading

The environmental load cases will be applied unidirectional, i.e. all external conditions are from the same direction. This is in many cases the worst possible loading condition, but not necessarily for all. When e.g. current gives higher damping effects in one direction and the wind and wave loads are from another, the loss of damping may induce larger loads to the structure as well as larger body movements. These kind of effects are not studied, but what is worth remembering is that for a complete study, all possible (within reasonable probabilities) loading directions should be applied.

9 Base Case Analyses

To be able to understand changes to the concept as well as having data for comparisons, studies on the base case are carried out. The techniques for the analyses are also more thoroughly discussed for the studies on the base case, and in such a way that the reader may have a better understanding on how the procedures in the analyses are. Complete geometry and mass distribution for the base case analysis model is presented in Appendix C.1.

9.1 Mooring system

The focus of this thesis is as mentioned earlier not on the mooring system. To be able to find the theoretical natural period in surge and sway, as well as understanding aspects about the mooring system, analyses are carried out.

There are different methods and analysis techniques for finding the mooring lines' contribution to the system stiffness, here a quasi-static approach has been utilized. Being quasi-static equation (5.1) reduces to:

$$\{F_C(\eta)\} = \{F(t)\} \tag{9.1}$$

Where in this case $\{F(t)\}$ is a ramp force increased slowly so that the velocity and acceleration terms in equation (5.1) are negligible.

For all analyses herein the ramp force is set to $0.1\,\mathrm{kN\,s^{-1}}$ and applied at the mooring line attachment point for the base case. The ramp force is applied for 8000 s.

9.1.1 Mooring system: Expected behavior

To verify that the mooring system behaves in an expected behavior, an analysis is run with all degree of freedom free and the ramp force applied in surge. In Figure 9.1 the time series plot can be seen.

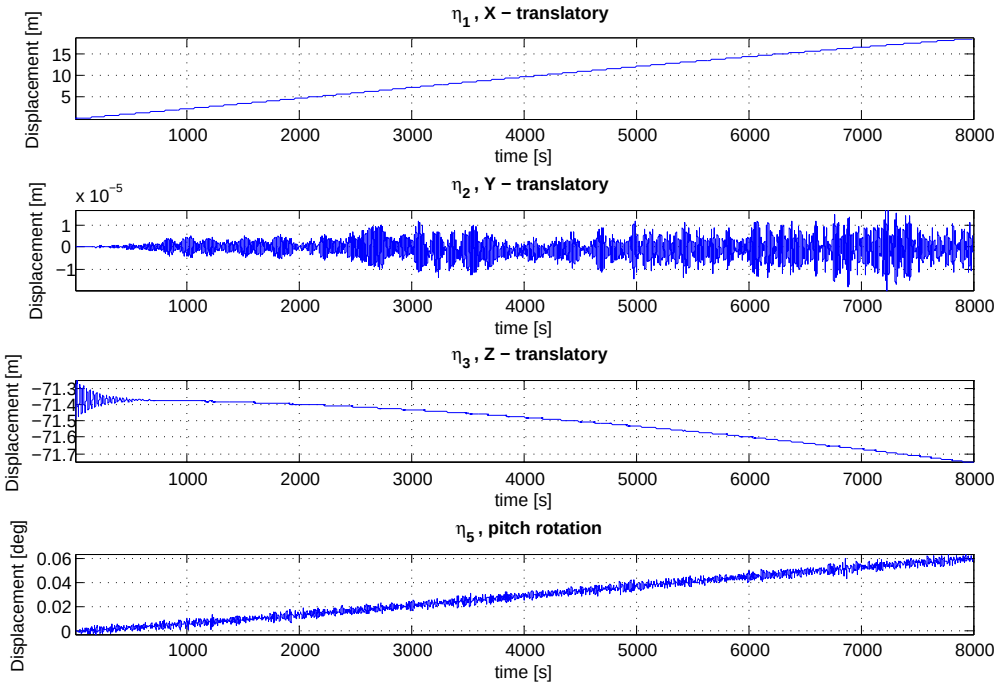

Figure 9.1: Surge displacement time series

As seen from Figure 9.1 the motion in surge seems quite linear by just looking at the displacement plot. What is also seen is that the motions in sway is practically zero, which is expected and reassuring since the mooring lines have a 120° spacing and one of the mooring lines has it center in the surge direction, which makes the other two symmetrical with regards to the displacement in surge.

9.1.2 Mooring stiffness

Since the applied force is known, the stiffness in surge and sway C_{ii} can be found as:

$$C_{ii} = 0.1\frac{\Delta t}{\Delta \eta_1} \tag{9.2}$$

Where Δt and $\Delta \eta_1$ is time and distance between two consecutive time steps respectively.

Considering surge first, the C_{11} element in the stiffness matrix is an uncoupled element, thus all other DOF is fixed when carrying out the analysis. A quite high damping ratio (approx. 10% of critical damping) is applied in all DOF to reduce resonance experienced when applying the ramp force. The stiffness plot can be seen in Figure 9.2.

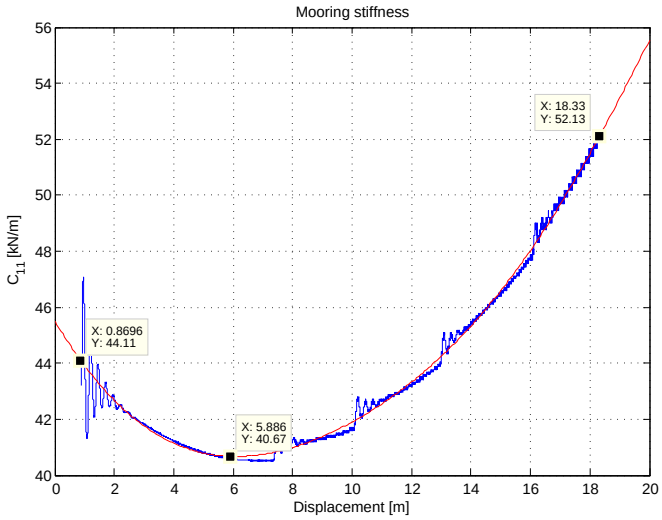

Figure 9.2: Mooring stiffness surge, only surge DOF free

A 6th degree polynomial is fitted to the signal to show the non-linearity better. It can be seen that no single value can represent the mooring line stiffness, but that it varies from $40\,\mathrm{kN\,m^{-1}}$ to $52\,\mathrm{kN\,m^{-1}}$ within the displacements considered.

By applying the ramp force in the sway direction, which is 90° off the surge direction, and keeping the other DOF fixed, a larger stiffness increase is observed, see Figure 9.3.

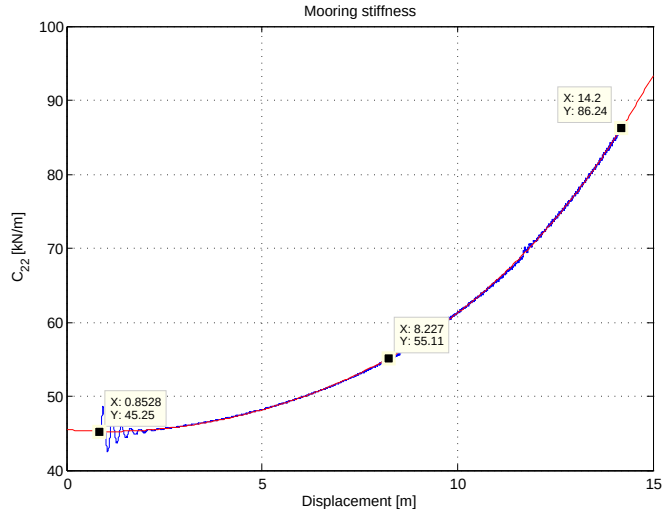

Figure 9.3: Mooring stiffness sway, only sway DOF free

Here, a 4th degree polynomial is fitted. Remembering the 120° spacing of the mooring lines, the sway motion will not have symmetrical mooring lines, which gives rise to an even higher non-linearity. In terms of what is observed, i.e. the high non-linearity and increase in stiffness, it is in good agreement with model tests performed on the Hywind concept [27].

9.2 Rigid body movement: Natural periods and hydrodynamic damping

Decay simulations have been carried out to find estimates to the linear and quadratic damping coefficients. The system is allowed to freely float for 400 s to ensure equilibrium, then a ramp force is applied for 120 s. The applied ramp force is dependent on which degree of freedom one investigates, and the applied ramp forces can be seen in Table 9.1. The theory behind the estimates for the damping coefficients can be reviewed in Section 5.4.1.

Degree of freedom	Ramp force
Surge (η_1)	$5\,\mathrm{kN\,s^{-1}}$
Sway (η_2)	$5\,\mathrm{kN\,s^{-1}}$
Heave (η_3)	$5\,\mathrm{kN\,s^{-1}}$
Roll (η_4)	$1500\,\mathrm{kN\,m\,s^{-1}}$
Pitch (η_5)	$1500\,\mathrm{kN\,m\,s^{-1}}$

Table 9.1: Decay analysis, ramp forces.

The results are compared to model tests done on the Hywind concept in the scale of 1:47 in the Ocean Basin laboratory at MARINTEK [27], the results from the report are not reproduced in the thesis but comparisons are made in the text. The model tests geometry is different from the base case analysis model, but conclusions related to the influence of different factors discussed in the following are deemed similar. Also, decay tests refer to the previous mentioned model test and decay simulations refer to the simulations conducted in this thesis.

The base case analysis model and mooring system have lateral quadratic drag $C_D = 1$ for each element, which can be said to "produce" the quadratic damping. The bottom of the wind turbine has a linear damping coefficient in the axial direction, which is somewhat tuned to the decay tests. The reason for using a linear damping coefficient is to avoid numerical problems at low velocities. Using linear damping is also beneficial to damp out the transient response, due to the fact that the analysis model is not in complete equilibrium after the static analysis. The time series and estimation technique for the heave motion can be seen in Figure 9.4. By using this technique, natural periods and damping estimates are found for the base case configuration, see Table 9.2.

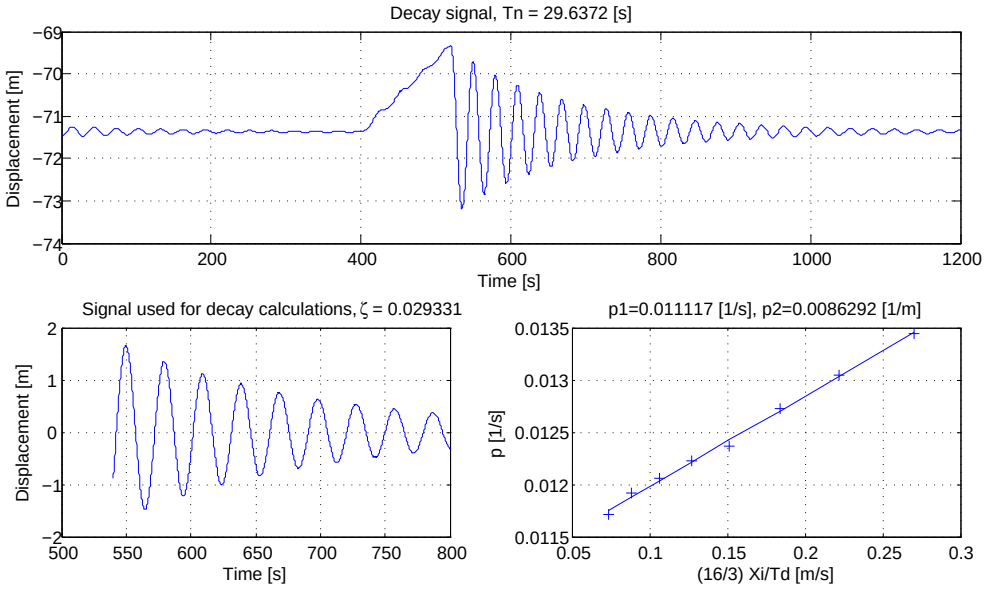

Figure 9.4: Base case decay, heave motion.

	Theoretical	Decay simulation			
Degree of freedom	T_n [s]	T_n [s]	ζ* (%)	p1 [1/s]	p2 [1/m]
Surge (η_1)	106	105.4	4.4	0.00021	0.0402
Sway (η_2)	106	105.4	4.3	0.00019	0.0409
Heave (η_3)	30.7	29.6	2.9	0.01112	0.0086
Roll (η_4)	26.5	26.1	2.6	0.00092	0.0231
Pitch (η_5)	26.5	26.1	2.8	0.00069	0.0236

Table 9.2: Natural periods and damping, base case. *Mean damping over decay simulation amplitude range.

The reason for taking the mean over the amplitude range, in terms of the relative damping (ζ), is because of the quadratic term in equation (5.17) which is highly velocity dependent. Taking surge motion as an example, it will range from 7.5 % to 2.6 % in the amplitude range considered. This also demonstrates that the drag term will be dominating at higher velocities, which is also of importance in terms of the viscous forces generated from wave kinematics.

Acceptable agreement is seen between the theoretical and decay simulation natural periods. In terms of damping, it is seen that all degrees of freedom except heave[1], is mainly quadratic damped due to the drag coefficient. The quadratic dominance is also seen in the decay tests. In terms of the magnitude of the damping ratio, the damping is set lower than what is shown in the decay tests. The reason for doing this is that model tests in ocean basins gives higher estimates than what is seen in full scale, because of different Reynolds numbers [28]. Therefore, as one wishes to be conservative, no external damping except for the linear damping included in heave and the "natural" damping from the drag coefficients is added to the analysis model.

[1]To avoid possible confusions it should be mentioned that yaw motion (η_6) is also linearly damped through SIMO to avoid possible numerical problems.

9.3 Wave induced resonance

Quite early in the thesis work when the estimates for damping were sorted out, a significant resonance contribution was observed in heave. This was first thought of as a mistake by the author when doing damping estimates, but further investigations have shown that it is physical, backed up by the model tests.

9.3.1 Analysis with wave induced resonance

By applying only waves with a $H_s = 6$ and $T_p = 12$ (representable wave parameters from the metocean data [25]) the spectrum for surge, pitch and heave motions together with the wave spectrum can be seen in Figure 9.5

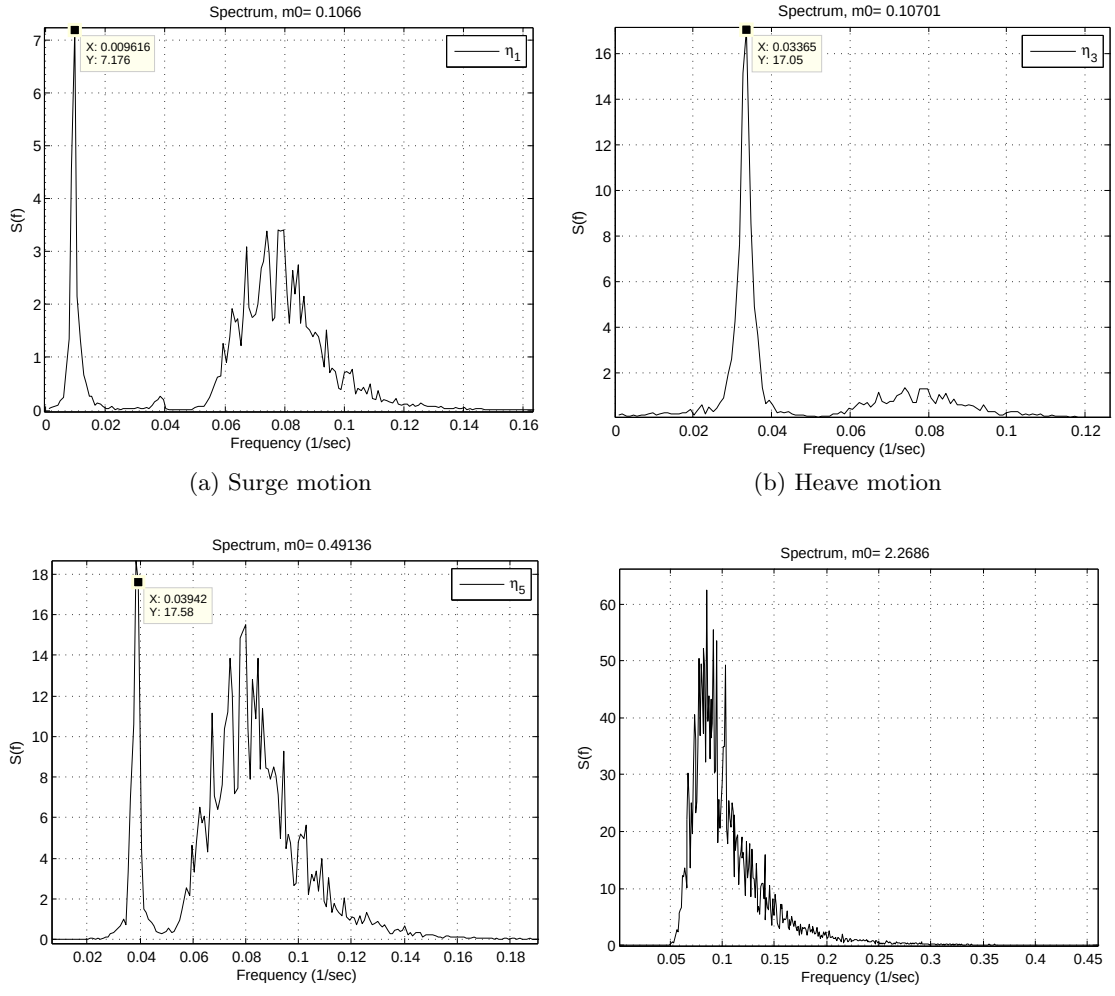

(a) Surge motion

(b) Heave motion

(c) Pitch motion

(d) Wave elevation

Figure 9.5: Power spectrums, rigid body motions, wave with $H_s = 6$ and $T_p = 12$.

Considering surge and pitch in Figure 9.5a and Figure 9.5c, respectively. They are mostly dominated by the wave excitation, but there is also some energy within their natural periods. Since the wave is dominating these degrees of freedom, the resonance is of less concern in an instability point of view. It can also be mentioned that there is a small coupling term with pitch that can be seen in the surge motion spectrum, see Figure 9.5a close to 0.04 Hz.

The heave motion on the other hand, is as one can see from Figure 9.5b largely dominated by resonance (f_3 =0.033 Hz), and the wave excitation induces a much less contribution to the heave motion. Before one proceeds, it should be mentioned that the heave motion amplitude corresponds to a significant value of $2 \times \sqrt{m_0} = 0.65$ m, and is not considered critical with a significant wave height of 6 m. It should also be mentioned that similar spectrum are seen for the model tests [27], which confirms the physical nature of what is observed.

Since there is resonance one would expect the wave spectrum to have energy within the natural periods of the rigid body movements, as can be seen in Figure 9.5d there is no energy over a period of 20 s where the natural periods are located. A reason for the large resonance within the heave natural period is investigated in the following.

9.3.2 Second order heave force contribution: surge and pitch interaction

The analyses in RIFLEX are non-linear, thus forces are calculated at displaced positions. This will include second order heave forces, and can give a physical explanation to what is observed in the previous. In the following only mass forces are considered and pitch angles are assumed small. See Figure 9.6 for an illustration of the interaction.

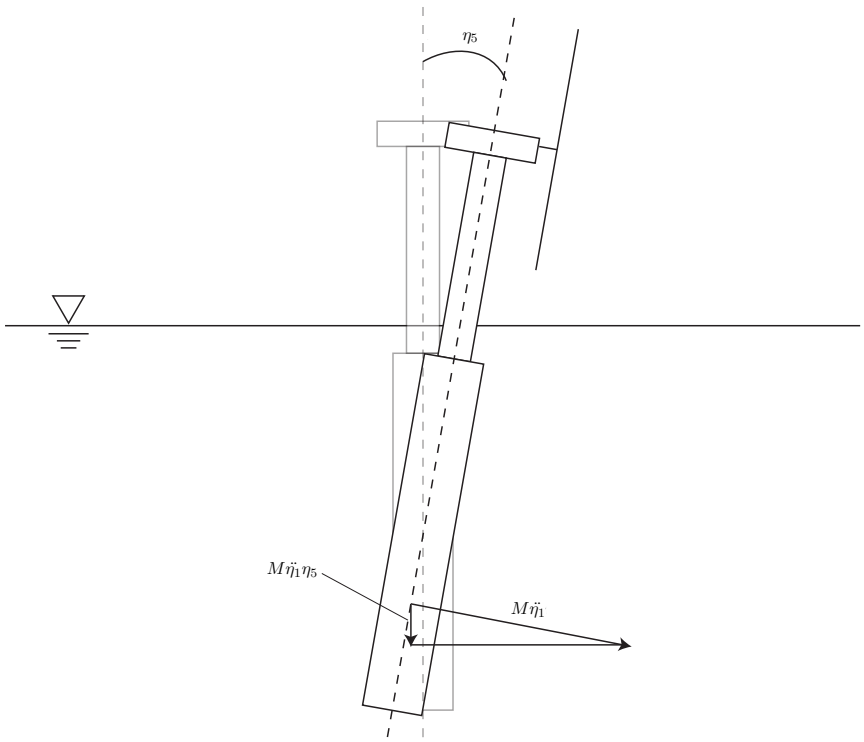

Figure 9.6: Second order heave force.

When the body is pitching a second order heave force contribution can be expressed as follows:

$$F_3 = -M\ddot{\eta}_1\eta_5 \tag{9.3}$$

Surge/pitch motion and acceleration can be expressed in terms of a circular frequency as:

$$\eta_i = \eta_{iA} cos(\omega t) \tag{9.4a}$$

$$\ddot{\eta}_i = -\omega^2 \eta_{iA} cos(\omega t) \tag{9.4b}$$

Where ω is the circular frequency, the subscript A denotes amplitude and i = 1,5. Difference in phase is disregarded.

By using equation (9.4a) and (9.4b) in equation (9.3) the second order heave force contribution for any single circular frequency can be written as:

$$F_3 = M\omega^2 \eta_{1A} cos(\omega t) \eta_{5A} cos(\omega t) \tag{9.5}$$

If the circular frequency is set to $\omega = \omega_{wave}$, i.e. some circular wave frequency, and using a trigonometric rule for double angle identities[2] F_3 can be written as:

$$F_3 = \frac{M\omega_{wave}^2 \eta_{1A} \eta_{5A}}{2}(1 + cos(2\omega_{wave} t)) \tag{9.6}$$

Ignoring the constant part of equation (9.6) and remembering that the circular frequency can be written as $\omega = 2\pi/T$, the wave period producing the resonance can be written in terms of the natural period in heave for the base case as:

$$T_{wave} = 2T_3 = 2 \times 30.7 = 61.4s \tag{9.7}$$

Within this wave period there is no energy, thus the wave can not be said to produce the resonance seen in Figure 9.5b by this derivation.

Turning back to equation (9.5) and setting the circular frequency for the pitch motion to the natural circular frequency in pitch (ω_5), and the circular frequency for the surge motion to some wave circular frequency (ω_{wave}). By using a trigonometric rule for product to sum identities[3] the heave force can be written as:

$$F_3 = \frac{M\omega_{wave}^2 \eta_{1A} \eta_{5A}}{2}(cos[(\omega_{wave} + \omega_5)t] + cos[(\omega_{wave} - \omega_5)t]) \tag{9.8}$$

The circular frequency difference in equation (9.8) is of importance in this context :

$$(\omega_{wave} - \omega_5) = (\frac{2\pi}{T_{wave}} - \frac{2\pi}{T_5}) \tag{9.9}$$

Setting this equal to the natural circular frequency in heave and rearranging, a wave period inducing resonance can be written for the base case as:

$$T_{wave} = \frac{1}{\frac{1}{T_3} + \frac{1}{T_5}} = \frac{1}{\frac{1}{30.7} + \frac{1}{26.5}} = 14.22s \tag{9.10}$$

Which corresponds to a frequency $f_{wave} = 0.07$, and as can be seen from Figure 9.5d the frequency lies where most of the wave energy is. The reason for pitch resonance can be reviewed in Section 5.5.3, where the Mathieu instability was briefly discussed, and an important instability region exist when there is considerable wave energy half the natural period in pitch, i.e. $T_5/2 = 13.25$ where there is considerable wave energy, see Figure 9.5d.

Since the Mathieu instability is dependent on the heave motion, the Mathieu instability together with the second order heave force may magnify each other and induce larger instabilities. Due to the complex loading situation with irregular waves and damping

[2] $cos(2x) = 2cos^2(x) - 1$

[3] $cos(x)cos(y) = \frac{1}{2}(cos(x+y) + cos(x-y))$

effects, the instability will be interrupted and not given the "time" it needs to develop, and is thus of a less concern. The reader may refer to the article by *H. A. Haslum and O. M. Faltinsen* [3] where this mutual interaction effect is more thoroughly discussed, and where it has shown of outmost importance in pure regular waves.

9.4 Structural damping

Structural damping is here meant as damping related to the material in terms of axial, shear, torsional and bending deformations. This damping can be seen as energy dissipated within the structure itself, while the damping in Section 9.2 can be viewed as external damping in terms of the fluid surrounding the structure.

9.4.1 Rayleigh damping

The structural damping model included in RIFLEX is by a Rayleigh damping formulation and can be written as:

$$[C] = \alpha_1[M] + \alpha_2[K] \tag{9.11}$$

Where [C] is the damping matrix, [M] is the mass matrix and [K] is the element-stiffness matrix. α_1 and α_2 are denoted as the mass and stiffness proportional damping coefficients, respectively. The matrices presented here follows a "structural" notation, and should not be confused with the hydrodynamic notation in other sections.

Since the structure investigated in this thesis has rigid body movements, equation (9.11) should be used with care. The stiffness proportional damping can be interpreted physically to model the energy dissipating arising from deformations. The mass proportional has a less physical interpretation, but can be viewed as damping due to external conditions, which are accounted for in Section 9.2. For dry structures these two contributions have shown good accuracy in practical applications [29]. For the floating structure investigated in this thesis on the other hand, the mass proportional damping is usually omitted to avoid unphysical structural damping due to the rigid body motions (i.e. $\alpha_1 = 0$) [19].

The damping ratio arising from the Rayleigh formulation in equation (9.11) can be written as:

$$\zeta_i = \frac{1}{2}(\frac{\alpha_1}{\omega_i} + \alpha_2\omega_i) \tag{9.12}$$

Where ω_i is circular frequency related to the i-th mode of the structure. To further clarify on the previous discussion equation (9.12) can be plotted for a range of frequencies ($f = \frac{\omega}{2\pi}$), see Figure 9.7.

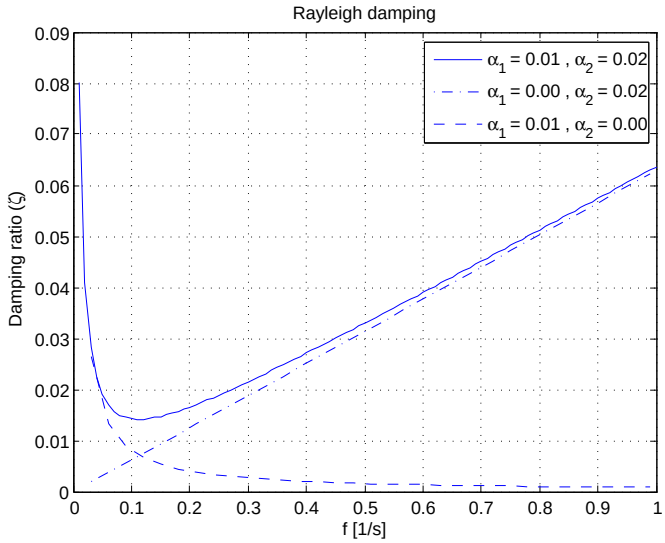

Figure 9.7: Rayleigh damping, magnitude for different frequencies.

What is clear from Figure 9.7 is that the mass proportional damping has a high contribution for low frequencies, these frequencies are dominated by the wind and wave excitation frequencies, thus unphysical high damping may be included in this region.

Wave (JONSWAP spectrum) and wind (Kaimal spectrum) realizations are shown in Figures 9.8a and 9.8b to exemplify their frequency contribution. It should be noted that the area under the curves represent energy within the given frequencies, and that the energy in the wind spectrum is increasing with lower frequencies, where as the wave frequency is banded around the mean frequency with the highest energy contribution around the peak frequency. Also, as mentioned earlier, most of the energy in the wave lies within the frequency range 0.05 Hz to 0.25 Hz, this can also be seen in the wave realization in Figure 9.8.

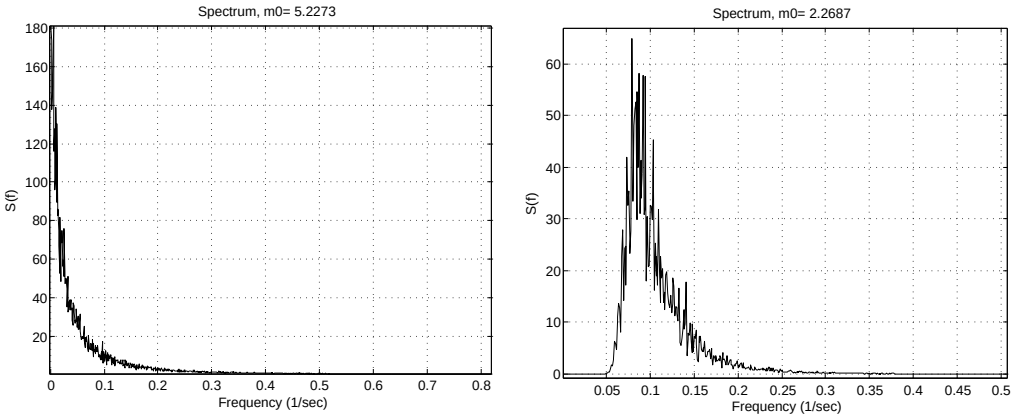

(a) Wind, $U_{mean} = 22.1$, $I_u = \frac{\sqrt{m_0}}{U_{mean}} = 0.1$

(b) Wave, $H_s = 4\sqrt{m_0} = 6$, $T_p = 11.9$

Figure 9.8: Power spectrums, wind and wave realizations

9.4.2 High frequency resonance

The structure has natural vibration frequencies which are connected to the modes of vibration. These frequencies and modes can be found by solving the eigenvalue problem of structural dynamics, but that is not to the authors knowledge well implemented in RIFLEX and thus problematic the formal way.

By applying unidirectional wave and wind with the properties given in Figure 9.8, and applying a low Rayleigh damping, i.e. $\alpha_1 = 0.0$ and $\alpha_2 = 0.001$. The two first frequencies, corresponding to the first and second bending mode, can be identified in the spectrum of the shear force, see Figure 9.9. The same can be seen in the bending moment spectrum, but only the first mode frequency can be identified (not shown).

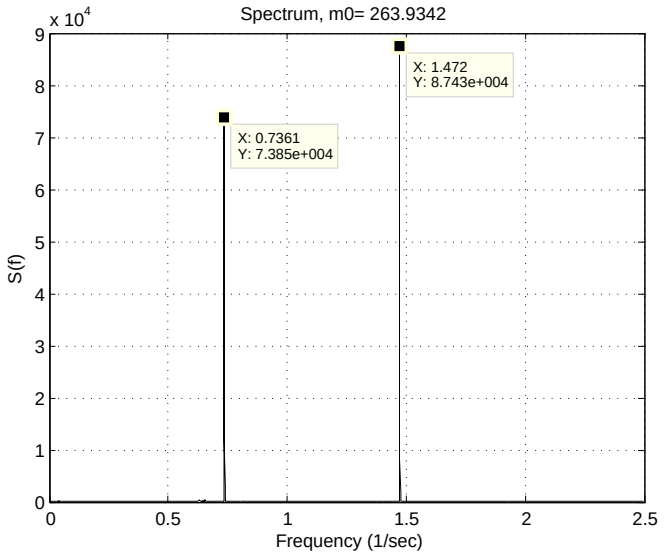

Figure 9.9: Power spectrum shear force, $\alpha_2 = 0.001$.

The low damping applied in the previous mentioned analysis is unreasonable low, in terms of the damping ratio it contributes to $\zeta_1 = \frac{0.001}{2} \times 2\pi \times 0.736 = 0.2\%$ for the first bending mode. Confering a table with recommended damping values [29], welded steel and reinforced concrete usually utlizes a damping ratio of 2-3 %. Thus setting $\alpha_1 = 0.0$ and $\alpha_2 = 0.01$, a 2 % damping ratio for the first bending mode frequency is applied, this damping ratio is also used for all further analyses.

A new analysis is run with the same environmental conditions as in the preceding. The resonance has diminished from the shear force spectrum (not shown), and as can be seen by the spectrum of the bending moment in Figure 9.10, the high frequency resonance is barely visible at a frequency of 0.736 Hz. While referring to the bending moment, the wave can be seen as the largest contributor to the bending moment, contribution from pitch resonance can also be seen. The wind contribution is barely visible, but can be seen for the frequencies lower than pitch resonance. The reader may refer to Table 9.2 to confer the rigid body motion natural periods.

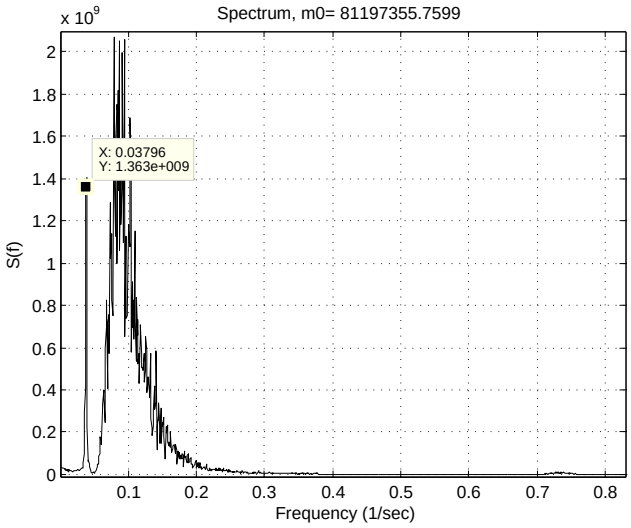

Figure 9.10: Power spectrum bending moment, $\alpha_2 = 0.01$.

The resonance within these high frequencies is not of much concern for further analyses carried out in the thesis, but may be of large concern in a complete wind turbine analysis. The main reason for this is excitation forces related to rotor blade rotation. At rated wind production, the turbine utilized for the Hywind concept has a mean rotor speed at 17 rpm[4], thus the mean frequency of rotation is 0.28 Hz, this frequency is usually denoted 1P and the excitation force is mainly related to mass imbalance in the rotor blades. The 1P frequency is not in the vicinity of any of the natural frequencies considered in this thesis, but it should be mentioned that with high yaw stiffness from the mooring system the natural period in yaw is low and may be in the vicinity of the 1P frequency.

There is also an excitation force related to the number of rotor blades, denoted 3P. This frequency is mainly due to differences in the three dimensional wind velocity and turbulence field, due to e.g. vertical wind shear and/or a blade passing the tower, if this happens to one of the blades an excitation force with a frequency 3P = 0.84 Hz can be induced, which is quite close to the natural frequency of the first bending mode and resonance may occur due to low damping levels. The 3P frequency is seen as the most critical and is also a weakness with the wind thrust code utilized (TDHMILL), which does not include this effect. More complex aeroelastic codes as HAWC2 has the possibility to include these effects, and research is ongoing to include this for offshore floating wind turbines [15].

When the rotor speed is increasing or decreasing below 17 rpm, passing of natural periods will be in effect and triggering of resonance may also happen due to the change in rotor speed below rated wind speed.

[4]It will vary somewhat making the frequency spectrum more broad banded.

9.5 Ultimate limit state

To compare response in an extreme environmental state, analyses are carried out for the ULS environmental conditions described in Section 8.2.

9.5.1 Structural forces

The structural forces are checked by creating an envelope of the forces from the entire time series. The envelope represents maximum and minimum forces which could have happened at any time during the analysis, and gives the analyst a feel with the forces acting within the structure. The envelope for case ULS1 can be seen in Figure 9.11.

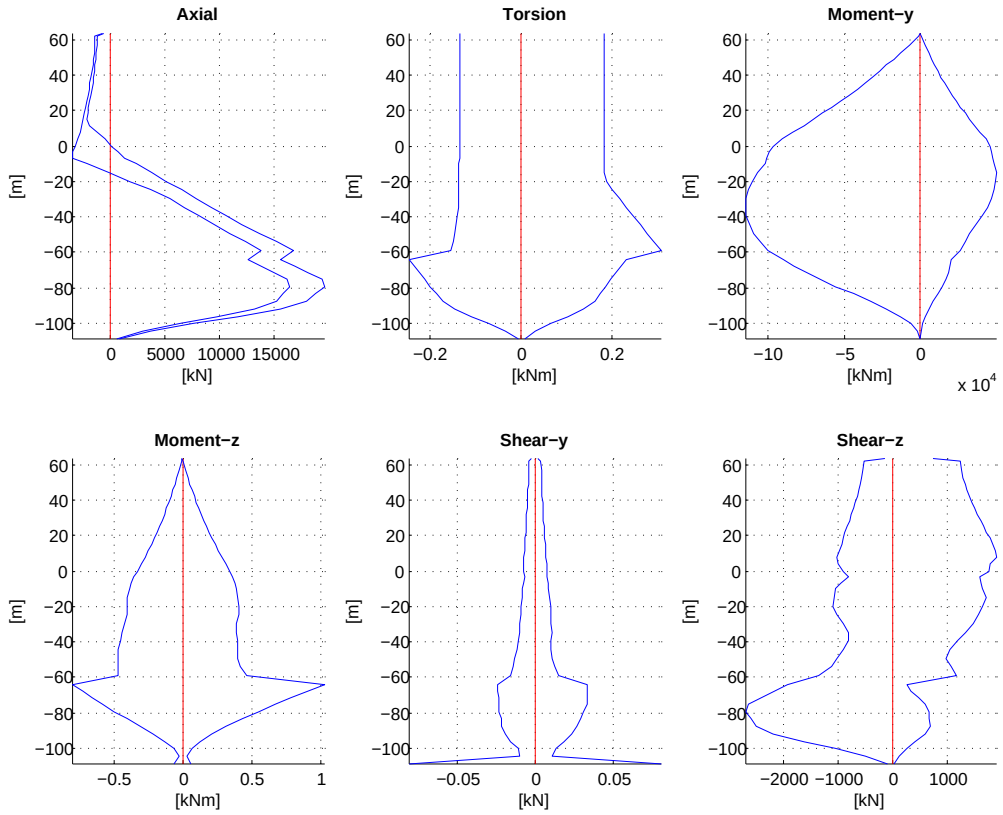

Figure 9.11: Envelope of structural forces, ULS1.

By using a handbook with formulas for structural stresses [30] and assuming a yielding stress at $\sigma_{yield} = 355\,\text{MPa}$, the resisting bending moment for the mean water line can be written as:

$$M_{res} = \sigma_{yield} W = (355 \times 10^3 kN/m^2) \times (0.97 m^3) = 34.4 \times 10^4 \text{kNm} \tag{9.13}$$

Where W is the section modulus, the diameter at the waterline is 6 m and the thickness is 0.035 m.

What is clear from the envelope in Figure 9.11, is that the bending moment about the local y-axis of the sections is dominating. With reference to equation (9.13), the resistance to yielding is more than satisfying at the mean water line, and the other ULS cases do not show any significant difference. Further investigations are not carried out in terms of the structural stresses in the ULS condition, although in a complete study all sections must be investigated. The Matlab script for envelope extraction can be seen in Appendix A.4.

9.5.2 Rigid body motions

The motions that are by the author considered important to investigate and compare is the heave and pitch motion of the structure. The surge motion is of course important as well, but realizing that the surge motion is highly dependent on the restoring from the mooring lines it is considered of less concern for the body's movements in terms of changes to the structural geometry. Since there is a large mass in the top of the tower, pitch motions are important for the bending moment by inertia forces due to the dynamic pitching.

Time series plots are seldom shown in the thesis, but are shown in Figure 9.12 for case ULS1 to give the reader a feel for the dynamic motions of the structure. The heave motion is normalized to a zero value at equilibrium, and the motions are taken out close to the center of gravity to reduce coupling terms.

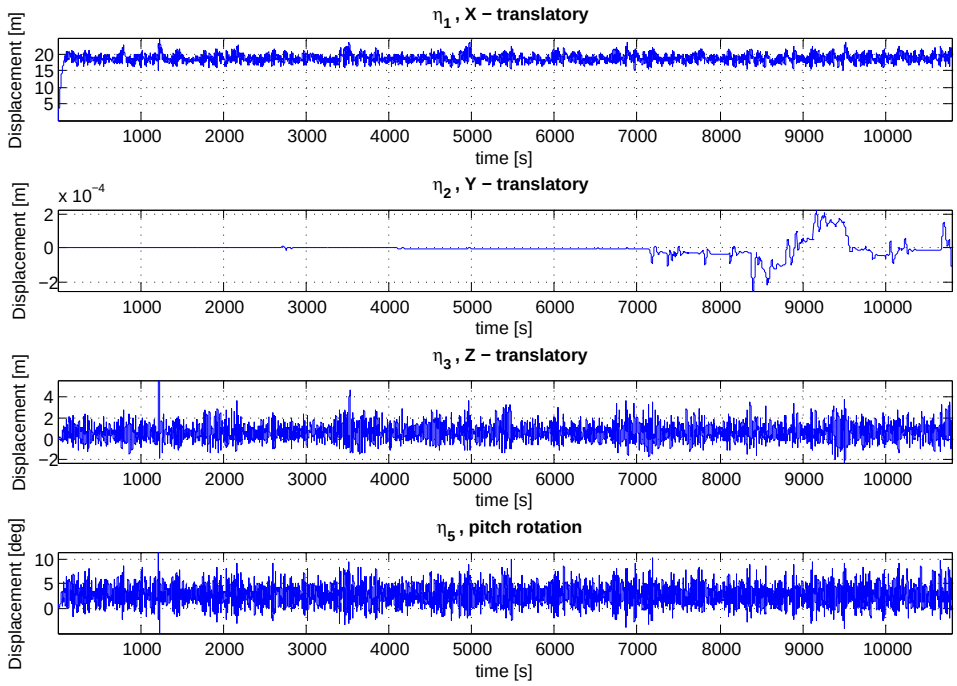

Figure 9.12: Time series of Base case motions, ULS1.

Referring to Figure 9.12, some factors can be deduced. The surge motion is taken to a stable position at around 19 m, the static contribution causing this is from the mean wind velocity and the constant current velocity. Sway motion can be seen as more or less zero, which is expected as the loading is unidirectional. The heave and pitch motions are more thoroughly investigated by statistical estimates.

Before one continues the reader may have observed the large spike at approximately 1200 s in the heave and pitch motion from Figure 9.12. By investigating the wave realization for the analysis, shown in Figure 9.13, the peak in the motion is due to a large wave height from the wave realization at the same time interval.

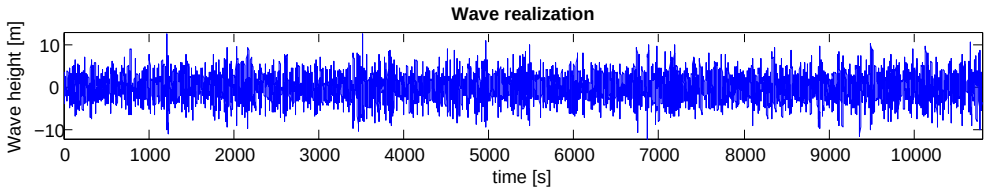

Figure 9.13: Time series of wave realization, ULS1.

What is known from statistics in terms of waves, is that if the wave elevation process is stationary Gaussian distributed, narrow banded and the dynamic system linear, then the response peak values may be predicted by the Rayleigh distribution [5]. The heave and pitch motions are plotted in a normal probability plot in Figures 9.14. If the motions are normal distributed, the sampled motions (represented by crosses) will follow the theoretical normal distribution in a straight line [31].

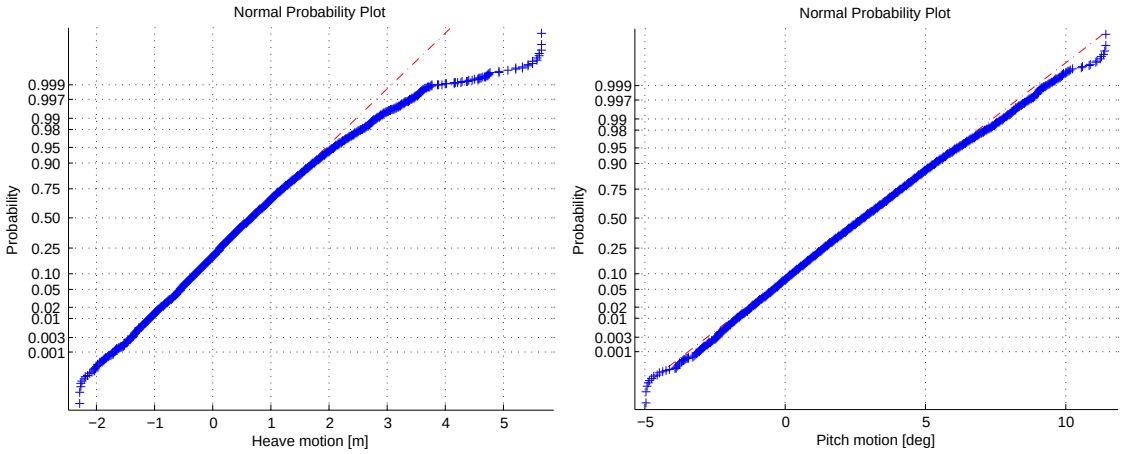

(a) Heave motion

(b) Pitch motion

Figure 9.14: Normal probability plot, heave and pitch motion for ULS1

As can be seen from Figure 9.14a the heave motion deviate somewhat from the normal distribution and can be said to have a "heavy tail", this also indicate that the Rayleigh distribution is "heavy tailed" and non-conservative in terms of peak values. From Figure 9.14b it can be seen that the pitch motion follows a Gaussian process in an acceptable manner. Although the heave motion deviates somewhat from a Gaussian process and more sophisticated statistical methods can be utilized[5], the author has decided to fit peak values to the Rayleigh distribution as it has a convenient analytical expression shown in the following.

Peak values can be found in different ways, the author has decided to use peak values obtained from an average zero-up-crossing period strategy. A zero-up-crossing period for a regular sinusoid will be the period. For a wide banded process, as the present case is, it is the time it takes to go from the mean value, cross it and then reach the mean value. The most probable maximum (mpm) response during a short-term time can then be written as:

$$R_{mpm} = R_{mean} + R_{dyn.mpm} = R_{mean} + \sqrt{2m_0 ln(\frac{t}{T_2})} \tag{9.14}$$

[5]For the interested reader it can be mentioned that a 3-parameter Weibull distribution in many instances can be used to predict better peak values for a process deviating from the Gauss process [32].

Where R_{mean} is the mean response, t is the analysis duration, ln is the natural logarithm, m_0 and T_2 are the response variance and mean period (average zero-up-crossing period) obtained from spectral analysis, respectively. t/T_2 is the number of zero-up-crossings. What should be noted is that R_{mpm} is the most probable largest value and that there is a probability ($P(R > R_{mpm}) = T_2/t$) that this will be exceeded.

The standard deviation (std), which is an indication of the averaged amplitudes or dynamic response, is also identified as an important factor to compare. The mean, which is an indication of the static contribution, is also kept to compare with the other cases. The response for all ULS cases are given in Table 9.3.

	Heave motion (η_3)			Pitch motion (η_5)		
Load case	R_{mean} [m]	R_{std} [m]	R_{mpm} [m]	R_{mean} [deg]	R_{std} [deg]	R_{mpm} [deg]
ULS1	0.69	0.81	3.58	2.78	1.99	9.98
ULS2	0.69	0.84	3.67	2.79	2.11	10.38
ULS3	0.69	0.85	3.72	2.79	2.22	10.78
ULS4	0.67	0.80	3.52	2.78	2.18	10.62

Table 9.3: Results from ULS cases, Base case motions

Referring to Table 9.3 the ULS response is quite similar, which can be expected as the difference in wave properties are small between them. As all of the analyses have different realizations, but similar wave properties, it can also be assumed that the difference between realizations is small for the ULS cases. The Matlab script for calculations can be seen in Appendix A.5.

9.6 Fatigue limit state

This section deals with lifetime assessments based on the environmental cases described in Section 8.1. As mentioned in Section 6.1.1 TDHMILL has a notch filter which intention is to simulate a rotor blade-pitch control system and the relevance of this is further clarified within this section. The significance of coupled analyses with wind and waves is also investigated.

9.6.1 FLS - No notch filter

All environmental conditions for the FLS state is here run for the base case without a notch filter. The developed Matlab script (see Appendix A.3) loads the bending moment at the mean water line and calculates the bending stress for that cross section. Turning points are found and rainflow cycles are calculated from the turning points. The stress ranges found are then placed in a frequency histogram with a division of a thousand buckets and damage calculations based on DNV-RP-C203 [22] are carried out. Figure 9.15 shows the stress time series and stress range histogram for case FLS1.

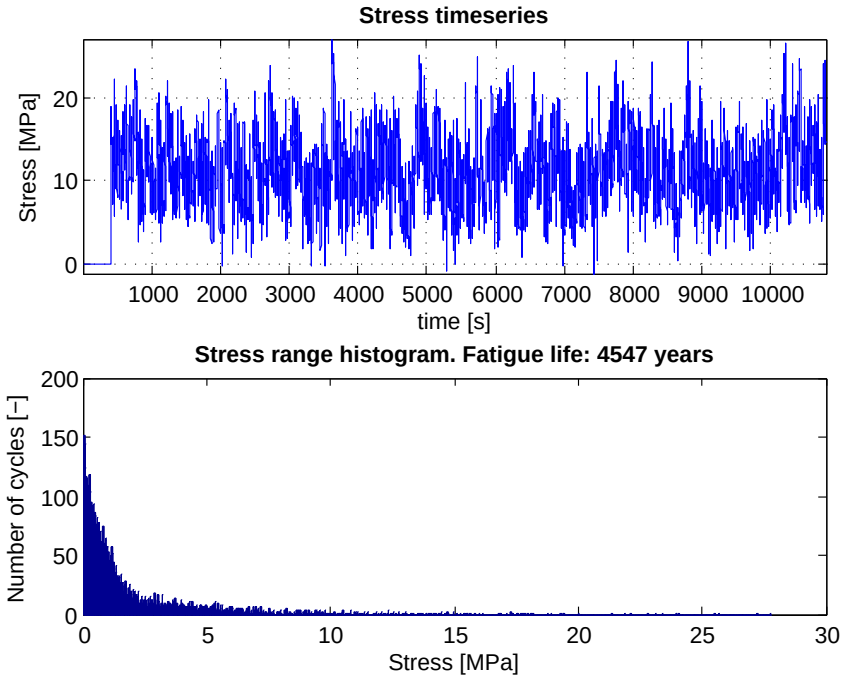

Figure 9.15: FLS1 Fatigue life Base case

Referring to Figure 9.15, the damage (inverse of fatigue life) is quite low for the FLS1 condition, but as mentioned earlier the total damage over a 50-year period is of interest and is calculated as:

$$D_{total} = \sum_{i=1}^{10} D(FLSi)P(FLSi) = \sum_{H_s=1}^{10} D(H_s)P(H_s) \tag{9.15}$$

Since the subscript i is equivalent to the significant wave height in each case the total damage is expressed in terms of H_s, it is reminded that H_s is related to the mean wind velocity as well as the spectral peak period and the reader may refer to Section 8.1 for more information. $D(H_s)$ is the damage in a year for case i and $P(H_s)$ is the probability for the given environmental condition. The probability for a significant wave height is given in Table 8.1.

The results for the lifetime assessment without a notch filter are given in Table 9.4. Stress standard deviation which is calculated from the time series is included in the table as a rough indication that the rainflow counting is performed correctly, the stress standard deviation is also discussed in the end of this section.

Load case	Std stress [MPa]	Lifetime [years]	$D(H_s)P(H_s)$ [1/year]
FLS1	4.5	4546.7	0.00007
FLS2	6.3	460.3	0.00088
FLS3	10.7	22.3	0.00775
FLS4	8.7	35.1	0.00202
FLS5	8.4	35.7	0.00087
FLS6	9.5	17.5	0.00074
FLS7	10.8	9.1	0.00057
FLS8	12.2	5.1	0.00039
FLS9	13.5	3.4	0.00022
FLS10	14.8	2.3	0.00017
		Total damage	0.01368
		Total lifetime	73 years

Table 9.4: Fatigue life base case - No notch filter

Referring to Table 9.4 it can be seen that by this approach the base case has a lifetime in terms of fatigue on the mean water line section of 73 years. As will be shown, this is a conservative lifetime assessment.

The observant reader may have noticed that case FLS3 "steals" most of the structures lifetime and further investigations are thus carried out. The spectrum of the bending moment for case FLS3 can be seen in Figure 9.16.

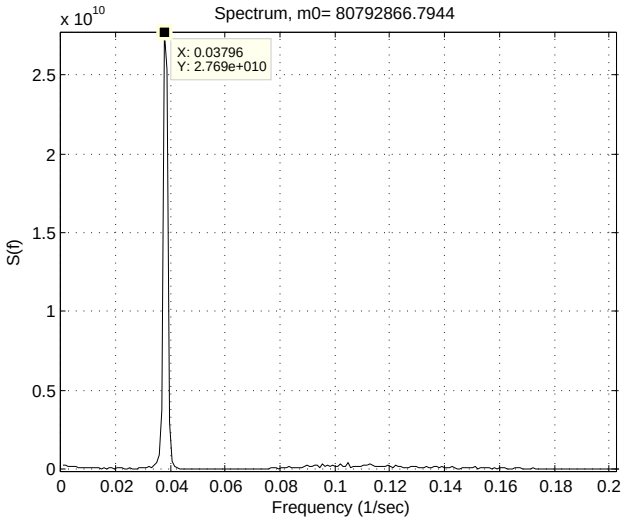

Figure 9.16: Power spectrum bending moment FLS3, without notch filter.

What can be seen in Figure 9.16 is that the bending moment is dominated by resonance at the natural frequency in pitch ($f_5 = 0.037\,\mathrm{Hz}$), wave and wind energy can also be barely recognized at the high and low frequencies, respectively. The reason for the resonance at the pitch natural frequency is that with a conventional control system (no notch filter) negative damping is added to the system and the wind turbine truly acts as a "perfect fatigue machine". This is further explained in Section 9.6.2.

Before one proceeds the author wish to comment on the relation between the standard deviation of the stress and the lifetime. It is seen for most FLS cases in Table 9.4 that the lifetime decreases with increasing stress standard deviation but there is not a one-to-one relation. In Figure 9.17 the bending moment spectrums for case ULS3 and ULS6 are shown, it is observed that with more energy within the higher frequencies stress oscilla-

tions will be larger (more zero-up-crossings) and increase fatigue damage. This is also of importance in regards to the 1P and 3P frequencies discussed in Section 9.4.2 which are high frequency contributions to the bending moment.

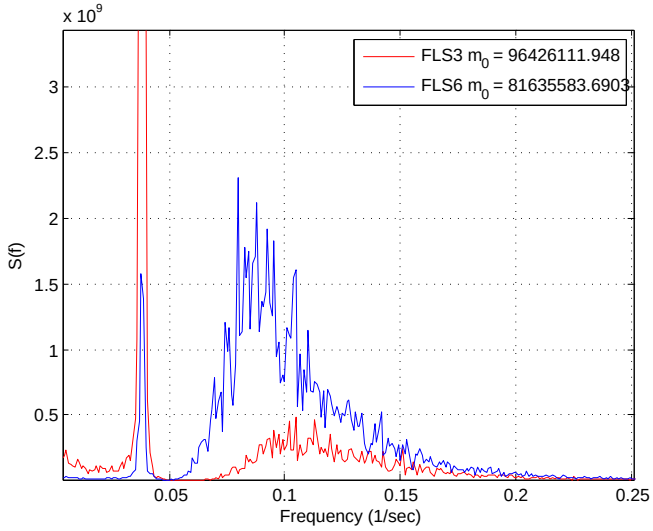

Figure 9.17: Power spectrum bending moment FLS3 and FLS6, without notch filter.

9.6.2 Control system: Negative damping

The theoretical approach is based on derivations for non-constant thrust coefficients by F. G. Nielsen [13]. By assuming that the thrust coefficients varies linearly with the relative mean wind velocity it can be written as:

$$C_T = C_{T0}(1 + k_{CT}\frac{U_d}{U_w}) \tag{9.16}$$

Where C_{T0} is a thrust coefficient at the mean wind velocity, $U_d(= U_{rel} - U_w)$ is the dynamic variation of the wind velocity due to turbulence and/or wave induced motions (the derivations are based on wave induced motions alone) and U_w is the mean wind velocity. K_{CT} is the slope and is of importance in the following. Phase lags are disregarded. The thrust force can now be expressed by equation (6.1) as:

$$T = KC_{T0}(1 + k_{CT}\frac{U_d}{U_w})U_{rel}^2 \tag{9.17}$$

It can be shown by assuming a larger mean wind velocity than dynamic motion and computing the dissipated energy over a cycle, assuming harmonic motions in a two DOF system, that the linearized damping in surge due to the wind thrust can be written as [13]:

$$B_{11} = \frac{1}{2}\rho_a \pi R^2 U_w C_{T0}(1 + \frac{k_{CT}}{2}) \tag{9.18}$$

The factor in the brackets is of importance, as this term for a $k_{CT} < -2$ will make the wind induced damping negative. The damping B_{15} and B_{55} contains the same term.

Dividing equation (9.17) by U_{rel} and differentiate with respect to the dynamic motion, k_{CT} can be expressed as:

$$\frac{d(T/U_{rel}^2)}{dU_{rel}} = \frac{KC_{T0}k_{CT}}{U_w} \quad \Rightarrow \quad k_{CT} = \frac{U_w}{KC_{T0}}\frac{d(T/U_{rel}^2)}{dU_{rel}} \tag{9.19}$$

Using this with the thrust force constants utilized in TDHMILL for the analyses, a plot can be made of k_{CT} versus mean wind velocity, which is assumed equal to the relative mean wind velocity, see Figure 9.18.

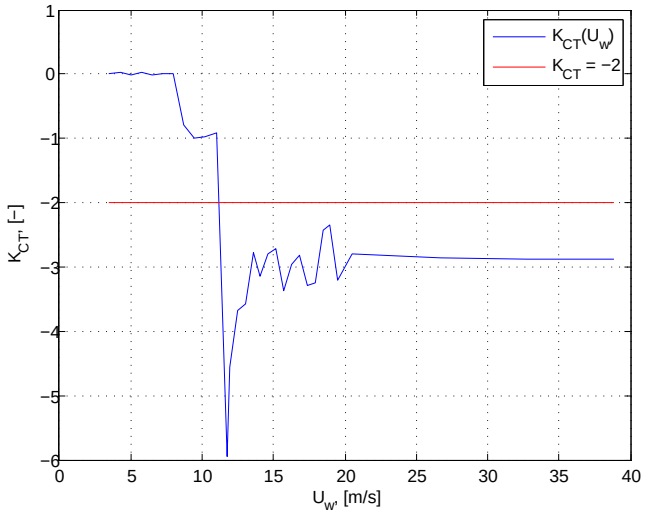

Figure 9.18: k_{CT} for thrust coefficients in analyses.

It can be seen from Figure 9.18 that the negative damping is highest for a mean wind velocity around the rated wind speed, interaction with waves will induce damping due to the quadratic drag term and this may counteract the negative wind induced damping and be of less concern for higher wind velocities where the wave damping will be higher (in regards to the environmental data described in Chapter 8).

As was shown in Section 9.6.1, not accounting for the negative damping by an active blade-pitch control system (notch filter) produces a resonant bending moment. Research is ongoing with Hywind prototype outside Karmøy to produce effective control systems to counteract this effect, where preliminary results are promising and the use of a notch filter in the analyses is justifiable [33].

9.6.3 FLS - With notch filter

Not using a notch filter will make the lifetime assessments and comparisons with other cases highly dependent on damping and the fact that reducing the draft of the analysis model will reduce the drag terms associated with the reduction, the notch filter is applied in the analyses for load cases over rated wind speed[6] where negative damping is present, i.e. FLS3-10 have the notch filter applied. The new lifetime assessment is presented in Table 9.5.

Load case	Std stress [MPa]	Lifetime [years]	Difference*	$D(H_s)P(H_s)$ [1/year]
FLS1	4.5	4546.7	0 %	0.00007
FLS2	6.3	460.3	0 %	0.00088
FLS3	7.2	112.2	403 %	0.00154
FLS4	7.2	76.6	118 %	0.00092
FLS5	8.1	42.6	20 %	0.00073
FLS6	9.3	19.0	9 %	0.00068
FLS7	10.7	9.5	5 %	0.00054
FLS8	12.0	5.4	5 %	0.00037
FLS9	13.4	3.5	4 %	0.00022
FLS10	14.7	2.4	3 %	0.00017
			Total damage	0.00611
			Total lifetime	164 years

Table 9.5: Fatigue life base case - Notch filter. *Percentage difference in lifetime assessment from Table 9.4.

Referring to Table 9.5 it is seen that in correspondence with what was discussed in Section 9.6.2 the load cases FLS3 and FLS4 have the highest increase in lifetime due to the reduction in negative damping by the notch filter. The reader may also refer to Table 8.1 for the load case properties as well as Figure 9.18 for the K_{CT} factor that together illustrate for which cases negative damping will be reduced the most.

In Figure 9.19 the bending moment spectrum is shown for case FLS3 with and without the notch filter. It is seen from the spectrum that the total energy is better distributed between wave and wind, but there is still some pitch resonance mainly due to the resonant frequencies in the wind spectrum and the reader may refer to Section 6.1.1 where the notch filter was briefly explained for a further clarification. The increase in total lifetime from 73 years to 163 years also clearly illustrates the importance of counteracting the negative damping at rated power production.

[6]For the interested reader it is mentioned that applying the notch filter for cases under rated wind speed the notch filter induced high resonance in pitch. The reason for this is still unknown and due to a limited time frame it is not investigated any further by the author.

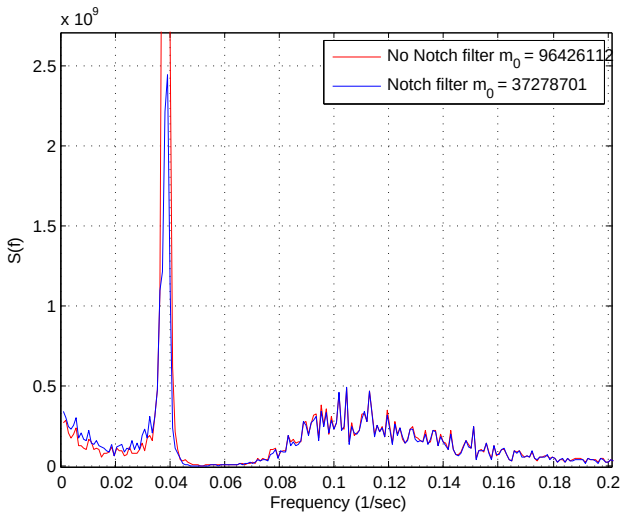

Figure 9.19: Power spectrum bending moment FLS3, notch filter significance.

The notch filter parameters (ζ_N,ζ_D) were as mentioned in Section 6.1.1 set to (0.001,0.2) for the results presented in Table 9.5. The effect of using a broader filter set to (0.1,1) has also been investigated, the total lifetime is increased to 170 years with a broad filter (0.1,1) compared to 164 years with the steep filter (0.001,0.2). The difference is not large, but the reason for the difference is important.

In Figure 9.20 the bending moment spectrum is shown for case FLS3 with the two mentioned combinations of parameters, it is observed that the broad filter parameters filters out less energy at pitch energy than the steep filter, but the steep filter has the most energy (see m_0 in Figure 9.20), this is also seen for other FLS cases (not shown). Thus, to avoid filtering out pitch motion induced by other frequencies than the pitch resonance frequency, the steep filter parameters are utilized.

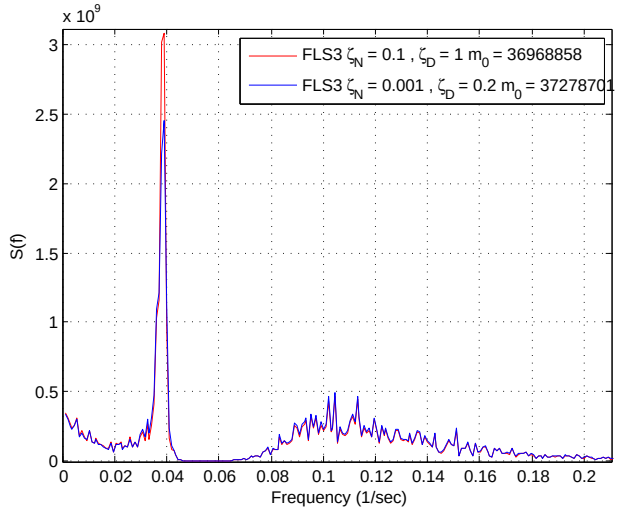

Figure 9.20: Power spectrum bending moment FLS3, notch filter parameters.

9.6.4 FLS - Only waves

The author wishes to emphasize the importance of coupled analyses for the Hywind concept where wind and wave induced loads are included together. Wind is removed from the analyses and in Table 9.6 a lifetime assessment is given which only include wave induced loads.

The almost double increase in lifetime from the lifetime assessment in Table 9.5 clearly illustrate the importance of including wind and wave loads together. It should also be observed that with increasing FLS case (increasing H_s) the wave induced fatigue is dominating in the analyses, but the FLS cases relative probability of occurrence mainly "favours" the FLS cases with low numbering (see Table 8.1) and increase the importance of wind induced fatigue.

Load case	Std stress [MPa]	Lifetime [years]	Difference*	$D(H_s)P(H_s)$ [1/year]
FLS1	1.4	147455.7	3143%	0.00000
FLS2	2.9	4630.3	906%	0.00009
FLS3	4.4	612.8	447%	0.00028
FLS4	5.9	145.3	90%	0.00049
FLS5	7.4	51.5	21%	0.00060
FLS6	8.9	21.6	13%	0.00060
FLS7	10.4	10.6	11%	0.00049
FLS8	11.8	5.9	10%	0.00034
FLS9	13.2	3.8	7%	0.00020
FLS10	14.6	2.6	6%	0.00016
			Total damage	0.00324
			Total lifetime	309 years

Table 9.6: Fatigue life base case - Only waves. *Percentage difference in lifetime assessment from Table 9.5.

10 Reduced Draft Analyses

The new concept with the heave plate configuration is made with a draft of 80 m, the base case configuration has a draft of 110 m and if one assume that a clearing of 20 m is needed, the new concept may be suitable for water depths of 100 m. The author has decided, due to a limited time frame, to limit the studies within the thesis to 80 m draft versions and elaborate on the consequences by physical behavior of the draft reductions performed.

10.1 Heave plate damping

The heave plate has been reported with important beneficial damping in heave. The article by Fischer et al. [4] investigates heave damping by model trials for spar buoys with the heave plate configuration. Damping amplifications factors of 3-5 times were achieved with a single heave plate having a diameter of 1.3 times the bare-cylinder diameter. Fischer et al. also investigated heave damping with multiple plates distributed from the keel, but the highest increase was achieved with only the bottom heave plate, the heave damping amplifications can be seen in Figure 10.1.

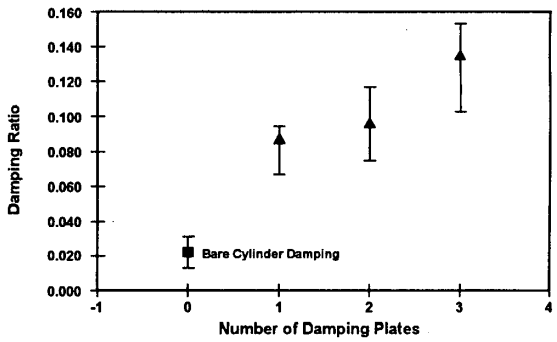

Figure 10.1: Heave plates, damping amplification [4].

The source of the increase in damping is mainly because of separation of the fluid stream and shedding of eddies over the heave plate edges, and should strictly speaking be added as an increase in the drag coefficient in terms of vertical drag. Quadratic damping on the other hand is more difficult to control in terms of the relative damping, thus the heave damping is increased in terms of linear relative damping from approx. 3 % for the base case, to approx. 5.5 % for the new concept with the heave plate. The results presented by Fischer et al. gives higher damping amplitudes than used in the analyses, but as mentioned in Section 9.2 model tests usually gives higher damping estimates than what is seen in full scale.

10.2 Reduced draft configurations and properties

The configurations and important properties for the 80 m draft versions can be seen in Table 10.1 together with the base case configuration. More detailed analysis models are for the interested reader given in Appendix C. Also, as was mentioned in Section 6.4, the water line diameter is not changed as it changes the steel tower.

As will be shown later, the reduced draft configurations have worse performance than the base case configuration and to better see the significance of the heave plate, a version similar to 80M-1 without the heave plate is also analysed.

The configurations are obtained by utilizing optimization techniques in excel by the solver function [34]. The driving factor has not been to create an optimal structure but to have the static pitch and natural periods within desired limits by changing the key parameters. What was mentioned in Section 5.5 the two properties static pitch and the natural period in pitch are conflicting, thus the 80M-1 configuration is created by keeping the natural period in pitch high while having an overall slender structure to reduce wave forces experienced by the structure. The 80M-2 configuration is created by keeping the static pitch low and to experience the performance of an overall larger structure.

	Base case	80M-Cyl	80M-1	80M-2
Draft hull	110 m	80 m	80 m	80 m
Displacement	6274 tons	5412 tons	5667 tons	6745 tons
Diameter cylinder	8.6 m	9.5 m	9.5 m	10.2 m
Diameter heave plate	-	-	14 m	18 m
Thickness heave plate	-	-	3 m	3 m
Theoretical static pitch	2.8°	4.4°	3.9°	2.8°
Natural period pitch	26.1 s	24.1 s	23.8 s	22.0 s
Damping pitch	2.8 %	2.8 %	2.7 %	2.4 %
Natural period heave	29.6 s	27.7 s	29.6 s	34.0 s
Damping heave	2.9 %	3.0 %	5.5 %	5.6 %

Table 10.1: Configurations and important properties for reduced draft analyses. Natural periods and damping are from decay simulations

10.3 Ultimate limit state

All ULS cases from Section 8.2 are run for the configurations given in Table 10.1. The difference in response between the configuration's ULS cases is small and including all of them in this section is not necessary as it does not provide any additional information, therefore only case ULS3 is used for comparisons. Rigid body motions response tables for all ULS cases are given in Appendix D.1 for the interested reader.

Many aspects can be compared and the author has gone through a large set of response spectrums as well as statistical calculations, and what is given here is by the author deemed as the most important factors to be aware of.

10.3.1 Wave kinematics in ULS state

From the infinite water depth velocity potential in equation (3.6) it can easily be shown that the water particle velocity and acceleration decays with e^{kz}, where $k = 2\pi/\lambda$. It is common to say and quite clear that when the wave length equals the water height (z) with opposite signs, the water particle acceleration and velocity is negligible (z is defined as zero at the mean water line and positive upwards). The decay in shallower waters is different and may give an advantage for the reduced draft configurations, but the relation shown here in term of the analyses is unchanged.

In Figure 10.2 the dispersion relation (see equation (3.7)) is plotted for a range of wave periods. It is seen that at a wave period of 16 s which is the peak period of ULS3 the wave length is 400 m and significant wave particle acceleration and velocity can be expected at the bottom of all configurations.

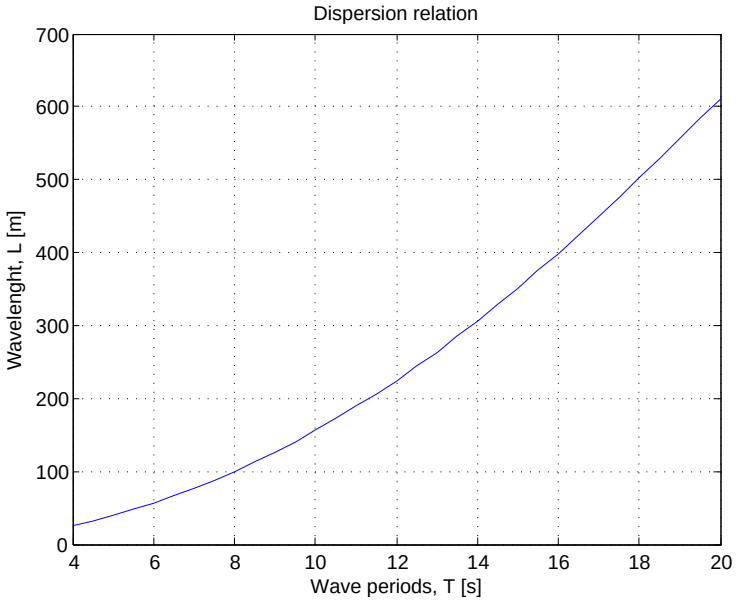

Figure 10.2: Wave period and wave length.

10.3.2 Rigid body motions

The response results for case ULS3 in percentage difference from the base case response are presented in Table 10.2.

	Heave motion (η_3)			Pitch motion (η_5)		
Configuration	R_{mean} [%]	R_{std} [%]	R_{mpm} [%]	R_{mean} [%]	R_{std} [%]	R_{mpm} [%]
80M-Cyl	2.8	19.9	17.5	30.5	35.2	34.0
80M-1	7.3	16.3	15.4	18.6	39.0	33.7
80M-2	31.9	31.5	32.1	-8.6	73.6	52.1

Table 10.2: ULS3 Percentage difference from base case

Overall the response performance is worse for all of the configuration from the base case except for the mean pitch motion of 80M-2, which is probably due to a larger displacement increasing the static restoring. 80M-2 has the largest deviations from the base case, which in the ULS state is due to the reduced draft and increase in overall diameter thus increasing the wave forces present, this is also clear from Figure 10.3a where 80M-1 and 80M-2 pitch motion are plotted together and wave frequency contributions are larger for 80M-2. From the heave motion spectrum in Figure 10.3b the same is observed.

Comparing 80M-1 and 80M-Cyl, the effect of the heave plate in the ULS state can be clarified further. It is seen from Table 10.2 that the pitch motion standard deviation, which is a measure on the dynamic response, is larger for the pitch motion of 80M-1 and can also be seen from the spectrum in Figure 10.3c. The mean on the other hand is less for 80M-1 and is easily explained by a larger static pitch. The pitch most probable max is because of these factors approximately the same. The reason for the worse dynamic behavior in pitch motion for the heave plate configuration is probably influenced by the increased diameter at the bottom where wave kinematics is of significance, see Section 10.3.1. From Table 10.2 it can be seen that the dynamic heave motion for 80M-1 is better than 80M-Cyl, this can also be seen from Figure 10.3d where it is also observed that some of the improvement in dynamic response is from the increased damping in 80M-1 because of the heave plate.

Comparing 80M-1 and the base case, it can be seen from the pitch motion spectrum in Figure 10.3e that 80M-1 has worse performance over all wave frequencies, the increase is mainly influenced by the reduction in draft and increase in overall diameter. The reduction in draft gives the base case larger restoring where wave kinematics is less and 80M-1 does not have that advantage. For the heave motion spectrum in Figure 10.3f it is observed that 80M-1 has better performance at heave resonance due to an increase in damping but that where most of the wave energy lies the performance is worse which is also due to the reduction in draft. The same can be deduced from the heave and pitch motion spectrum for 80M-2 (see Figure 10.3a where it is compared to 80M-1), which has an even larger deviation in the spectrum from the base case because of a larger overall diameter and implies that increasing the diameter is disadvantageous in the ULS state.

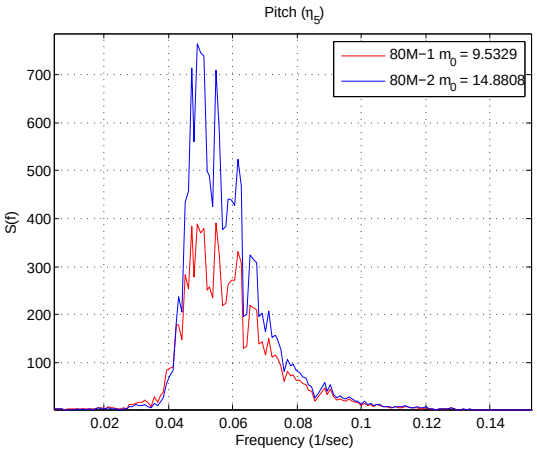

(a) Pitch motion, 80M-1 and 80M-2.

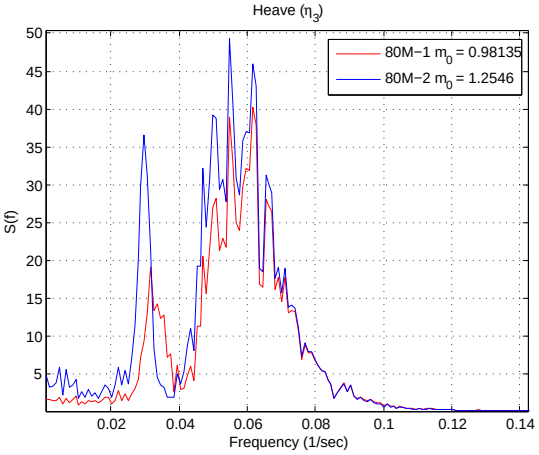

(b) Heave motion, 80M-1 and 80M-2.

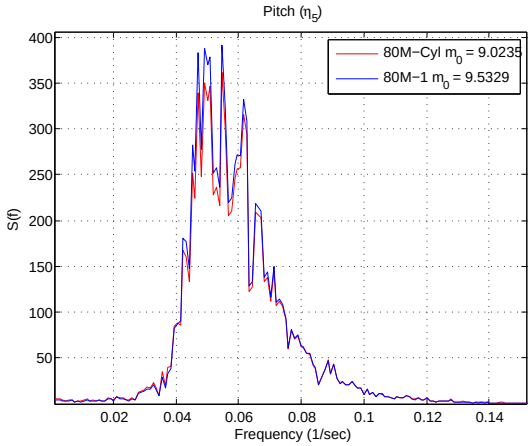

(c) Pitch motion, 80M-1 and 80M-Cyl.

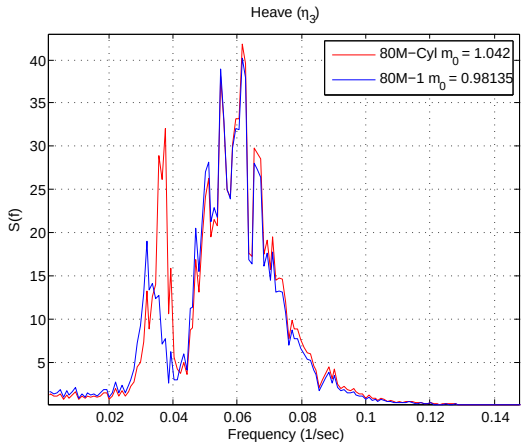

(d) Heave motion, 80M-1 and 80M-Cyl.

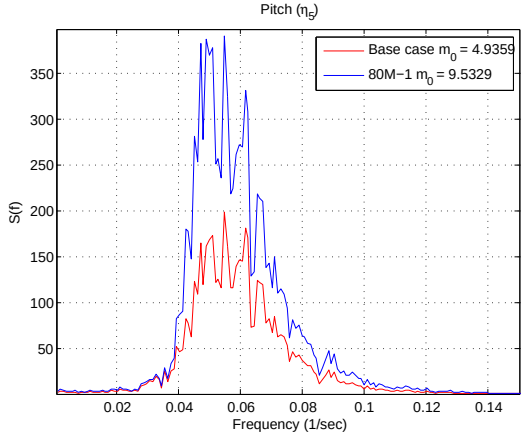

(e) Pitch motion, 80M-1 and Base case.

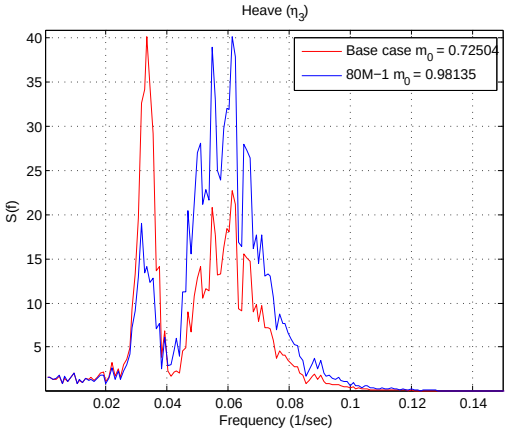

(f) Heave motion, 80M-1 and Base case.

Figure 10.3: ULS3 Comparisons power spectrum, rigid body motions.

10.3.3 Structural forces - Bending moment

The bending moments for case ULS3 are presented in Figure 10.4 for all configurations given in Table 10.1. The maximum bending moment is increased for all configurations in regards to the base case, it does however not present any threat in terms of yielding at the mean water line (the reader may refer to equation (9.13)). It is observed from Figure 10.4 that 80M-1 has an overall larger bending moment over the structure compared to 80M-Cyl due to the larger dynamic motions (see Table 10.2), the difference is however negligible.

Another important factor from Figure 10.4 is that the maximum bending moment for all configurations in the ULS state is found under the mean water line and implies that the largest fatigue damage may be found there, as mentioned in Section 6.5 the fatigue damage is calculated at the mean water line and does not necessarily give the highest fatigue damage.

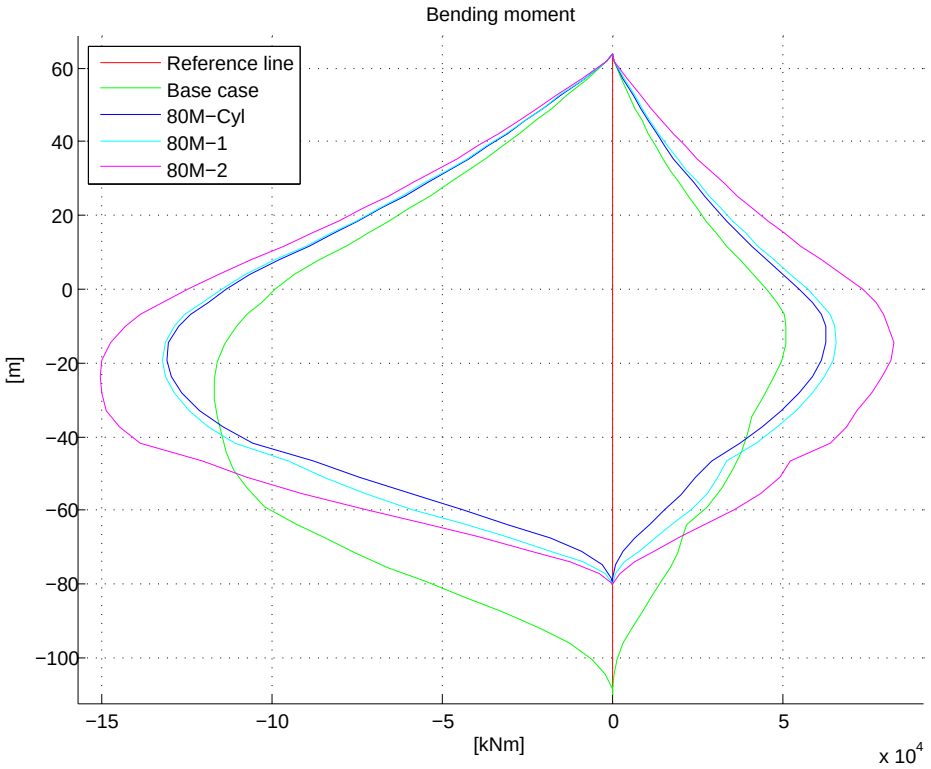

Figure 10.4: ULS3 Bending moment for all configurations.

(Page intentionally left blank)
(For readers convenience with figures and text in the following)

10.4 Fatigue limit state

All FLS cases from Section 8.1 are run for the configurations given in Table 10.1. As mentioned in Section 9.6.3 the notch filter is utilized in the analyses for all FLS cases at rated power production (FLS3-10).

10.4.1 Total lifetime

The total lifetime (inverse of total damage, see equation 9.15) is presented in Table 10.3 for all configurations. Tables with more detailed analysis results are presented in Appendix D.2 for the interested reader.

	Base case	80M-Cyl	80M-1	80M-2
Total lifetime	164 years	58 years	61 years	53 years
Dev. Base case	1	0.35	0.37	0.32

Table 10.3: Total lifetime and deviation from base case for all cases.

Referring to Table 10.3 it is seen that all of the new configurations have a significantly worse lifetime than the base case. The heave plate configuration 80M-1 has better fatigue life than 80M-Cyl, but the improvement from the bare cylinder to the heave plate on three years is however negligible in a practical point of view. Another interesting result is that the 80M-2 configuration which has larger overall diameter and displacement, has the least lifetime.

10.4.2 Base case and 80M-1 comparison

In Figure 10.5 the bending moment spectrum is shown for the base case and 80M-1. It is seen for all FLS cases shown that in the wave frequency range 80M-1 has a higher energy contribution than the base case. It is observed that 80M-1 has a larger resonance frequency contribution for FLS2-6, which is probably due to the restoring and drag coefficients "lost" by the reduction of the draft.

With increasing FLS case it is also observed that the wave energy is increasing in the bending moment and that the pitch resonance within the bending moment is decreasing. This is also the case for FLS7-10 (not shown)[1], which insinuate higher significance of wave kinematics for increasing FLS cases and is in correspondence with the findings in Section 9.6.4.

[1]The reader may refer to Figure 10.10 where 80M-1 is shown in relation to 80M-Cyl.

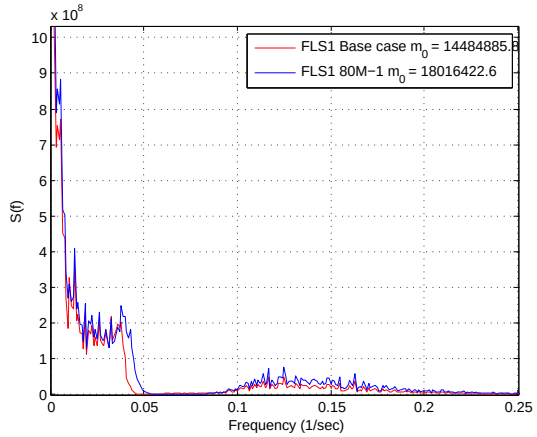

(a) FLS1

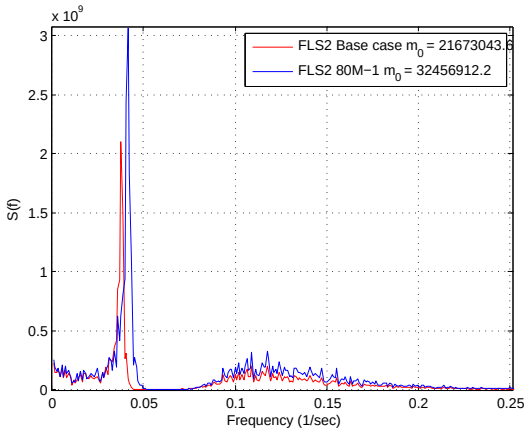

(b) FLS2

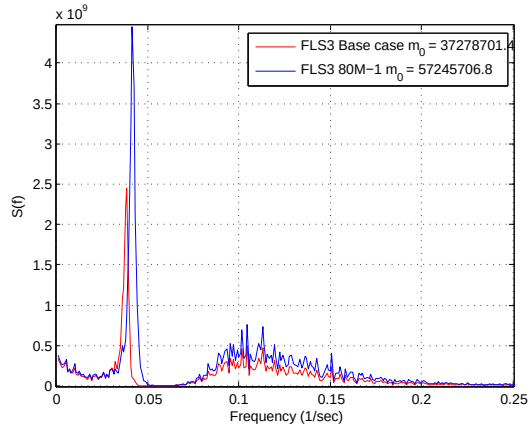

(c) FLS3

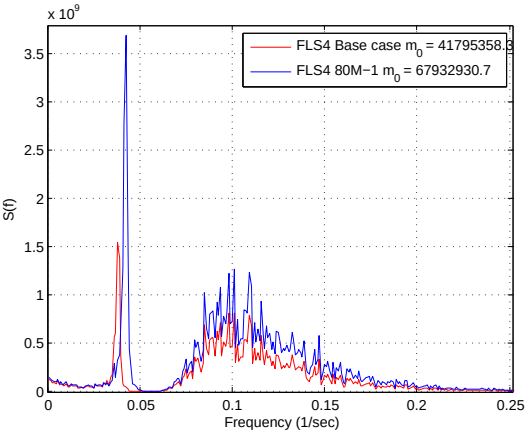

(d) FLS4

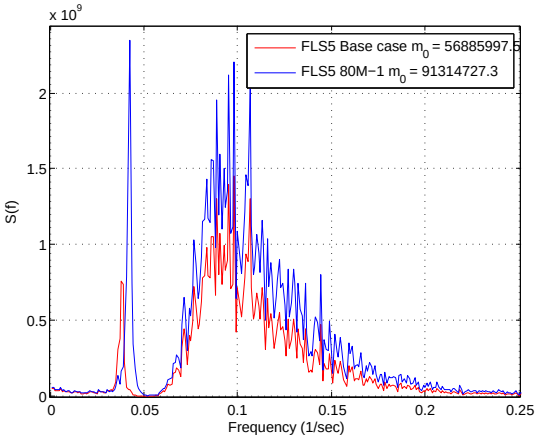

(e) FLS5

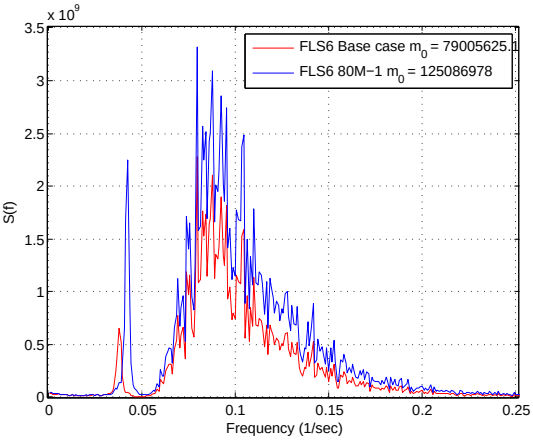

(f) FLS6

Figure 10.5: FLS Base case and 80M-1 comparisons power spectrum bending moment.

10.4.3 Comparison of all configurations

For a better view of the configurations fatigue damage over the range of analyses compared to the base case, each FLS case damage for each configuration is normalized by the base case damage for each FLS case and is shown in Figure 10.6.

Referring to Figure 10.6, 80M-1 have better performance than 80M-Cyl where the thrust force is greater and wave kinematics with depth is less (approx. FLS1-5), for the cases where mainly wave kinematics is of concern (approx. FLS6-10) the two configurations converges and 80M-1 tends to worse performance than 80M-Cyl, the latter is also in agreement with the results for dynamic pitch motion in the ULS state (see Section 10.3.2).

80M-2 has better performance (FLS1-3) than 80M-1 and 80M-Cyl where thrust force is large and wave kinematics less, but the damage is significantly increased (FLS4-10) with the increase in wave kinematics. It is reminded that these comparisons are in relation to the base case.

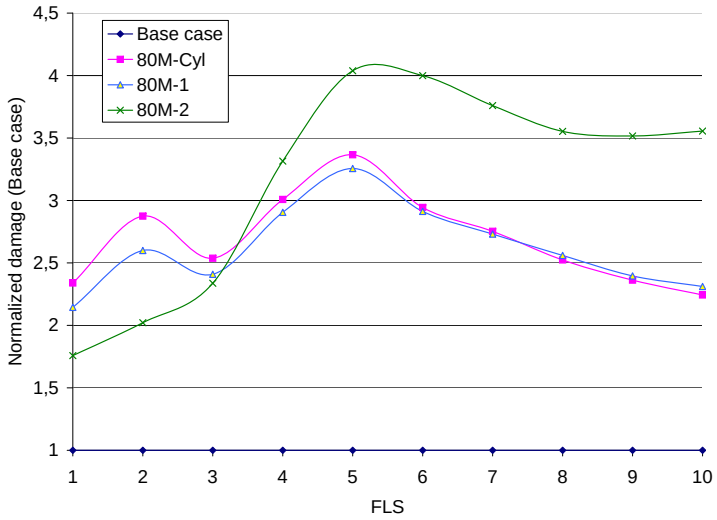

Figure 10.6: Comparison of damage for all FLS cases and configurations normalized on base case. Each FLS case damage for each configuration is normalized by the base case damage for each FLS case.

In terms of the total damage given in Table 10.3 it is interesting to see for which FLS cases the configurations accumulate its respective damage. Each FLS case for each configuration is normalized by the configuration's total damage and is shown in Figure 10.7.

Referring to Figure 10.7 FLS3 is clearly identified as the largest contributor to the damage for all configurations, the combination of high thrust force, moderate sea state and the third highest probability of occurring FLS case (P(FLS3) = 0.173) are the driving factors.

In the range FLS4-6 it is seen that base case and 80M-2 deviate from 80M-Cyl and 80M-1, which is probably because of the wave kinematics with depth (see Section 10.3.1) where the base case has larger restoring due to a longer draft and 80M-2 has larger overall diameter which increases the wave forces induced. It is reminded that the plots in Figure 10.7 includes the relative probability of occurrence for each FLS case.

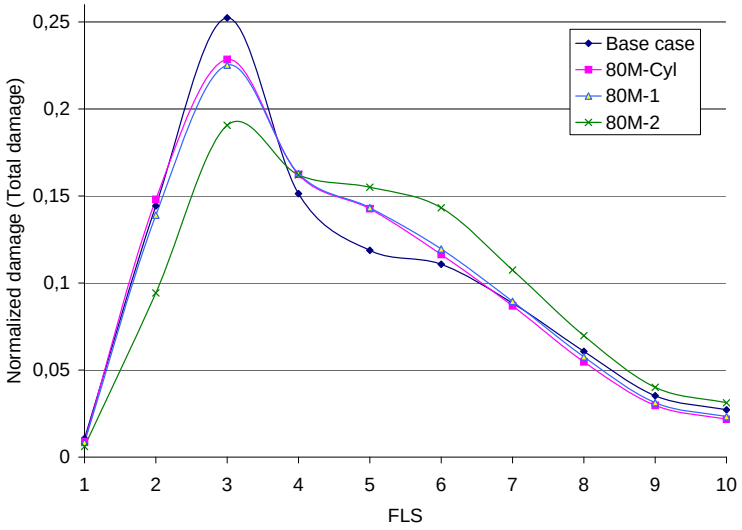

Figure 10.7: Comparison of relative damage ($D(H_s)P(H_s)$) for all FLS cases and configurations normalized on total damage. Each FLS case for each configuration is normalized by total damage (see equation 9.15) for each configuration.

The damage induced in each analysis uncorrelated to the FLS case relative probability of occurrence is shown in Figure 10.8. With increasing FLS case the wind thrust is of less importance (the reader may refer to Section 9.6.4) and wave kinematics induces large fatigue damage in the structure which is expected and clear from Figure 10.8 for all configurations. This also illustrate the importance of accounting for the load cases relative probability of occurrence when analysing structures with stochastic loading, where decisions must be made on the basis of determined probability levels.

What also should be observed from Figure 10.8, is that the long draft of the base case proves for excellent hydrodynamic properties with increasing wave kinematics in terms of fatigue compared to the other configurations, which is difficult to maintain when reducing the draft.

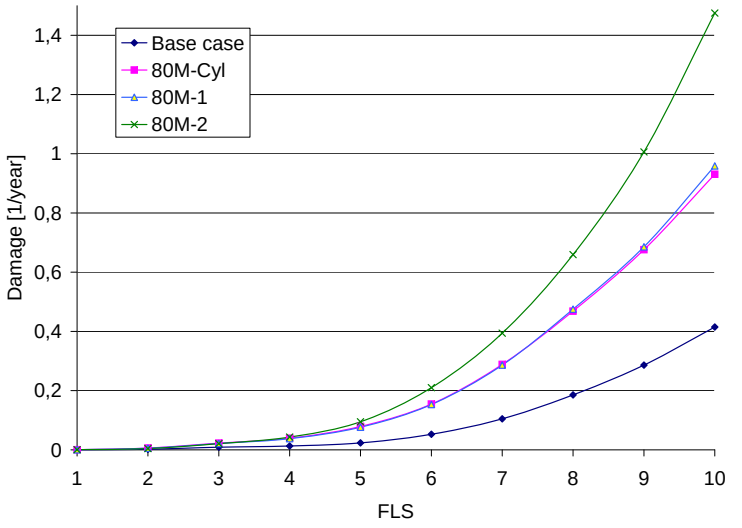

Figure 10.8: Comparison of damage for all FLS cases and configurations based on analysis damage. No normalization.

10.4.4 Heave plate significance

In Figures 10.9 and 10.10 the bending moment spectrum is shown for 80M-Cyl and 80M-1 for all FLS cases. The comparison of spectrums is performed to increase the knowledge of frequency contributions in the loading which gives a better view of the heave plate significance.

The energy differences between 80M-1 and 80M-Cyl in the spectrums are small, as can be expected since the difference in lifetime is minimal, therefore the heave plate dimensions should have been increased to investigate if this would increase the lifetime further for the heave plate configuration. Due to a limited time frame an increase in heave plate dimensions is not performed, but difference in the spectrums can still be observed and is further investigated in the following.

For FLS1 it is observed that 80M-Cyl has more energy for low frequencies due to the wind, this can also be seen FLS2-5 although in a more limiting matter. Based on this it seems that the heave plate configuration withstand wind turbulence in a larger degree.

In terms of pitch resonance it can be seen from FLS2 that there is a relative larger energy part for 80M-Cyl, but the pitch resonance is not larger for 80M-Cyl in all spectrums (the opposite in FLS4) and it can not be concluded that the increase in lifetime is based on better damping alone.

It is seen for all FLS cases that 80M-Cyl has more energy for the higher frequencies of the wave energy in the bending moment, which means 80M-1 seems better for smaller wave periods. The opposite is seen for lower wave frequencies and is in correspondence with earlier discussion in this chapter (see e.g. Section 10.3.2) on the increase in wave induced loads with depth because of the heave plate.

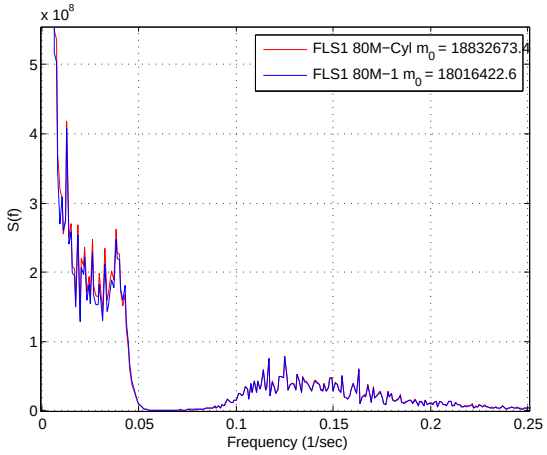

(a) FLS1

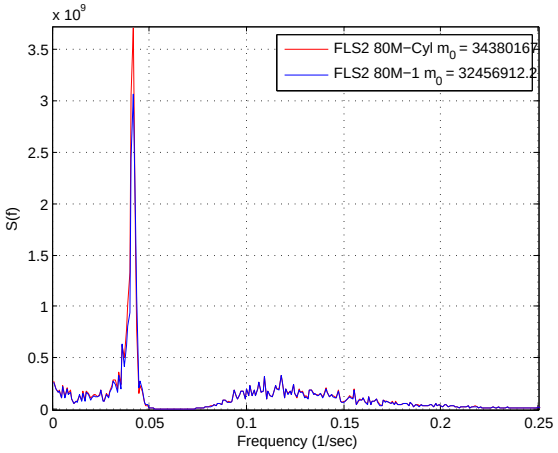

(b) FLS2

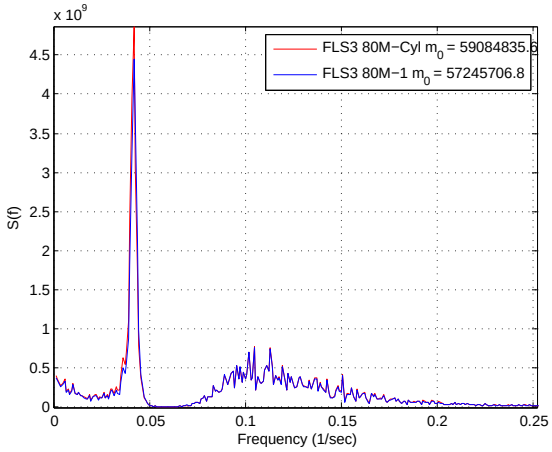

(c) FLS3

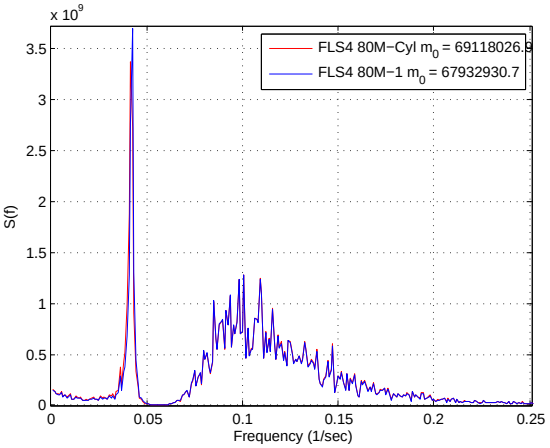

(d) FLS4

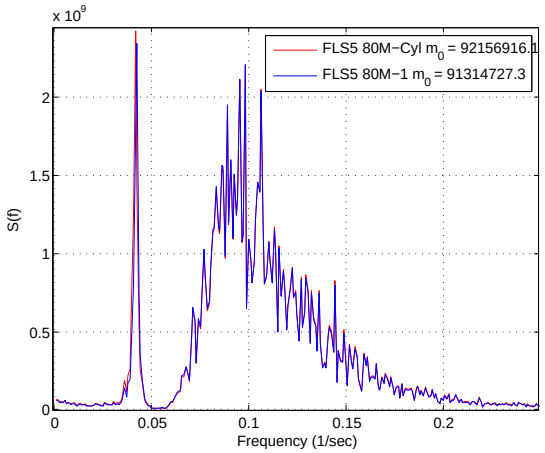

(e) FLS5

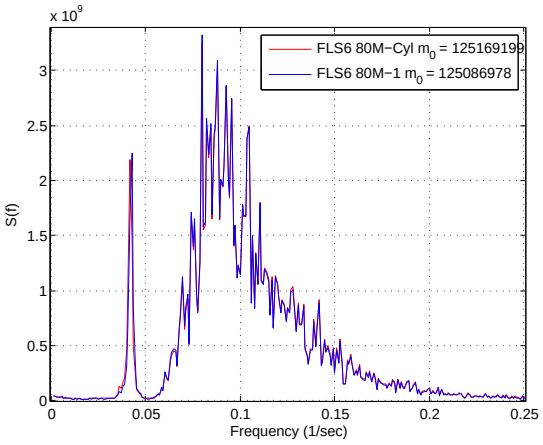

(f) FLS6

Figure 10.9: FLS 80M-Cyl and 80M-1 comparisons power spectrum bending moment.

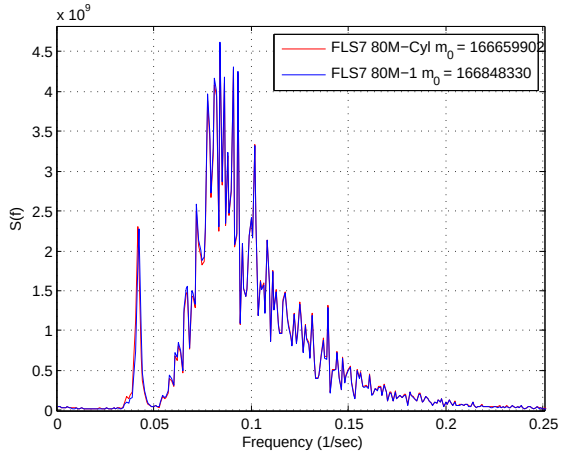

(a) FLS7

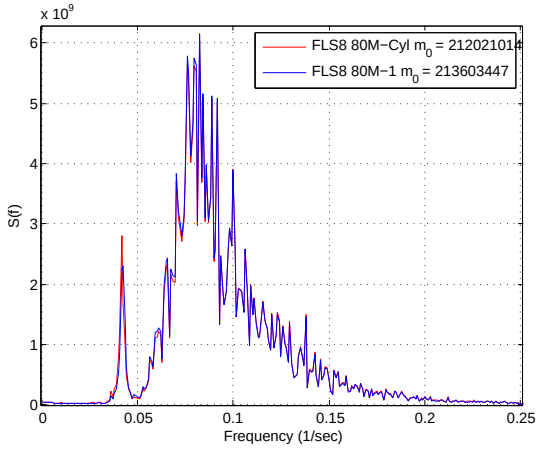

(b) FLS8

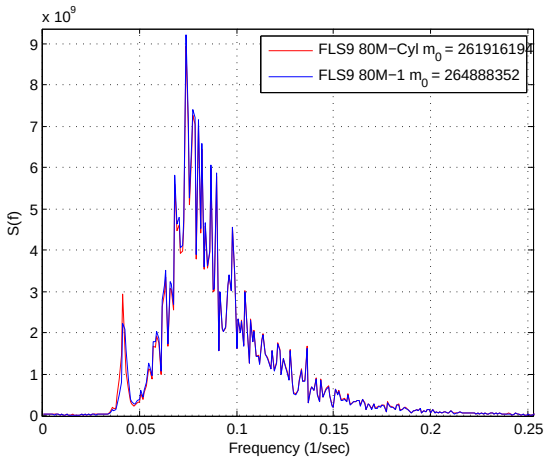

(c) FLS9

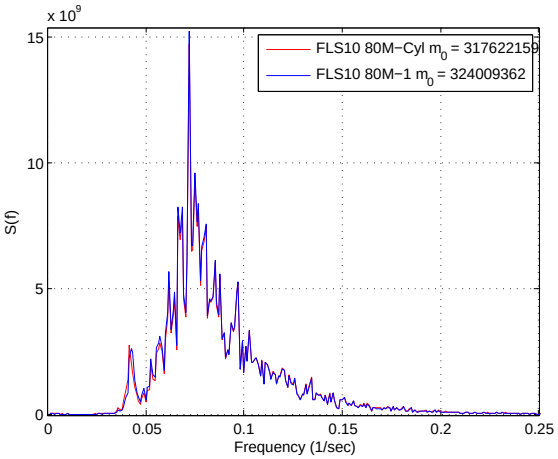

(d) FLS10

Figure 10.10: FLS 80M-Cyl and 80M-1 comparisons power spectrum bending moment. Cont'd

11 Summary, Concluding Remarks and Recommendations for Further Work

11.1 Summary and concluding remarks

The purpose of the thesis work has been to evaluate performance in terms of the fatigue and ultimate limit state for reduced draft configurations of the Hywind concept, where the inclusion of a heave plate has been investigated. To obtain reliability and confidence in the results an important focus with the work has been to lay the foundation and understanding for the analysis parameters, where also consequences has been elucidated. The Hywind concept has introduced new theoretical foundations for wind turbines where especially the negative damping induced at rated power production is of importance.

The support structure's key parameters have been extracted on the base of the static pitch angle and the natural periods with the rigid body motions. The static pitch angle and the natural periods provides the analyst with important limitations in the change of geometry prior to running time consuming dynamic analyses. It is emphasized that the rigid body motions natural periods should be kept out of the range of significant wave energy to avoid excessive motions. The natural period in pitch and heave should also be kept apart due to the Mathieu instability.

A design basis for the heave plate has been established in the thesis work by the panel program WAMIT. An analytical expression for the heave added mass has been found in the literature and is found acceptable with the analyses performed. The surge normalized added mass is on average found to be reduced when introducing the heave plate, and an added mass reduction factor for the segment containing the heave plate has been investigated and utilized in the time domain analyses. The heave plate configurations have also been shown to introduce negligible frequency dependence compared to the bare cylinder configuration. The heave plate also provides additional added mass in heave, which can be utilized as a simple measure to increase the natural period in heave.

Load cases based on the Hywind meteorological and oceanographic design basis have been established in the ultimate limit state (ULS) and fatigue limit state (FLS). The FLS load cases are based on 50-year scatter tables for wave and wind. They have been developed in a conservative manner, joined with wind by the significant wave height and the number of load cases have been limited by weighting the spectral peak period. The ULS load cases have been developed by including 50-year wind and waves as well as a 10-year current, where wind was simplified as a point load by a method named equivalent radius in the thesis.

Thorough investigations have been performed on the 110 m draft base case. Natural periods and hydrodynamic damping have been estimated and related to both theory and model trials on the Hywind concept. Wave energy that induced resonance outside the wave energy range has been investigated, and theory relating to a second order heave

force contribution and the Mathieu instability shows the physical nature and possibility of what is observed, directly related to the analyses. Structural damping in terms of the Rayleigh damping formulation has been investigated and damping coefficients related to the first bending mode established. The 1P and 3P frequencies in wind turbine engineering have been defined and the 3P frequency is found to be in the vicinity of the first bending mode frequency of the base case, but further studies have not been performed due to limitations in the wind thrust code utilized.

The importance of a wind turbine control system which strives for active damping at rated power production, simulated by a notch filter in the analyses, has been shown for the base case. The increase in lifetime from 73 to 164 years by including the notch filter clearly illustrate this importance. The notch filter parameters have also been evaluated and the author recommends using a steep filter to avoid filtering out other motions than the pitch natural frequency. The importance of including both waves and wind is emphasized, where only including waves increased the lifetime assessment to 309 years for the base case.

By reducing the draft with 30 m the lifetime is decreased from 164 to 61 years for the heave plate configuration (80M-1). The reduction in lifetime is mainly related to the reduction in draft and is identified as a challenge for taking the Hywind concept to shallower depths. Increasing dimensions for the reduced draft configuration has also been shown to reduce the lifetime. Although the heave plate configuration has a minimal improvement compared to the bare cylinder configuration with the dimensions utilized, the present study shows an improvement and increasing the heave plate dimensions may increase the lifetime further.

The ULS analyses have shown that the wave induced motions are larger for the reduced draft configurations and increasing dimensions further amplifies this. It is also seen from the ULS that the heave plate configuration has better dynamic performance in heave motion, but worse in dynamic pitch motion than the bare cylinder configuration. The bending moment in the ULS condition is not deemed as critical based on a check of yielding at the mean water line, it is however emphasized that all cross sections should be checked in a complete study due to variations in dimensions over the structure. The ULS analyses have also served to increase the understanding of the FLS analyses, by providing more knowledge of the behavior in an extreme sea state.

The special purpose computer codes SIMO/TDHMILL and RIFLEX have proven advantageous for the analysis of the floating offshore wind turbine concepts in the thesis work, and with the developed Matlab scripts fast and reliable post processing has been achieved. The developed Matlab scripts has been written for the use with the utilized computer codes, but have been developed with generality in mind for the use with other computer codes as well as usability for others than the author. The developed batch script has also been of outmost importance during the thesis work and should prove useful for others running coupled analyses with the special purpose computer codes.

11.2 Recommendations for further work

It is recommended in direct relation with the present study to increase the heave plate dimensions to investigate any further improvements in fatigue life, and also to have a better view of the frequency contributions in the bending moment. It should be mentioned that by increasing the heave plate dimensions wave induced forces can be of a larger concern at the bottom and may not increase the lifetime. As the basis for analyses on heave plate configurations are presented in the study, utilizing the information herein is directly applicable for further analyses.

An important factor which has barely been discussed in the thesis is the mooring lines. They may prove as a limiting factor for taking the Hywind concept to shallower waters and should thus be thoroughly investigated for reduced draft configurations in shallower depths. Clearing, line segment length and composition, attachment point, clump weight, buoyancy elements, pretension and bridle arrangement are all mentioned as possible characteristics to investigate for mooring lines in shallower depths.

Resonance within pitch motion has been shown to play an important role in the lifetime assessments. Increasing the active pitch motion damping potential of the wind turbine control system is under research and could also serve as an interesting topic for a master student with a background in cybernetics. An increase in pitch damping by the attaching vertical strakes (increase shedding of eddies) to the hull can also serve as an interesting research topic, and it is mentioned that the placement starting from the keel, where wave kinematics are less, should be investigated.

It has been experienced by the author that changing geometry, pre-analysis in terms of verifications of damping and natural periods, running the coupled analyses for a number of loading conditions and post-processing the results is a time consuming task. The entire process could be further improved by programming a streamlined shell around it, coupling all of the underlying processes. This can be highly advantageous in optimization studies on the Hywind concept and other similar concepts as the heave plate configuration.

Bibliography

[1] Finn Gunnar Nielsen. Tuning the geometric and mass properties of hywind. *Statoil (Internal document)*, 2009.

[2] Longbin Tao and Shunqing Cai. Heave motion supression of a spar with a heave plate. *Elsevier Ltd.*, 2003.

[3] H. A. Haslum and O. M. Faltinsen. Alternative shape of spar platforms for use in hostile areas. *Offshore Technology Conference, Houston, Texas.*, 1999.

[4] F. J. Fischer and R. Gopalkrishnan. Some observations on the heave behaviour of spar platforms. *Journal of Offshore Mechanics and Arctic Engineering*, 1998.

[5] O. M. Faltinsen. *Sea loads on ships and offshore structures.* Cambridge university press, 1990.

[6] Geir Moe. *Kompendium, Introduksjon til bø lger og bø lgekrefter.* Department of structural engineering, NTNU, 2005.

[7] Einar Strømmen. *Theory of Bridge Aerodynamics.* Springer-Verlag Berlin Heidelberg, 2006.

[8] International standard. *IEC 61400-1: Wind turbines - Part 1: Design requirements*, 3rd edition, 2007.

[9] International standard. *IEC 61400-3: Wind turbines - Part 3: Design requirements for offshore wind turbines*, 1st edition, 2009.

[10] J.F. Manwell, J.G. McGowan, and A.L. Rogers. *Wind Energy Explained - Theory, Design and Application.* John Wiley and Sons Ltd, 2002.

[11] Turgut Sarpkaya and Michael Isaacson. *Mechanics of wave forces on offshore structures.* Litton Educational Publishing, Inc., 1981.

[12] John Nicholas Newman. Transient axisymmetric motion of a floating cylinder. *Journal of Fluid Mechanics, 157 , pp 17-33*, 1985.

[13] Finn Gunnar Nielsen. Design brief for offshore floating wind-mills. *Statoil (Internal document)*, 2007.

[14] Karl Rottmann. *Matematisk formelsamling.* Spektrum forlag, 2003.

[15] Tor David Hanson (Statoil). Personal communication, 2010.

[16] Finn Gunnar Nielsen. *Lecture notes in marine operations.* Department of marine hydrodynamics, NTNU, 2007.

[17] Rune Yttervik. TDHMILL3D - User documentation. *Statoil (Internal document)*, 2009.

[18] Bjørn Skaare. Matlab notch filter plot (notchfilterplot.m). *Statoil (Internal file)*, 2010.

[19] MARINTEK. *RIFLEX Theory Manual*, 2008.

[20] MARINTEK. *SIMO - User's Manual*, 2008.

[21] MARINTEK. *RIFLEX User Manual*, 2008.

[22] Det Norske Veritas (DNV). *Fatigue Design of Offshore Steel Structures (DNV-RP-C203)*, 2008.

[23] P.A. Brodtkorb, P. Johannesson, G. Lindgren, I. Rychlik, J. Rydén, and E. Sjö. WAFO - a Matlab toolbox for the analysis of random waves and loads. In *Proc. 10'th Int. Offshore and Polar Eng. Conf., ISOPE, Seattle, USA*, volume 3, pages 343–350, 2000.

[24] American Society for Testing and Materials (ASTM). *Standard Practices for Cycle Counting in Fatigue Analysis, E 1049*, 2005.

[25] Einar Nygaard and Martin Mathiesen. Hywind metocean design basis. *MBM-MGE-RA 32, Statoil (Internal document)*, 2008.

[26] Frank M. White. *Fluid mechanics, 6th edition*. McGraw-Hill, 2008.

[27] Rune Yttervik (Project manager). Model test of offshore floating wind turbine. *Statoil (Internal document)*, 2006.

[28] Finn Gunnar Nielsen (Statoil). Personal communication, 2010.

[29] Anil K. Chopra. *Dynamics of structures. Theory and applications to earthquake engineering*. Pearson Prentice Hall, 2007.

[30] Fridtjov Irgens. *Formelsamling mekanikk*. Tapir Akademisk Forlag, 1999.

[31] The MathWorks. *Matlab Documentation, Version: R2008b*, 2008.

[32] Nils Rune Sødahl. *Methods for Design and Analysis of Flexible Risers*. PhD thesis, The Norwegian Institute of Technology (NTH), 1991.

[33] Rune Yttervik (Statoil). Personal communication, 2010.

[34] Microsoft Corporation. *Office Excel Manual*, 2003.

Appendices

A Matlab Scripts

Presented here are some of the Matlab scripts developed throughout the thesis, the scripts found here are referred to in the thesis text. With the author's background within computer programming, attention has been made to write fast, reliable and easy to use scripts.

The Matlab scripts can be found in their native form in the folder /Matlab/ on the attached disk. The Matlab folder on the attached disk also includes other Matlab scripts developed in the thesis work, which may prove beneficial for further work, but only scripts referred to in the text are given here to reduce the size of the appendix.

A.1 Dispersion relation

```
%%%%%%%%%%%%%%%%%%%%%%%%%%%%%%%%%%%%%%%%%%%%%%%%%%%%%%%%%%%%%%%%%%%%%%%%%%%%%%%
% Script for solving the dispersion relation for different wave periods   %
% Wave periods of T = [4,20] [s] are typical.                             %
%                                                                         %
% Eirik Wie Furunes                                                       %
% Spring 2010                                                             %
%%%%%%%%%%%%%%%%%%%%%%%%%%%%%%%%%%%%%%%%%%%%%%%%%%%%%%%%%%%%%%%%%%%%%%%%%%%%%%%
clc
clear all
close all

%%%%%%%%%%%%%%%%%%%%%%%%%%%%%%%%%% input %%%%%%%%%%%%%%%%%%%%%%%%%%%%%%%%%%%%%%
d = 220; % depth [m]
D = 9.5; % cylinder diameter [m]
T = 4:.5:20; % periods [s]
initial_guess = 1; % initial guess for wavenumber used in fsolve


%%%%%%%%%%%%%%%%%%%%%%%%%%%%%%%% calculations %%%%%%%%%%%%%%%%%%%%%%%%%%%%%%%%

g = 9.81; % acc. gravity [m/s^2]

omega = (2*pi)./T; % wave frequency [rad/s]
L = zeros(1,length(omega)); % preallocating wavelength [m]
dL_ratio = zeros(1,length(omega)); % preallocating depth
                                   % divided by wavelength


% solve the dispersion relation by the wavenumber k for each wave period T
for i=1:length(omega);
    dispersion = @(k) omega(i).^2 - g.*k*tanh(k.*d); % dispersion relation
    options=optimset('Display','off');
    k_res = fsolve(dispersion,initial_guess,options);

    % compute wavelength from wave number
    L(i) = (2*pi)./k_res;
```

```
    % ratio for small body approximation
    dL_ratio(i) = L(i)/D;
end


%%%%%%%%%%%%%%%%%%%%%%%%%%%%%%%% plots %%%%%%%%%%%%%%%%%%%%%%%%%%%%%%%%

% Plot wave lengths versus periods
figure(1)
plot(T,L);
grid on
xlabel('Wave periods, T [s]')
ylabel('Wavelenght, L [m]')
title('Dispersion relation')


% Plot wavelenght / diameter versus limit of 5
figure(2)
plot(T,dL_ratio);
hold on
xlabel('Wave periods, Tp [s]')
ylabel('\lambda/D [-]')

plot([T(1) T(length(T))],[5 5],'black');
legend(['\lambda/D = \lambda/',num2str(D),],'\lambda/D = 5','Location',...
'NorthWest')
title('Slender body')
grid on

%%%%%%%%%%%%%%%%%%%%%%%%%%%%%%%% eof %%%%%%%%%%%%%%%%%%%%%%%%%%%%%%%%
```

A.2 Decay script

```
%%%%%%%%%%%%%%%%%%%%%%%%%%%%%%%%%%%%%%%%%%%%%%%%%%%%%%%%%%%%%%%%%%%%%%%%%%%%%%%
% Decay calculations                                                            %
%                                                                               %
% In heave, an equilibrium position from the static analysis can be             %
% difficult to obtain, derfor it is recommended to apply the load after         %
% some time.                                                                    %
% The equilibrium position is then calculated as the mean and a threshold       %
% stops decay calculations based on 2x the standard deviation - this is         %
% to minimize error.                                                            %
%                                                                               %
% For the other modes the equilibrium is taken as the first entry in the        %
% global coordinate system.                                                     %
%                                                                               %
% Modes:                                                                        %
%   surge: x translation                                                        %
%   sway:  y translation                                                        %
%   heave: z translation                                                        %
%   pitch: rotation about y-axis                                                %
%   roll:  rotation about x-axis                                                %
%                                                                               %
% Eirik Wie Furunes                                                             %
% Spring 2010                                                                   %
%%%%%%%%%%%%%%%%%%%%%%%%%%%%%%%%%%%%%%%%%%%%%%%%%%%%%%%%%%%%%%%%%%%%%%%%%%%%%%%
clc
clear all
close all

%%%%%%%%%%%%%%%%%%%%%%%%%%%%%%%%%% input %%%%%%%%%%%%%%%%%%%%%%%%%%%%%%%%%%%%

load 'C:\Analyses\80M-Cyl\Damping - Natural periods\noddis.asc'; % load file

node = 8; % node to extract data from, COG - almost uncoupled motions

mode = 3; % 1 is surge, 2 is sway, 3 is heave, 4 is roll, 5 is pitch

time_before = 400; % time before load is applied [s] RIFLEX: TIMEON
                   % heave calculations are dependent on this to have
                   % a satisfying equilibrium position

time_load = 140; % how long the load is applied for [s]
                 % RIFLEX: TIMEOFF - TIMEON
                 % to remove the first amplitude this can be extended

time_end = 800;    % how much of the timeseries to extract after loading
                   % time_end = 0, is until end of timeseries

%%%%%%%% mode = 4 or 5, extra data for pitch/roll calculations

node_extra = 20; % Select a node different from the one before


%%%%%%%%%%%%%%%%%%%%%%%% read relevant data from files %%%%%%%%%%%%%%%%%%%%%%%

time = noddis(:,1); % time

% displacements, time is in column 1 so node 1 is in column 2, etc.
x = noddis(:,node*3 - 1); % x-dir
y = noddis(:,node*3); % y-dir
z = noddis(:,node*3 + 1); % z-dir
```

```
if mode == 5 && node_extra ≠ 0
    x_2 = noddis(:,node_extra*3 - 1); % x-dir
    z_2 = noddis(:,node_extra*3 + 1); % z-dir
end

if mode == 4 && node_extra ≠ 0
    y_2 = noddis(:,node_extra*3); % x-dir
    z_2 = noddis(:,node_extra*3 + 1); % z-dir
end


dt = time(2)-time(1); % timestep [s]

%%%%%%%%%%%%%%%%%%%%%%%%%%%%%% calculations %%%%%%%%%%%%%%%%%%%%%%%%%%%%%%

total_r = floor(1 + (time_before + time_load)/dt); % points to remove
trans_r = floor(1 + time_before/dt); % transitive points
trans_s = floor(1 + time_before/(2*dt)); % half of transitive

if time_end == 0
    time_end = length(time);
else
    time_end = time_end/0.2;
end

% zp is the mean of the last half of the transitive state
% zp gives the z coordinate around which the system oscillates
% disp is the amplitudes with zp as reference line
% entire variable is entire time series

%  threshold parameter
std_z = 0.01;

if mode == 1
    zp = 0; % correct static position for mode 1
    entire = x;
    disp = entire(total_r:time_end) - zp;

elseif mode == 2
    zp = 0; % correct static position for mode 2
    entire = y;
    disp = entire(total_r:time_end) - zp;

elseif mode == 3
    zp = mean(z(trans_s:trans_r)); % take mean of the upper half transitive
    std_z = std(z(trans_s:trans_r));
    entire = z;
    disp = entire(total_r:time_end) - zp;

elseif mode == 4 && node_extra ≠ 0
    length_node = z(1) - z_2(1); % length between nodes
    y_rel = y - y_2; % relative y translational distance

    % calculate angle between nodes
    entire = (asin(y_rel./length_node))*(180/pi); % (rad) -> deg
    disp = entire(total_r:time_end);

elseif mode == 5 && node_extra ≠ 0
    length_node = z(1) - z_2(1); % length between nodes
    x_rel = x - x_2; % relative x translational distance

    % calculate angle between nodes
    entire = (asin(x_rel./length_node))*(180/pi); % (rad) -> deg
```

```
    disp = entire(total_r:time_end);

end


% counter for new vectors
j = 1;

% go through displacement amplitudes and store peaks and troughs
for i=2:(length(disp) -1)
    if disp(i-1) < disp(i) && disp(i) > disp(i+1) && disp(i) > 2*std_z
        amp(j) = disp(i);
        time_d(j) = dt*i;
        j = j+1;
    end
end

% calculate periods and damping
for i=1:length(amp)-1
    ld(i) = log(amp(i)/amp(i+1));
    Td(i) = (time_d(i+1) - time_d(i));
    ratio(i) = ld(i)/(sqrt(4*pi^2 + ld(i)^2));
    Tn(i) = Td(i)*sqrt(1-ratio(i)^2);
end

% Mean of periods
T_damped = mean(Td)
T_undamped = mean(Tn)
Ratio_mean = mean(ratio)


%%% Linear and quadratic damping

% from measurements
p = ((4*pi)./Tn).*ld./(sqrt(4*pi^2 + ld.^2));

for i=1:length(amp)-1
   ampT(i) =  (16/3)*(amp(i+1)+(amp(i)-amp(i+1))/2)/(Td(i));
end

% fit a poly of order 1
p_fit = polyfit(ampT,p,1)

%%%%%%%%%%%%%%%%%%%%%%%%%%%%%%%% plots %%%%%%%%%%%%%%%%%%%%%%%%%%%%%%%%%%%%%%%%

% plot signal and signal used
scrsz = get(0,'ScreenSize');
figure('OuterPosition',[1 scrsz(4)/2 scrsz(3)/2.2 scrsz(4)/2.2])

subplot(2,2,[1 2])
plot(time,entire)
xlabel('Time [s]')

if mode == 4 || mode == 5
    ylabel('Displacement [deg]')
else
    ylabel('Displacement [m]')
end
title(['Decay signal, Tn = ',num2str(T_undamped),' [s]'])
grid on

subplot(2,2,3)
plot(time(total_r:time_end),disp)
```

```
xlabel('Time [s]')

if mode == 4 || mode == 5
    ylabel('Displacement [deg]')
else
    ylabel('Displacement [m]')
end
title(['Signal used for decay calculations, \zeta = ',num2str(Ratio_mean)])
grid on

% plot linear and quadratic damping estimates
subplot(2,2,4)
plot(ampT,p,'+',ampT,p_fit(1)*ampT + p_fit(2),'b')
xlabel('(16/3) Xi/Td [m/s]')
ylabel('p [1/s]')
grid on

damp_con = ['p1=',num2str(p_fit(2)),' [1/s], p2=',num2str(p_fit(1)),' [1/m]']
title(damp_con)

%%%%%%%%%%%%%%%%%%%%%%%%%%%%%%%% eof %%%%%%%%%%%%%%%%%%%%%%%%%%%%%%%%%%%%%%%%
```

A.2.1 Verification study

To verify the results obtained by the script another script supplied by Finn Gunnar Nielsen was used. The script supplied simulates a system with linear stiffness and linear damping. To be able to verify the quadratic damping estimation the script was extended to include quadratic damping as well.

The verification is done as follows. The system is given an initial offset and released with no external forces acting. The damping coefficients in the equation of motion is varied and compared to the damping coefficients obtained by the decay script shown in the previous section. Table A.1 shows verification cases, the tabulated values do not show an exact recreation of the coefficients but is deemed acceptable. A visualization of the decay signal and interpolation is shown in Figure A.1 for case 4.

	Simulation script		Decay script		% difference	
Case	p1	p2	p1	p2	p1	p2
1	0	0.0512	-0.001	0.0504	0	1.57
2	0.0310	0	0.0286	0	8	0
3	0.0310	0.0512	0.0289	0.0504	7	1.57
4	0.1550	0.0854	0.1531	0.0822	1.23	3.8
5	0.1550	0.8537	0.1556	0.7939	0.39	7.2

Table A.1: Simulated and estimated damping coefficients. p1 [1/s], p2 [1/m].

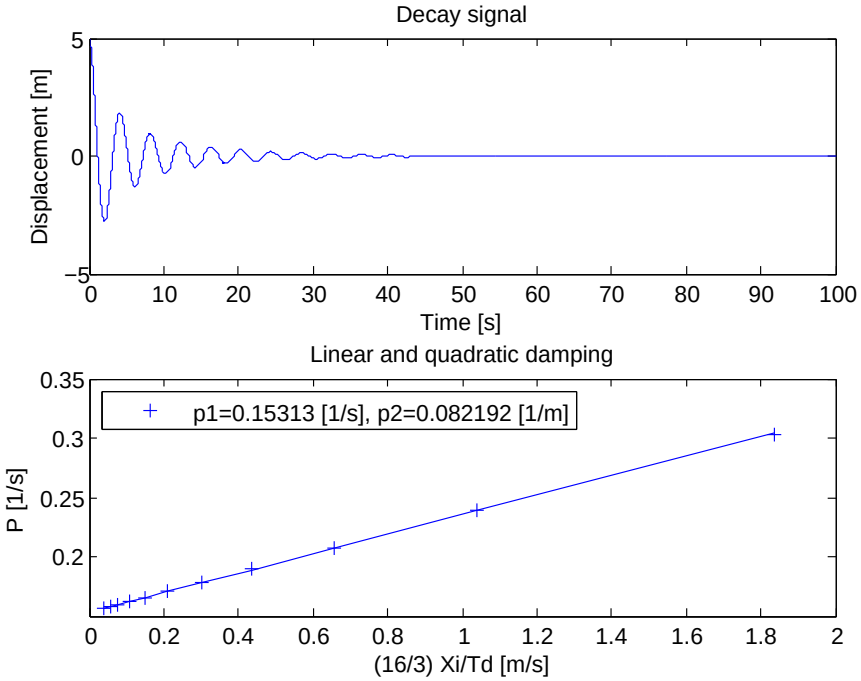

Figure A.1: Case 4: Decay signal and damping estimates

A.3 Fatigue calculations

```
%%%%%%%%%%%%%%%%%%%%%%%%%%%%%%%%%%%%%%%%%%%%%%%%%%%%%%%%%%%%%%%%%%%%%%%%%%%%%%%
% Script for calculating fatigue damage based on rainflow counting,       %
% Palmgren-Miner accumulated damage and DNV-RP-C203                       %
%                                                                         %
% Requires: WAFO-Toolbox (http://www.maths.lth.se/matstat/wafo/)          %
%                                                                         %
% Eirik Wie Furunes                                                       %
% Spring 2010                                                             %
%%%%%%%%%%%%%%%%%%%%%%%%%%%%%%%%%%%%%%%%%%%%%%%%%%%%%%%%%%%%%%%%%%%%%%%%%%%%%%%
clc
clear all
close all


%%%%%%%%%%%%%%%%%%%%%%%%%%%%%%%%%% input %%%%%%%%%%%%%%%%%%%%%%%%%%%%%%%%%%%%%%%%

dir = 'C:\Analyses\80M-1\FLS-NOTCH\FLS10\'; % Directory with elmfor.asc

% store fatigue results
% store = 1. Storage and plot.
% store = 2. Storage without plot.
% store = 0. No storage, but plot.
% file is stored in subfolder of specified dir (..//)
store = 0;

% file read input
el_col = 2; % Starting column for force extraction,
              % ie. DOF = 1. for relevant node. Refer to key_elmfor.txt

el_end = 1; % Element end, 1 or 2, required for moment and shear force.


% cross section input
D = 6; % Cross section outer diameter [m]
t = 0.035; % Cross section thickness [m]

% fatigue specific input
trans_time = 400; % removal of transitive state [s].

division = 1000; % division of stress amplitude range [-].
                 % eg. stress range 0 - 100 MPa. A division of 10 will
                 % divide into buckets of 10 MPa
                 % Should never be less than 20 (DNV-RP-C203)

%%%%%%%%%%%%%%%%%%%%%%% DNV-RP-C203 parameters %%%%%%%%%%%%%%%%%%%%%%%%%%%%%%%

% Table 2-2 S-N curves in seawater with cathodic protection - D curve

t_ref = 0.025; % (2.4.3) Reference thickness (welded connections) [m]
k = 0.20; % (2.4.3) thickness exponent
N_lim = 10^6;

% N ≤ 10^6 cycles
m_1 = 3; % (2.4.3) negative inverse slope of the S-N curve [-]
log10_a_1 = 11.764; % (2.4.3) intercept of log N axis [-]

% N > 10^6 cycles
m_2 = 5; % (2.4.3) negative inverse slope of the S-N curve [-]
log10_a_2 = 15.606; % (2.4.3) intercept of log N axis [-]
```

```
%%%%%%%%%%%%%%%%%%% read relevant data from files %%%%%%%%%%%%%%%%%%%%%%%%%

eval(['load ''',dir,'elmfor.asc''',';']); % load element forces from file

time = elmfor(:,1); % time [s]

% element forces
axial = elmfor(:,el_col); % DOF 1

if el_end == 1
    mom_y = elmfor(:,el_col+2); % DOF 3
else
    mom_y = elmfor(:,el_col+3); % DOF 4
end

clear elmfor; % clear up memory

%%%%%%%%%%%%%%%%%%%%%%%%%%%% calculations %%%%%%%%%%%%%%%%%%%%%%%%%%%%%%%%

dt = time(2) - time(1); % timestep

trans_r = floor(1 + trans_time/dt); % number of transitive steps [-]


r_o = D/2; % outer radi
r_i = r_o - t; % inner radi

A = pi*(r_o^2-r_i^2); % area
W = (pi/(4*r_o))*(r_o^4-r_i^4); % section modulus

%preallocate for speed, also secure zero stress in transitive state.
s = zeros(length(time),1);

% loop through timeseries and calculate stress, ignore transitive.
for i=trans_r:length(time);
    s(i) = -mom_y(i)/W; % stress, positive mean is most conservative

end

%convert from [kN/M^2] to [MPa]
s = s./(1e3);


%%%%%%%%%%%% rainflow counting

tp = dat2tp([time s],0.05,'none');   % Turning points, filter out noise.
                                     % Noise defined as second parameter

rfc = tp2rfc(tp); % Rainflow cycles (residual included), 4-point algorithm.

stress_range = rfc(:,2)-rfc(:,1); % Stress range, (Smax - Smin).

[n_cycles,ds] = hist(stress_range,division); % freq. count and bin locations


%%%%%%%%%%%% DNV-RP-C203 S-N curve
% log N = log10(a) - m*log10(Δ_sigma*(t/t_ref)^k)

damage = 0; % accumulated damage

for i=1:length(ds)
    log_N = log10_a_1 - m_1*log10(ds(i)*(t/t_ref)^k);
```

```
    if 10^log_N > N_lim
        log_N = log10_a_2 - m_2*log10(ds(i)*(t/t_ref)^k);
    end

    damage = damage + n_cycles(i)/(10^log_N);
end

% damage in a year
damage_year = damage*(60*60*24*365)/(time(length(time))-time(trans_r));

life = round((1/damage_year)); % life in years
disp(['Directory: ',dir])
disp([' '])
disp(['Fatigue life: ',num2str(life),' years'])
disp([' '])
disp(['Mean stress: ',num2str(mean(s)),' [MPa]'])
disp(['Standard deviation stress: ',num2str(std(s)),' [MPa]'])


%%%%%%%%%%%%%%%%%%%%%%%%%%%%%%%% plots %%%%%%%%%%%%%%%%%%%%%%%%%%%%%%%%%%%%%%%%

if store ~= 2
    figure (1)

    subplot(2,1,1)
    plot(time,s)
    xlabel('time [s]')
    ylabel('Stress [MPa]')
    title('Stress timeseries','FontWeight','bold')
    grid on
    axis tight

    subplot(2,1,2)
    hist(stress_range,division)
    ylabel('Number of cycles [-]')
    xlabel('Stress [MPa]')
    title(['Stress range histogram. Fatigue life: ',...
            num2str(life),' years'],'FontWeight','bold')
end

%%%%%%%%%%%%%%%%%%%%%%%%%%%%%%%% storage %%%%%%%%%%%%%%%%%%%%%%%%%%%%%%%%%%%%%%%%
if store == 1 || store == 2
    eval(['cd ''',dir,'''',';']);
    fid = fopen('..//fatigue_res.eifu','a');
    fprintf(fid,'%60s\n',['Filedir: ''',dir,''' Damage in a year: ',...
            num2str(damage_year),', Life in years: ',num2str(life),...
            ', Mean stress: ',num2str(mean(s)),', [MPa] ',...
            ' Standard deviation stress: ',num2str(std(s)),' [MPa]']);
    fclose(fid);
    fid = fopen('..//fatigue_res_excel.eifu','a');
    % Fatigue damage, Std stress. Easy to use excel format
    fprintf(fid,'%60s\n',[num2str(damage_year),'    ',num2str(std(s)),' ']);
    fclose(fid);
end

%%%%%%%%%%%%%%%%%%%%%%%%%%%%%%%% eof %%%%%%%%%%%%%%%%%%%%%%%%%%%%%%%%%%%%%%%%%
```

A.4 Envelope of forces

```
%%%%%%%%%%%%%%%%%%%%%%%%%%%%%%%%%%%%%%%%%%%%%%%%%%%%%%%%%%%%%%%%%%%%%%%%%%%%%%%
% Reads element forces and extracts an envelope with maximum force        %
% distribution over structure.                                            %
%                                                                         %
% Requires: Model length information which can be aquired from stamod.res %
%                                                                         %
% Eirik Wie Furunes                                                       %
% Spring 2010                                                             %
%%%%%%%%%%%%%%%%%%%%%%%%%%%%%%%%%%%%%%%%%%%%%%%%%%%%%%%%%%%%%%%%%%%%%%%%%%%%%%%
clc
clear all
close all

%%%%%%%%%%%%%%%%%%%%%%%%%%%%%%%%% input %%%%%%%%%%%%%%%%%%%%%%%%%%%%%%%%%%%%%%%

load 'C:\Analyses\80M-2\ULS\ULS3\elmfor.asc'; % Load file
load 'C:\Analyses\80M-2\ULS\ULS3\nodes.eifu'; % Model length information.

%%%%%%%%%%%%%%%%%%%% read relevant data from files %%%%%%%%%%%%%%%%%%%%%%%%%%
dof = 10; % number of dofs
time = elmfor(:,1); % time

el_end = 2; % Element end, 1 or 2, required for moment and shear force.

% file read input
el_col_s = 2; % Starting column for force extraction,
              % ie. DOF = 1. for relevant element. Refer to key_elmfor.txt

el_col_e = length(elmfor(1,:)); % ending column for force extraction,
                                % ie. dof 10 for relevant element


% element forces
axial = elmfor(:,el_col_s:dof:el_col_e-9); % DOF 1

torsion = elmfor(:,el_col_s+1:dof:el_col_e-8); % DOF 2

if el_end == 1
    mom_y = elmfor(:,el_col_s+2:dof:el_col_e-7); % DOF 3
else
    mom_y = elmfor(:,el_col_s+3:dof:el_col_e-6); % DOF 4
end

if el_end == 1
    mom_z = elmfor(:,el_col_s+4:dof:el_col_e-5); % DOF 5
else
    mom_z = elmfor(:,el_col_s+5:dof:el_col_e-4); % DOF 6
end

if el_end == 1
    shear_y = elmfor(:,el_col_s+6:dof:el_col_e-3); % DOF 7
else
    shear_y = elmfor(:,el_col_s+7:dof:el_col_e-2); % DOF 8
end

if el_end == 1
    shear_z = elmfor(:,el_col_s+8:dof:el_col_e-1); % DOF 9
else
    shear_z = elmfor(:,el_col_s+9:dof:el_col_e); % DOF 10
end
```

```
clear elmfor; % clear up memory

%%%%%%%%%%%%%%%%%%%%%%%%%%%%%%%% calculations %%%%%%%%%%%%%%%%%%%%%%%%%%%%%%%%

ref_line = nodes(:,4); % create a reference line based on configuration
%ref_line = (1:1:length(axial(1,:))); % non-length reference line

% min_max: row is node, column is min max for each force. i.e 12 col.
min_max = zeros(length(axial(1,:)),12);

col = 0;
for i=1:length(min_max(:,1));
    min_max(i,1) = min(axial(:,i));
    min_max(i,2) = max(axial(:,i));
    min_max(i,3) = min(torsion(:,i));
    min_max(i,4) = max(torsion(:,i));
    min_max(i,5) = min(mom_y(:,i));
    min_max(i,6) = max(mom_y(:,i));
    min_max(i,7) = min(mom_z(:,i));
    min_max(i,8) = max(mom_z(:,i));
    min_max(i,9) = min(shear_y(:,i));
    min_max(i,10) = max(shear_y(:,i));
    min_max(i,11) = min(shear_z(:,i));
    min_max(i,12) = max(shear_z(:,i));
end

%%%%%%%%%%%%%%%%%%%%%%%%%%%%%%%% plots %%%%%%%%%%%%%%%%%%%%%%%%%%%%%%%%%%%%%%%%

figure('Name','Envelope, forces over nodes','NumberTitle','off')

    subplot(2,3,1)
    line([0 0],[ref_line(1) ref_line(length(ref_line))],'Color','r');
    hold on
    plot(min_max(:,1),ref_line);
    plot(min_max(:,2),ref_line);
    hold off
    xlabel('[kN]')
    ylabel('[m]')
    title('Axial','FontWeight','bold')
    grid on
    axis tight

    subplot(2,3,2)
    line([0 0],[ref_line(1) ref_line(length(ref_line))],'Color','r');
    hold on
    plot(min_max(:,3),ref_line);
    plot(min_max(:,4),ref_line);
    hold off
    xlabel('[kNm]')
    ylabel('[m]')
    title('Torsion','FontWeight','bold')
    grid on
    axis tight

    subplot(2,3,3)
    line([0 0],[ref_line(1) ref_line(length(ref_line))],'Color','r');
    hold on
    plot(min_max(:,5),ref_line);
    plot(min_max(:,6),ref_line);
    hold off
    xlabel('[kNm]')
    ylabel('[m]')
```

```
    title('Moment-y','FontWeight','bold')
    grid on
    axis tight

    subplot(2,3,4)
    line([0 0],[ref_line(1) ref_line(length(ref_line))],'Color','r');
    hold on
    plot(min_max(:,7),ref_line);
    plot(min_max(:,8),ref_line);
    hold off
    xlabel('[kNm]')
    ylabel('[m]')
    title('Moment-z','FontWeight','bold')
    grid on
    axis tight

    subplot(2,3,5)
    line([0 0],[ref_line(1) ref_line(length(ref_line))],'Color','r');
    hold on
    plot(min_max(:,9),ref_line);
    plot(min_max(:,10),ref_line);
    hold off
    xlabel('[kN]')
    ylabel('[m]')
    title('Shear-y','FontWeight','bold')
    grid on
    axis tight

    subplot(2,3,6)
    line([0 0],[ref_line(1) ref_line(length(ref_line))],'Color','r');
    hold on
    plot(min_max(:,11),ref_line);
    plot(min_max(:,12),ref_line);
    hold off
    xlabel('[kN]')
    ylabel('[m]')
    title('Shear-z','FontWeight','bold')
    grid on
    axis tight

%%%%%%%%%%%%%%%%%%%%%%%%%%%%%% eof %%%%%%%%%%%%%%%%%%%%%%%%%%%%%%%%%%%%%%
```

A.5 Rigid body movements and mode spectrums

```
%%%%%%%%%%%%%%%%%%%%%%%%%%%%%%%%%%%%%%%%%%%%%%%%%%%%%%%%%%%%%%%%%%%%%%%%%%%%%%%
% Adaptive script to check rigid body movements and their spectrums.      %
%                                                                         %
%                                                                         %
% Requires: SPEGEN_T.m, SPEGEN_T_stat.m                                   %
%                                                                         %
% Eirik Wie Furunes                                                       %
% Spring 2010                                                             %
%%%%%%%%%%%%%%%%%%%%%%%%%%%%%%%%%%%%%%%%%%%%%%%%%%%%%%%%%%%%%%%%%%%%%%%%%%%%%%%
clc
clear all
close all


%%%%%%%%%%%%%%%%%%%%%%%%%%%%%%%%% input %%%%%%%%%%%%%%%%%%%%%%%%%%%%%%%%%%%%%%%%
load 'C:\Analyses\Base case\FLS-NOWIND\FLS10\noddis.asc'; % load file

node = 1; % node to output timeseries from

node_pitch = 2; % Select a node larger from previous

trans_time = 400; % removal of transitive state [s]. Does not effect
                  % time series representation

mode_spec = 99;  % 0 = spectrum from all modes, 1 = x, 2 = y, 3 = z, 4 = pitch
                 % anything else => no spectrum

spec_div = 10;  % power spectrum division. for smoothing

norm_heave = 999; % Normalize heave (initial pos - pos)
                  % norm_heave = 999, no normalization
                  % norm_heave = 0, initial position is taken from riflex
                  % norm_heave = value, value is taken as inital position
                  % NB: z is defined as zero at MWL and positive upwards.

print_stat = 0; % print peak value statistics, yes = 0, no = other


%%%%%%%%%%%%%%%%%%%%%%%% read relevant data from files %%%%%%%%%%%%%%%%%%%%%%%%

time = noddis(:,1); % time

dt = time(2) - time(1); % timestep

trans_r = floor(1 + trans_time/dt); % number of transitive steps [-]

total_time = time(length(time))-time(trans_r); % time minus transitive [s]

% displacements, time is in column 1 so node 1 is in column 2, etc.
x = noddis(:,node*3 - 1); % x-dir
y = noddis(:,node*3); % y-dir
z = noddis(:,node*3 + 1); % z-dir


if node_pitch ~= 0
    x_2 = noddis(:,node_pitch*3 - 1); % x-dir
    z_2 = noddis(:,node_pitch*3 + 1); % z-dir
end
```

```
if node_pitch ≠ 0
    length_node = z(1) - z_2(1); % length between nodes
    x_rel = x - x_2; % relative x translational distance
    angle = (asin(x_rel./length_node))*(180/pi); % (rad) -> deg
end

% normalize heave
if norm_heave == 0
    z = z(1) - z;
elseif norm_heave == 999
    % do nothing
else
    z = norm_heave - z;
end

%%%%%%%%%%%%%%%%%%%%%%%% peak value statistics %%%%%%%%%%%%%%%%%%%%%%%%%%%

if print_stat == 0
    %%% Heave motion
    disp('eta_3 - Heave motion')
    [m0,T02,xtmean] = SPEGEN_T_stat(z(trans_r:length(z)),spec_div,dt);

    mpm = xtmean + sqrt(2*m0*log(total_time/T02));

    disp(['Mean from spectrum ',num2str(xtmean)])
    excel(1) = xtmean;
    disp(['Standard deviation dynamic ',num2str(sqrt(m0))])
    excel(2) = sqrt(m0);
    disp(['Most probable max motion(mean + dynamic) ',num2str(mpm),' [m]'])
    excel(3) = mpm;
    disp([' ']);

    %%% Pitch motion
    disp('eta_5 - Pitch motion')
    [m0,T02,xtmean] = SPEGEN_T_stat(angle(trans_r:length(angle)),spec_div,dt);

    mpm = xtmean + sqrt(2*m0*log(total_time/T02));

    disp(['Mean from spectrum ',num2str(xtmean)])
    excel(4) = xtmean;
    disp(['Standard deviation dynamic ',num2str(sqrt(m0))])
    excel(5) = sqrt(m0);
    disp(['Most probable max motion(mean + dynamic) ',num2str(mpm),' [deg]'])
    excel(6) = mpm;
end

%%%%%%%%%%%%%%%%%%%%%%%%%%%%%% plots %%%%%%%%%%%%%%%%%%%%%%%%%%%%%%%%%%%%%%

% power spectrum S(f) (e.g. m^2*sec)

if mode_spec == 0
    SPEGEN_T(x(trans_r:length(x)),spec_div,dt);
    legend('\eta_1')

    SPEGEN_T(y(trans_r:length(y)),spec_div,dt);
    legend('\eta_2')

    SPEGEN_T(z(trans_r:length(z)),spec_div,dt);
    legend('\eta_3')

    SPEGEN_T(angle(trans_r:length(angle)),spec_div,dt);
    legend('\eta_5')
end
```

```
if mode_spec == 1
    SPEGEN_T(x(trans_r:length(x)),spec_div,dt);
    legend('\eta_1')
elseif mode_spec == 2
    SPEGEN_T(y(trans_r:length(y)),spec_div,dt);
    legend('\eta_2')
elseif mode_spec == 3
    SPEGEN_T(z(trans_r:length(z)),spec_div,dt);
    legend('\eta_3')
elseif mode_spec == 4
    SPEGEN_T(angle(trans_r:length(angle)),spec_div,dt);
    legend('\eta_5')
end


% time series plots
scrsz = get(0,'ScreenSize');
figure('OuterPosition',[scrsz(4)/2.4 scrsz(4)/3 scrsz(3)/2.2 scrsz(4)/1.8])

% Surge, X - translatory
subplot(4,1,1)
plot(time,x)
xlabel('time [s]')
ylabel('Displacement [m]')
title('\eta_1 , X - translatory','FontWeight','bold')
axis tight
grid on


% Sway, Y - translatory
subplot(4,1,2)
plot(time,y)
xlabel('time [s]')
ylabel('Displacement [m]')
title('\eta_2 , Y - translatory','FontWeight','bold')
axis tight
grid on

% Heave, Z - translatory
subplot(4,1,3)
plot(time,z)
xlabel('time [s]')
ylabel('Displacement [m]')
title('\eta_3 , Z - translatory','FontWeight','bold')
axis tight
grid on



% Pitch, Rotation about y
subplot(4,1,4)
plot(time,angle)
xlabel('time [s]')
ylabel('Displacement [deg]')
title('\eta_5 , pitch rotation','FontWeight','bold')
axis tight
grid on


%%%%%%%%%%%%%%%%%%%%%%%%%%%%% eof %%%%%%%%%%%%%%%%%%%%%%%%%%%%%%%%%%%%%%%%
```

B Batch Script for Running Coupled Analysis

Presented here is the batch script developed during the thesis work for running coupled analyses with the analysis programs SIMO/TDHMILL and RIFLEX. The batch script verifies that the modules RIFLEX inpmod and RIFLEX stamod has succsesfully completed. An example on how to run the script in parallel and sequentially is included in the folder /Batch Script/ on the attached disk where also the following script can be found in its native form.

```
@ECHO OFF
REM %%%%%%%%%%%%%%%%%%%%%%%%%%%%%%%%%%%%%%%%%%%%%%%%%%%%%%%%%%%%%%%%%%%%%%%
REM %
REM % Batch file for running a single case with id defined below
REM %
REM %
REM % Eirik Wie Furunes, Spring 2010
REM %
REM %%%%%%%%%%%%%%%%%%%%%%%%%%%%%%%%%%%%%%%%%%%%%%%%%%%%%%%%%%%%%%%%%%%%%%%

REM %%%%% ID %%%%%

set id=main

REM %%%%% ID %%%%%


REM %%%%% DEFINE COMPLETION STRING %%%%%

set "inpmod=--- THE RIFLEX INPUT MODULE   I N P M O D   IS SUCCESSFULLY COMPLETED ---"
set "stamod=--- THE RIFLEX STATIC MODULE  S T A M O D   IS SUCCESSFULLY COMPLETED ---"

REM %%%%% DEFINE COMPLETION STRING %%%%%


REM
REM %%%%%%%%%%%% RIFLEX INPMOD %%%%%%%%%%%%
REM


call riflex inpmod %id%

set completed=-1
FOR /F "tokens=* eol=*" %%G IN (%id%_inpmod.res) DO (
    IF "%%G" == "%inpmod%" (
        set completed=1
    )
)
IF NOT %completed%==1 (
```

```
    ECHO ################################################
    ECHO.
    ECHO    RIFLEX INPMOD FAILED
    ECHO.
    ECHO ################################################
    pause
    goto:eof
)



REM
REM %%%%%%%%%%%% SIMO STAMOD %%%%%%%%%%%%
REM

call rsimo %id% dummy stamod batch sta



REM
REM %%%%%%%%%%%% RIFLEX STAMOD %%%%%%%%%%%%
REM

call riflex stamod %id%

set completed=-1
FOR /F "tokens=* eol=*" %%G IN (%id%_stamod.res) DO (
    IF "%%G" == "%stamod%" (
        set completed=1
    )
)
IF NOT %completed%==1 (
    ECHO ################################################
    ECHO.
    ECHO    RIFLEX STAMOD FAILED
    ECHO.
    ECHO ################################################
    pause
    goto:eof
)



REM
REM %%%%%%%%%%%% SIMO DYNMOD %%%%%%%%%%%%
REM

call rsimo %id% dummy dynmod batch dyn



ECHO ################################################
ECHO.
ECHO    Waiting to run riflex dynmod
ECHO.
ECHO    Current directory stated below
ECHO.
cd
ECHO.
ECHO ################################################

REM % Remove REM below to include pause before dynmod
REM pause
```

```
REM
REM %%%%%%%%%%%%% RIFLEX DYNMOD %%%%%%%%%%%%%
REM

call riflex dynmod %id%



REM
REM % Clean up, be careful if adjusting this depending on if you need s2x in simo
REM

del fort.4 fort.98 fort.99 *.mpf main_*.ffi stdin.inp *.lis main_*.sam



REM
REM %%%%%%%%%%%%% SIMO S2XMOD %%%%%%%%%%%%%
REM

REM rsimo %id% dummy s2xmod batch s2x



ECHO ################################################
ECHO.
ECHO    Run is complete, press any key to quit.
ECHO.
ECHO    Current directory stated below
ECHO.
cd
ECHO.
ECHO ################################################

pause
```

C Analysis Models

Presented here is geometry and mass distribution for the analysis models.

C.1 Base case

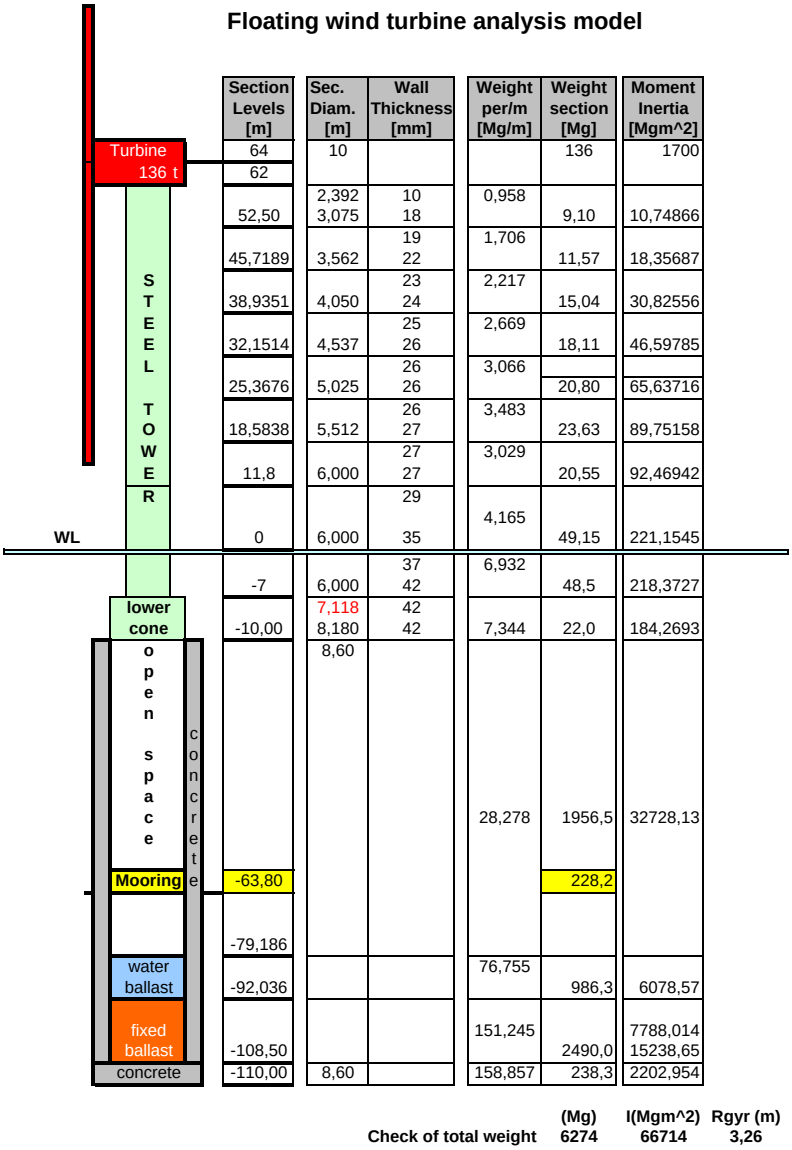

Figure C.1: Base case analysis model

C.2 80M-Cyl

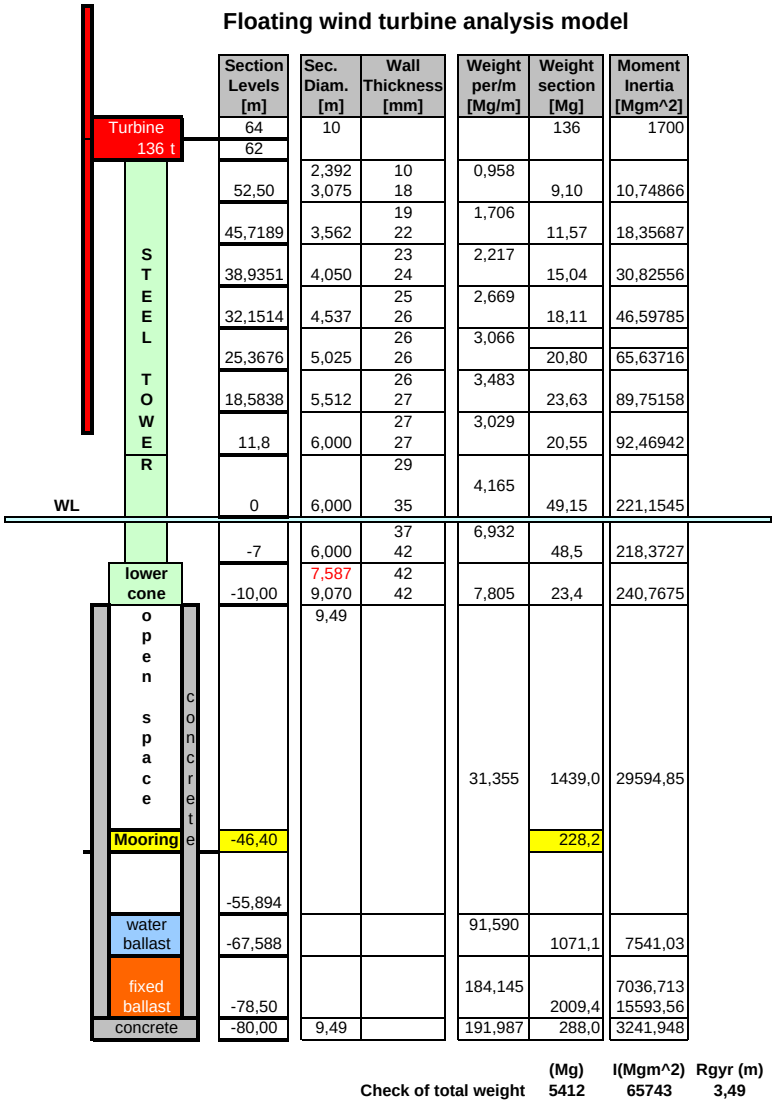

Section Levels [m]	Sec. Diam. [m]	Wall Thickness [mm]	Weight per/m [Mg/m]	Weight section [Mg]	Moment Inertia [Mgm^2]
64	10			136	1700
62					
	2,392	10	0,958		
52,50	3,075	18		9,10	10,74866
		19	1,706		
45,7189	3,562	22		11,57	18,35687
		23	2,217		
38,9351	4,050	24		15,04	30,82556
		25	2,669		
32,1514	4,537	26		18,11	46,59785
		26	3,066		
25,3676	5,025	26		20,80	65,63716
		26	3,483		
18,5838	5,512	27		23,63	89,75158
		27	3,029		
11,8	6,000	27		20,55	92,46942
		29	4,165		
0	6,000	35		49,15	221,1545
		37	6,932		
-7	6,000	42		48,5	218,3727
	7,587	42			
-10,00	9,070	42	7,805	23,4	240,7675
	9,49				
			31,355	1439,0	29594,85
-46,40				228,2	
-55,894					
			91,590		
-67,588				1071,1	7541,03
			184,145		7036,713
-78,50				2009,4	15593,56
-80,00	9,49		191,987	288,0	3241,948

	(Mg)	I(Mgm^2)	Rgyr (m)
Check of total weight	5412	65743	3,49

Figure C.2: 80M-Cyl analysis model

C.3 80M-1

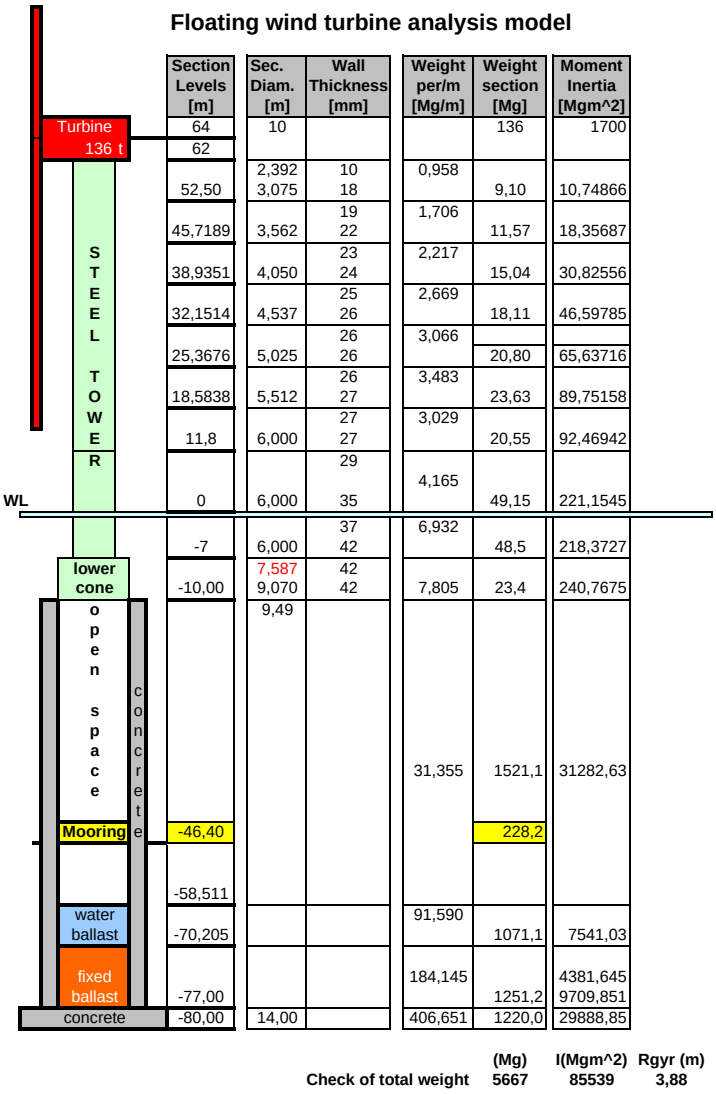

	Section Levels [m]	Sec. Diam. [m]	Wall Thickness [mm]	Weight per/m [Mg/m]	Weight section [Mg]	Moment Inertia [Mgm^2]
	64	10			136	1700
	62					
		2,392	10	0,958		
	52,50	3,075	18		9,10	10,74866
			19	1,706		
	45,7189	3,562	22		11,57	18,35687
			23	2,217		
	38,9351	4,050	24		15,04	30,82556
			25	2,669		
	32,1514	4,537	26		18,11	46,59785
			26	3,066		
	25,3676	5,025	26		20,80	65,63716
			26	3,483		
	18,5838	5,512	27		23,63	89,75158
			27	3,029		
	11,8	6,000	27		20,55	92,46942
			29			
				4,165		
WL	0	6,000	35		49,15	221,1545
			37	6,932		
	-7	6,000	42		48,5	218,3727
		7,587	42			
	-10,00	9,070	42	7,805	23,4	240,7675
		9,49				
				31,355	1521,1	31282,63
Mooring	-46,40				228,2	
	-58,511					
				91,590		
	-70,205				1071,1	7541,03
				184,145		4381,645
	-77,00				1251,2	9709,851
	-80,00	14,00		406,651	1220,0	29888,85

Check of total weight	(Mg)	I(Mgm^2)	Rgyr (m)
	5667	85539	3,88

Figure C.3: 80M-1 analysis model

C.4 80M-2

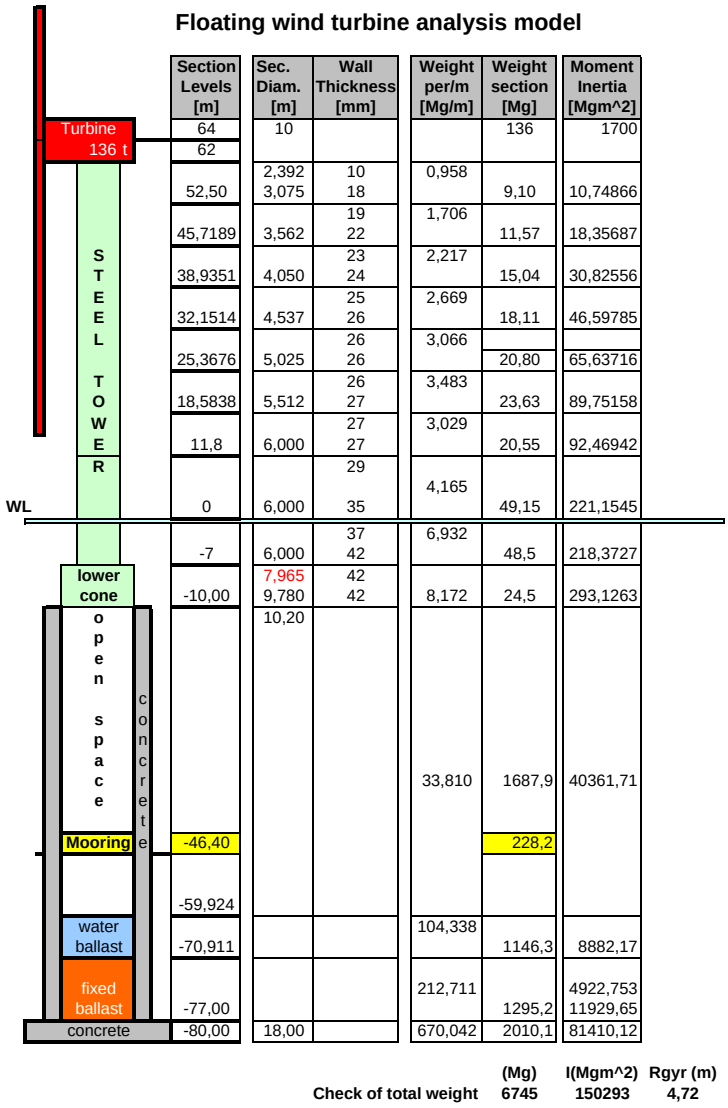

	Section Levels [m]	Sec. Diam. [m]	Wall Thickness [mm]	Weight per/m [Mg/m]	Weight section [Mg]	Moment Inertia [Mgm^2]
	64	10			136	1700
	62					
		2,392	10	0,958		
	52,50	3,075	18		9,10	10,74866
			19	1,706		
	45,7189	3,562	22		11,57	18,35687
			23	2,217		
	38,9351	4,050	24		15,04	30,82556
			25	2,669		
	32,1514	4,537	26		18,11	46,59785
			26	3,066		
	25,3676	5,025	26		20,80	65,63716
			26	3,483		
	18,5838	5,512	27		23,63	89,75158
			27	3,029		
	11,8	6,000	27		20,55	92,46942
			29			
				4,165		
WL	0	6,000	35		49,15	221,1545
			37	6,932		
	-7	6,000	42		48,5	218,3727
		7,965	42			
lower cone	-10,00	9,780	42	8,172	24,5	293,1263
		10,20				
open space				33,810	1687,9	40361,71
Mooring	-46,40				228,2	
	-59,924					
water ballast	-70,911			104,338	1146,3	8882,17
fixed ballast	-77,00			212,711	1295,2	4922,753 11929,65
concrete	-80,00	18,00		670,042	2010,1	81410,12

	(Mg)	I(Mgm^2)	Rgyr (m)
Check of total weight	6745	150293	4,72

Figure C.4: 80M-2 analysis model

D Datasheet

D.1 ULS - Rigid body motions

	Heave motion (η_3)			Pitch motion (η_5)		
Load case	R_{mean} [m]	R_{std} [m]	R_{mpm} [m]	R_{mean} [deg]	R_{std} [deg]	R_{mpm} [deg]
ULS1	0.69	0.81	3.58	2.78	1.99	9.98
ULS2	0.69	0.84	3.67	2.79	2.11	10.38
ULS3	0.69	0.85	3.72	2.79	2.22	10.78
ULS4	0.67	0.80	3.52	2.78	2.18	10.62

Table D.1: ULS Base case

	Heave motion (η_3)			Pitch motion (η_5)		
Load case	R_{mean} [m]	R_{std} [m]	R_{mpm} [m]	R_{mean} [deg]	R_{std} [deg]	R_{mpm} [deg]
ULS1	0.71	0.95	4.14	3.63	2.69	13.35
ULS2	0.71	0.99	4.27	3.64	2.84	13.87
ULS3	0.71	1.02	4.37	3.64	3.00	14.45
ULS4	0.69	0.98	4.19	3.62	2.95	14.22

Table D.2: ULS 80M-Cyl

	Heave motion (η_3)			Pitch motion (η_5)		
Load case	R_{mean} [m]	R_{std} [m]	R_{mpm} [m]	R_{mean} [deg]	R_{std} [deg]	R_{mpm} [deg]
ULS1	0.74	0.92	4.05	3.30	2.75	13.21
ULS2	0.74	0.96	4.19	3.30	2.91	13.78
ULS3	0.74	0.99	4.30	3.31	3.09	14.41
ULS4	0.72	0.94	4.10	3.30	3.04	14.21

Table D.3: ULS 80M-1

	Heave motion (η_3)			Pitch motion (η_5)		
Load case	R_{mean} [m]	R_{std} [m]	R_{mpm} [m]	R_{mean} [deg]	R_{std} [deg]	R_{mpm} [deg]
ULS1	0.88	1.03	4.56	2.52	3.39	14.74
ULS2	0.90	1.08	4.75	2.53	3.62	15.55
ULS3	0.91	1.12	4.91	2.55	3.86	16.40
ULS4	0.88	1.08	4.73	2.54	3.83	16.25

Table D.4: ULS 80M-2

D.2 FLS - Fatigue life with notch filter

Load case	Std stress [MPa]	Lifetime [years]	$D(H_s)P(H_s)$ [1/year]
FLS1	4.5	4546.7	0.00007
FLS2	6.3	460.3	0.00088
FLS3	7.2	112.2	0.00154
FLS4	7.2	76.6	0.00092
FLS5	8.1	42.6	0.00073
FLS6	9.3	19.0	0.00068
FLS7	10.7	9.5	0.00054
FLS8	12.0	5.4	0.00037
FLS9	13.4	3.5	0.00022
FLS10	14.7	2.4	0.00017
		Total damage	0.00611
		Total lifetime	164 years

Table D.5: FLS Base case

Load case	Std stress [MPa]	Lifetime [years]	$D(H_s)P(H_s)$ [1/year]
FLS1	5.1	1943.5	0.00015
FLS2	7.5	160.1	0.00254
FLS3	8.7	44.2	0.00391
FLS4	9.1	25.5	0.00278
FLS5	10.2	12.7	0.00244
FLS6	11.7	6.5	0.00199
FLS7	13.3	3.5	0.00149
FLS8	14.9	2.1	0.00094
FLS9	16.5	1.5	0.00051
FLS10	18.1	1.1	0.00037
		Total damage	0.01713
		Total lifetime	58 years

Table D.6: FLS 80M-Cyl

Load case	Std stress [MPa]	Lifetime [years]	$D(H_s)P(H_s)$ [1/year]
FLS1	4.9	2120.3	0.00014
FLS2	7.3	177.1	0.00229
FLS3	8.6	46.6	0.00372
FLS4	9.0	26.4	0.00269
FLS5	10.1	13.1	0.00236
FLS6	11.6	6.5	0.00197
FLS7	13.3	3.5	0.00148
FLS8	15.0	2.1	0.00095
FLS9	16.6	1.5	0.00052
FLS10	18.3	1.0	0.00038
		Total damage	0.01650
		Total lifetime	61 years

Table D.7: FLS 80M-1

Load case	Std stress [MPa]	Lifetime [years]	$D(H_s)P(H_s)$ [1/year]
FLS1	4.7	2586.2	0.00012
FLS2	6.9	227.7	0.00178
FLS3	8.4	48.0	0.00360
FLS4	9.0	23.1	0.00307
FLS5	10.5	10.6	0.00293
FLS6	12.3	4.8	0.00271
FLS7	14.3	2.5	0.00203
FLS8	16.3	1.5	0.00132
FLS9	18.5	1.0	0.00076
FLS10	20.9	0.7	0.00059
		Total damage	0.01891
		Total lifetime	53 years

Table D.8: FLS 80M-2